UNIVERSITÀ
DEGLI STUDI
DI PADOVA

UNIVERSITY OF PADOVA

DEPARTMENT OF INDUSTRIAL ENGINEERING

PhD COURSE IN INDUSTRIAL ENGINEERING

Curriculum: Chemical and Environmental Engineering

PhD THESIS IN INDUSTRIAL ENGINEERING

XXXII PhD CYCLE

EPOXIDATION OF VEGETABLE OILS BY CONVENTIONAL AND NON-CONVENTIONAL METHODS

Supervisor: Giuseppe Maschio, Full Professor

PhD student: Damiano Piccolo

ACADEMIC YEAR 2018-2019

Ai miei genitori

A Elisa

Abstract

The interest on epoxidised vegetable oils has been increasing in the last years thanks to their use as renewable and sustainable resource for a wide range of environmental-friendly and sustainable chemicals. The aim of this work is producing epoxidised soybean oil in newer, safer and more efficient ways. This PhD thesis is structured according to different experimental approaches, supported by a kinetic and mass transfer modelling to enable a complete understanding of the phenomena. The epoxidation process was carried out in two phases via peroxyacetic acid, produced by the reaction between acetic acid and hydrogen peroxide. Epoxidation of soybean oil was carried out in a batch calorimetric reactor, for an accurate study on kinetics, mass transfer and calorimetry. Furthermore, the microwave (MW) heating effect on the process was studied, by means of a comparative study using two geometrically similar reactors with different heating sources, conventional and MW heating. MW heating process is able to produce a uniform stable suspension halving the time to reach maximum yield. Epoxidation was tested also in a continuous system, for its potential industrial interest. The process was also effective in a continuous reactor, even though the mixture must be stabilised by means of a surfactant. The feasibility of using radiofrequency heating in the continuous reactor was tested for more controlled operation than MW heating.

Table of contents

Introduction

The interest on epoxidised vegetable oils has been increasing in the last years thanks to their use as a renewable and sustainable resource for a wide range of environmental-friendly and sustainable chemicals. Chemicals produced from vegetable oils can be obtained from different crops and exploited to produce a wide range of products. The annual production of vegetable oils is noticeable, equal to 182.3 million tons in 2017.

Palm oil is the most abundant, with a production of about 33% of the total, even if lands for its production are only 5.5% of the lands employed for its cultivation. In fact, palm oil is produced in large plantations thanks to its very high productivity. Nevertheless, soybean oil is the most widespread crop (40.1% of the total lands) despite its lower productivity. Oils are largely produced also from cottonseed (13.8%) and sunflower (10%).

Vegetable oils are renewable, non-toxic and can be easily functionalised to obtain other products. In the food industry, large amount of vegetable oils is used, instead of animal fats. Furthermore, they are also exploited for the production of soaps and cosmetic products. Oils can be used also for petrochemical industry, as bio-lubricants, bio-diesel via transesterification or green-diesel (Ecofining process by Eni).

Thanks to their high reactivity, epoxidised vegetable oils are exploited for the production of many chemicals such as alcohols, glycols, alkanolamines and in the production of epoxy resins, polyesters and polyurethanes. Moreover, it is recalled that epoxidised soybean oil is a valuable stabiliser and plasticiser for PVC, and its production is well implemented industrially since 1949 with several patented applications.

At the industrial scale, the production of epoxidized oils is based on large batch processes. The technique is quite widespread, and is based on the reaction between a peroxycarboxylic acid and the double bonds of the oil. The process is biphasic: the peroxycarboxylic acid is produced in the aqueous phase by reaction between the carboxylic acid and hydrogen peroxide, it then migrates to the oil phase and epoxidizes the oil. Hence, the process is composed of two steps of reaction and two of mass transfer. Commonly used acids are formic or acetic: the first is more reactive but can lower the selectivity, enhancing side reactions that break the oxirane ring. The epoxidation is carried out via peracid thanks to its solubility in the oil phase, sensibly higher than that of hydrogen peroxide. The process is catalysed by sulfuric or phosphoric acid.

In the literature, other methods can be found for oil epoxidation. An alternative method is the epoxidation using molecular oxygen with silver catalyst dispersed in the batch. The efficiency of the overall process is very low. Other methods are based on using solid catalyst as alumina or ion exchange resins. In this case, the process takes place in three phases and it exploits acid sites of the catalyst. The advantage of this process is mainly on the easy separation of the catalyst by simple filtration. Moreover, catalyst can be reused after regeneration (in the case of resins, regeneration was operated by concentrated sulfuric acid). Some researchers proposed a method based on ultrasound. In fact, ultrasound can be successfully used to produce micro-emulsions/suspension, with beneficial effects on mass transfer. Moreover, ultrasound locally creates high pressure and temperature spots. In this way, the process was faster, highly selective and more efficient. Other authors proposed MW heating, that mainly targets the aqueous phase. Its effect can be interesting to speed up the process. However, this technique was not well established, with few works on this field.

In addition to these methods, electrochemical epoxidation seems to be quite interesting. This method permits to electrochemically produce hydrogen peroxide *in situ*, and to achieve epoxidation both by the standard route and via chlorohydrin, thanks to hypochlorous acid that was electrochemically formed. Other methods can be found in the literature, with new challenging catalysts, but they were only developed at the laboratory scale.

The aim of this work is producing epoxidized soybean oil in newer, safer and more efficient ways. The study was organised in different experimental approaches and a biphasic kinetic and mass transfer modelling. Moreover, diluted hydrogen peroxide and acetic acid were chosen instead of commonly used concentrated hydrogen peroxide and formic acid for safer conditions. Soybean oil was preferred among different vegetable oils thanks to its large production.

This study involves the epoxidation in a batch calorimetric reactor, that is a batch, well-stirred, jacketed reactor. *Huber* thermocryostat guarantees an accurate thermal control of the system. This apparatus permitted to study the process in batch conditions, with high quality mixing and accurate data acquisition. This part of the study is a base case, enabling to obtain useful information for future scale-up and calorimetric data. The epoxidation process was carried out to obtain yield vs time curves, at different intermediate times and parametric with temperature. The set-up of this experimental apparatus required the implementation of a software for the temperature and pressure data acquisition in the reactor and the control of the impeller motor. Furthermore, the calibration of the stirrer required the realisation of an infrared velocity

measurement system. A deep study on the determination of the heat exchange coefficient was carried out, based on both thermal transients and steady states.

Moreover, the effect of MW heating in the reacting system was assessed, for a more effective energy delivery to the system. In fact, MW field has both thermal and kinetic effects in reacting systems made of polar species. Two systems were implemented, with same geometry but different heating source: MW and conventional heating. In this way, an accurate comparison was performed, evaluating the net effect of the MW field on the reactive system. The effect of the stirring velocity was assessed in both cases. Yield vs time curves were obtained for both processes, at different temperatures.

Furthermore, the feasibility of a continuous process was verified, and it was fully implemented and operated, obtaining the yield vs time curves. The biphasic mixture was stabilised by means of a surfactant, obtaining a stable emulsion. A study on the stability of the mixture was carried out, using different ionic and non-ionic surfactants.

In addition, radiofrequency heating was applied and tested on the continuous process, with several advantages in terms of electric control of the system compared to MW. An accurate electrical study by means of a Vector Network Analyser was performed for the correct operation of the system.

For all cases, a kinetic and mass transfer model was implemented to enable a complete understanding of the system. The biphasic mixture was studied according to the approach based on Whitman's two films theory, and described both all the reactions that take place in each phase and mass transfer between phases. The model permitted to determine mass transfer and kinetic parameters by means of a fitting, thanks to which it was possible to assess the overall rate determining step of the process and other relevant information.

Chapter 1

State of the art

In the last decades, industrial chemistry has been trying to solve the problem that petrol-derived chemicals represent, striving to find more sustainable and bio-degradable renewable substitutes. Vegetable oils (VO) can be a valid solution because they can be obtained from different crops and can be exploited to produce a wide range of products. Annual production in 2017 was equal to 182.3 million ton [1]. The most produced VO is palm oil with 33% of the total VOs world production even if its cultivation occupies only 5.5% of the lands employed for its cultivation [2]. However, soybean is the most widespread crop (40.1% of the total lands) despite its lower productivity. In the case of soybean, cottonseed and sunflower, the occupied lands are 40.1%, 13.8% and 10.0% respectively of the total land occupied by the cultivation of vegetable for the oil production. The production and the request of vegetable increase each year thanks to the new green technologies that attempt to substitute petroleum derivate products with new renewable ones.

Moreover, VOs are renewable, non-toxic and can be easily functionalised to obtain other products [3]. VOs are used in the food industry, to produce soaps but also as bio-lubricants [4], bio-diesel via transesterification or green-diesel (Ecofining process by Eni) [5]. Epoxidised vegetable oils (EVOs) are used mainly thanks to the high reactivity of the oxirane ring [3], [6]. In fact, EVOs are an intermediate product used in the synthesis of many chemicals such as alcohols, glycols, alkanolamines and in the production of epoxy resins, polyesters and polyurethanes [7], [8]. Moreover, it is recalled that epoxidised soybean oil is a valuable stabiliser and plasticiser for PVC and its production is well implemented at the industrial scale (2Mtons per year) since 1949 with patented applications [9],[10]. The use of the soybean oil as a plasticiser has been growing considerably in these years, thanks to the high quality of the material and the competitiveness over petrol-derived ones.

In this chapter, the different processes exploited for VO epoxidation are exposed, both as regards the industrial standard and the new solutions proposed by the literature. Moreover, since in this work exploits also microfluidic techniques, a short overview on this field is reported.

Furthermore, the physics of the microwave heating (MW) is explained since dielectric losses heating is one of the methods exploited in this work.

Moreover, since in this work also a mathematical modelling was performed, a short overview on the different approaches is reported.

1.1 Epoxidation reaction: features and possible ways

The epoxidation of the vegetable oils is the functionalisation, by partial oxidation the fat acids. It is useful to remind that vegetable oils have certain amount of unsaturations along the chain that depends on the kind of fat acid.

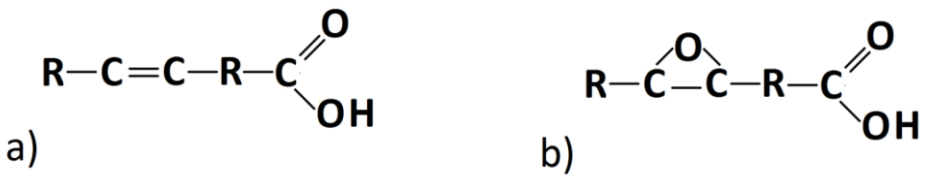

Figure 1.1. *Schematic representation of a fat acid and an epoxidized fat acid.*

There are many possibilities to perform the epoxidation that can be found in the literature. The process of epoxidation of vegetable oils is well known and exploited at the industrial scale since 1946 with patented applications [11]. The process was carried out preparing a solution of peracetic acid by reaction between hydrogen peroxide and acetic acid in presence of an acid catalyst such as sulfuric or phosphoric acid. After the reaction was completed, the solution was mixed with the soybean oil, obtaining a suspension in which the peroxyacetic acid can react with the unsaturations of the oil. Once the conversion of the double bonds was complete, the oil was separated and purified. As mentioned in the patent, one of the oldest methods to perform this process involved the use of perbenzoic acid, that is costly and difficult to separate from the oil. In modern processes, epoxidation is carried out in large batch reactors using acetic or formic acid, hydrogen peroxide and vegetable oil. Great plant investments are required with reactions durations up to 8 hours. Several drawbacks affect this process, such as the heat removal since the process is strongly exothermic, and the corrosiveness of the acids. Several other approaches can be found in the literature. Dinda *et al.* [12] and Chavan *et al.* [7] proposed a classification based on the different methods.

1. Epoxidation with peroxycarboxilic acids (Prilezhaev's epoxidation) obtained by generation *in situ* by reaction between hydrogen peroxide and carboxylic acids. Sometimes catalysts as sulfuric or phosphoric acids are used. This is the most used method, these acids are commonly used and available at relatively low cost and the by-product is simply water [13], [14], [15], [16];
2. epoxidation with peroxycarboxylic acids, in presence of solid catalyst (ion exchange resin or alumina) [3], [17], [18];
3. electrochemical epoxidation [19] that is an efficient method of electrochemically generating hydrogen peroxide *in situ* and achieving epoxidation by the traditional way and via chlorohydrin;
4. epoxidation using halohydrines, using hypohalous acids or salts [20];
5. epoxidation using gaseous oxygen and a metallic catalyst (silver). This process is the simplest one even though it permits to achieve very low yield;
6. other methods, with different catalysts al for example Nb2O5 on silica (Di Serio *et al.* [21]), molecular sieve containing niobium (Dworakowska *et al.* [22]), molybdenum catalysts (Farias *et al.* [23]) or other catalysts [24]

In the literature, hundreds of papers can be found, regarding different oils but all of them exploited one of these methods to carry out the epoxidation. The different methods are explained in the next paragraphs.

1.1.1 Biphasic epoxidation

The patent developed in 1946 [11] applied this method that is the most widespread at the plant scale. According to this patent, a peroxyacetic acid solution was obtained by reacting acetic acid and hydrogen peroxide. Successively, the epoxidized oil was obtained by reaction between the virgin oil and the peracid solution. The process was carried out in batch reactors with good selectivity and conversion. This process is also used nowadays, even though it is commonly modified using a single batch in which both perhydrolysis and epoxidation take place in the same reactor [6], [25]. Since hydrogen peroxide is not soluble in the organic phase, a vector of oxygen is needed, and for this reason acetic acid is used. Consequently, acetic is oxidised to peroxyacetic acid by hydrogen peroxide. Peracid is soluble in the organic phase and reacts with the double bonds of the oil producing epoxides and acetic acid. The cycle is completed once acetic acid diffuses from the organic to the aqueous phase. The process is made of four steps,

two of reaction (perhydrolysis and epoxidation) and two of mass transfer. The process is schematised in Figure 1.1.

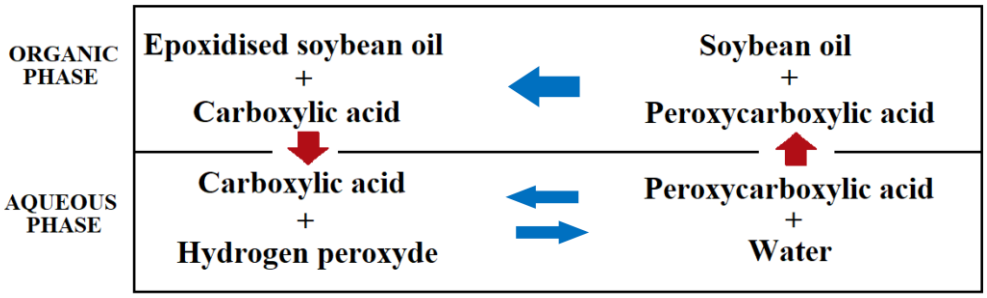

Figure 1.1. *Schematic representation of the process.*

Because of the presence of acids and water, epoxy ring opening reaction can take place and leads to the formation of different by-products, mainly glycols.

In general, the process can be carried out using different carboxylic acids, such as formic and acetic. Formic acid is strongly reactive, both in the formation of the peroxyformic acid and the epoxy ring opening. Acetic acid is sometimes used to increase selectivity whereas propionic acid is not commonly used because it is too weak. Sometimes an acid catalyst is used, such as sulfuric or phosphoric acid, to speed up the process. The formation of the peroxycarboxylic acid is often considered the rate determining step, even if according Santacesaria [26] epoxidation is the slowest reaction. These results can differ because they are strongly dependent on the type of carboxylic acid, on the use of an acid catalyst and the concentration of the hydrogen peroxide.

1.1.1.1 Presence of acid catalyst

The need of an acid catalyst is not well clear in the literature. The presence of an inorganic acid prevents the spontaneous decomposition of the peroxycarboxylic acid (according to Zhao *et al.*[27], [28]) thus promoting the epoxidation step. Moreover, the presence of an acid prevents the dissociation of the acetic acid. This dissociation should be detrimental for the formation of peroxycarboxylic acid and the oxirane even if this aspect is in contrast what it is said in by Li *et al.*[19]. Dinda *et al.* [29] demonstrated the great catalytic activity of phosphoric and sulfuric acid, both boosting the formation of the oxirane and its degradation. In this, way the conversion of oxygen to oxirane could extent to 67.5% in 10 hours and to 70% in 6 hours for the two acids respectively. The same authors also tested other acids as hydrochloric and nitric acid, with lower positive effects. Moreover, the beneficial effect of sulfuric and phosphoric acid is also proved

by Santacesaria *et al*.[26], who demonstrate a remarkable difference in their catalytic activity. In fact, sulfuric acid shows a relevant thermal exothermic peak, more intense than phosphoric acid. These results are not in line with Sinadinovic-Fiser *et al*. [3], who did not found a great catalyst activity of sulfuric acid. Moreover, in some works no sulfuric/phosphoric acid is used at all, i.e. Jia *et al*. [30] or de Quadros *et al.* [14].

In general, the presence of an acid catalyst strongly promotes the formation of the peroxyacid, but it is detrimental for the epoxides, because it promotes their degradation to glycols. Consequently, the concentration of acid catalyst must be a compromise. According to Aguilera *et al.* [31] pH lower than 3.5 permits the protonation of oxirane and its cleavage. Similarly, Dinda *et al.* [12] report that a mass fraction of sulfuric acid greater than 3% promotes this side-reaction so they choose an optimum value of 2%.

1.1.1.2 Choice and concentration of the carboxylic acid

The process can be carried out using formic, acetic or propionic acid. Nevertheless, propionic acid seems to have very low reactivity and for this reason is not commonly used [32]. Formic acid is strongly reactive, so that thermal control can be difficult to achieve. Moreover, formic acid is very corrosive and its high reactivity can be detrimental for epoxy stability [12]. Carboxylic acid concentration is crucial for the process since low concentration leads to an insufficient formation of peracid, and high concentration is detrimental for the stability of the epoxides. This aspect was studied by Dinda *et al.* [12] and Chavan *et al.* [33] who propose that a good compromise can be achieved with an acetic acid: double bonds molar ratio equal to 0.5:1, whereas values of concentration higher or lower than this one implies what stated before. This is in line with the results of Sinadinovic-Fiser *et al.* [3].

1.1.1.3 Concentration of hydrogen peroxide

Concentrated hydrogen peroxide is typically used for enhanced reactivity. Dinda *et al.* [12] used hydrogen peroxide with a massive concentration equal to 50wt.%, Santacesaria *et al.* [26] and De Quadros *et al.* [14] employed H.P. at 60wt.%. Sepulveda *et al.* [17] performed their experiments with H.P. at 70% and 100%. The latter demonstrated that pure hydrogen peroxide is not effective because a certain amount of water is needed for the formation of the peracid. Nevertheless, highly concentrated hydrogen peroxide involves also serious safety issues, because of its instability and the risk of detonation. For this reason, several researchers used

much weaker reaction conditions, using 30wt.% hydrogen peroxide as Jia *et al.* [30] and Sinadinovic-Fiser *et al.* [3].

Similarly to the previous case, H.P.: double bonds molar ratio is a relevant parameter in the process, even though its influence is weaker than that of the acetic acid. Assumed that this parameter cannot be lower than 1:1 (stoichiometric constraint), a common value is between 1.5:1 e 2:1, as demonstrated by Dinda *et al.* [12]. Lower values of this ratio do not guarantee enough oxygen for the system, whereas higher values can be detrimental for the stability of the epoxides. These results were obtained also by Sinadinovic-Fiser *et al.* [3].

1.1.1.4 Effect of the temperature

The process is usually carried out in a temperature range between 50 and 70°C. At the industrial scale, the temperature of 80°C is usually considered a safety threshold after which emergency procedures should be implemented [14]. High temperature could lead to an uncontrolled decomposition of the hydrogen peroxide with hazardous consequences. Tests on the sole aqueous phase without the oil, showed that the onset temperature at which runaway decomposition starts is of about 100°C, with acetic acid and H.P. 35wt.% [34]. This value can change depending on the concentration of hydrogen peroxide or using formic acid. However, in case of decomposition, high peaks of temperature and pressure (tens of bars) could be reached. Nevertheless, under safety conditions, temperature is an important process variable that strongly influences the quality of the product. High temperature permits to achieve high conversion in short residence time, but the stability of the epoxides is affected because the acid attack is enhanced. In fact, high temperature increases all the kinetics, both the desired and undesired ones. On the other hand, low temperature lead to slow kinetics. Even though kinetics are slow, epoxides are exposed to the acid phase for a long time, and thus easily degrade. Dinda *et al.* [12] suggest the temperature of 60°C as a good compromise, in line with Santacesaria *et al.* [26], and De Quadros *et al.* [14]. However, these values can slightly change according to the carboxylic acid and the concentration of the hydrogen peroxide.

The determination of the enthalpy of reaction is important for the thermal control of the process. A rigorous study was undertaken by Leveneur *et al.* [35], using formic acid. According to the authors, the enthalpy of the main reaction is equal to -116 kJ/mol, whereas the enthalpy of the side reactions was 50 kJ/mol. The authors obtained this result implementing a model that neglects mass transfer, since they suppose the process being in kinetic control. According to

other authors, enthalpy of reaction was -196 kJ/mol [14] and -230 kJ/mol [26], both using formic acid.

The main kinetic parameters are also available in the literature. Rangarajan *et al.* [25], in a study published in 1994, determined the activation energies of the peracetic acid formation, of the epoxidation and the epoxy ring opening and they were respectively equal to 77.9, 77.6 and 66.3 kJ/mol. Leveneur *et al.* [35] did a similar study with formic acid, and the values they obtained for the activation energy of the performic acid, the epoxidation and the epoxy opening reactions equal to 20, 72,7 and 34. These values are indicated in Table 1.1.

Table 1.1. *Thermodynamic and kinetic data of the main and the side reactions.*

	Rangarajan et al. [25] (acetic acid)	**De Quadros et al. [14] (formic acid)**	**Leveneur et al. [35] (formic acid)**	**Santacesaria et al. [26] (formic acid)**
Enthalpy of reaction of epoxidation	-	-196	-116	-230
Enthalpy of reaction of degradation	-	-	-50	-
Activation energy of formation of peracid	77.9	-	20	-
Activation energy of epoxidation	77.6	-	72.7	-
Activation energy of degradation	66.3	-	34	-

The main results previously exposed are reported in Table 1.2.

Table 1.2. *Typical values of process variables.*

Temperature	**H_2O_2**	**H_2O_2 : D.B. molar base**	**Carb acid : D.B molar ratio**	**Acid catalyst concentration**	**Time to total conversion**
50-70°C	30-60 wt.%	1.5:1	0.5:1	0-2wt.%	6-10h

1.1.2 Three-phase epoxidation.

This route is based on the use of a solid catalyst instead of sulfuric or phosphoric acid. The solid catalyst can be alumina or sulfonated ion exchange resin. The process is more complex, and separation of the catalyst can be achieved by simple filtration. The catalyst usually needs regeneration after re-use.

1.1.2.1 Ion Exchange resin

This technique was successfully implemented by Sinadinovic-Fiser *et al*. [3], using strongly acid Amberlite IR-120. The authors used castor oil diluted with benzene (1:1 mass ratio), acetic acid and 30wt.% hydrogen peroxide. Oil is diluted with benzene to lower the viscosity, especially when the conversion is high and to promote the diffusion in the ion exchange resin. Moreover, the dilution has beneficial effects on the selectivity and on the cleavage of the oxirane rings. The authors chose acetic acid instead of formic for selectivity reasons, as previously explained, with 0.5:1 acid : double bonds molar ratio. They also studied the effect of temperature, experimenting at 30, 50 and 75°C, and found a compromise between high reactivity and selectivity at 50°C. They also performed similar studies on hydrogen peroxide, determining a value equal to 1.5:1 a good value for this ratio.

The most interesting part is focused on the effect of the ion exchange resin, since the formation of the acetic acid is catalysed by the resin. The authors tested different loadings, 5, 10 and 15wt.%, determining higher reactivity with higher loadings. However, even though they noticed a great improvement in terms of rate of reaction between 5 and 10wt.% loading, they observed negligible differences between 10 and 15wt.%, so that 10wt.% was preferred. In fact, high loading can promote oxirane cleavage and moreover the catalyst would not be payed back. The authors also performed a study on the reusability of the catalyst, and they found that its efficiency decreases considerably. When reused, the maximum achievable yield decreases by 4% but the time required to reach the maximum increases by two hours.

1.1.2.1 Alumina

This method is based on findings by Sepulveda *et al.* [17] and uses alumina as solid catalyst thanks to its acid behaviour. The authors studied the epoxidation of methyl esters of vegetable

oils and they used also ethyl acetate. Concentrated hydrogen peroxide is used at 70wt.%, tests were carried out at 80°C and oil : catalyst equal to 1:5.
In this study, different alumina catalysts were used, Sol-gel, Fluka and Acros. The authors found different performances of the catalyst that were simply explained thanks to a BET analysis. In particular, the efficiency of the catalyst strongly depends on number of the active acid sites and consequently on the specific area of the catalyst, and the higher is the area, the higher is the efficiency of the catalyst. Specific areas span from 195 to 280 m^2/g.
Hydrogen peroxide is 4 times the amount required by the stoichiometry, to compensate its high decomposition catalysed by alumina. Reusability of the catalyst is possible because the yield loss is negligible.

1.1.3 Electrochemical epoxidation

This method is completely different from the previous ones and was implemented by Li *et al* [19]. This method is based on the electrochemical synthesis, and is easily controllable acting on the supply current that flows in the cell. The process is carried out in an electrolytic cell, with two compartments divided by an ion exchange membrane, in which the cathode is made of graphite whereas the anode is made of $Ti/SnO_2 + Sb_2O_4/PbO_2$. Each section is loaded with oil, formic acid and hydrochloric acid. A solution of $NaHCO_3$ is added to adjust the pH in the range of 5-7. Oxygen is bubbled in the reactor and the cell is connected to a power supply current controlled.
The mechanism of reaction is made of several reactions. In the cathodic compartment, hydrogen peroxide is electrochemically produced, thanks to which peroxyformic acid can be formed. Epoxidation is directly thanks to the reaction between double bonds and performic acid. In the cathodic compartment, hypochlorous acid is produced. This acid can epoxidize the oil via chlorohydrin. In this way, epoxidation can be carried out in both compartments, in different ways. A schematic representation of the process is shown in Figure 1.2.
The authors highlighted that pH is fundamental for this process. High pH promotes the dissociation of the formic acid, but affects the formation of hydrogen peroxide. Also, the bubbling rate was determining for the process since an excess of hydrogen peroxide highly promotes side reactions. Current density was a crucial variable, since a compromise should be found between enough current or hydrogen peroxide formation and side reaction that leads to the formation of molecular oxygen and chlorine.

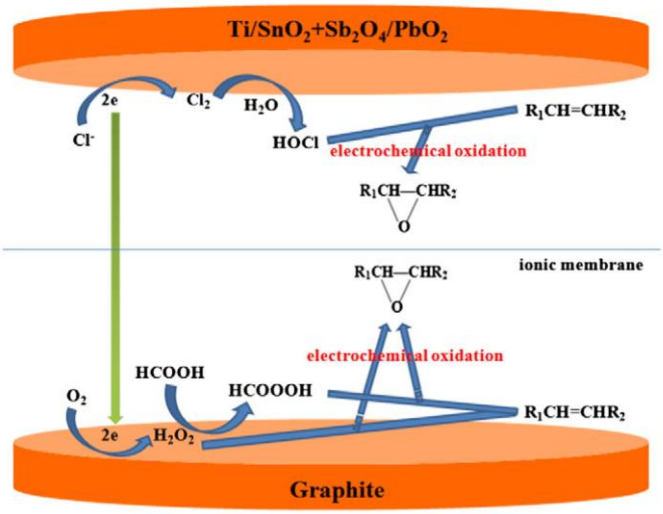

Figure 1.2. *Schematic representation of electrochemical epoxidation.*

1.1.4 Ultrasound and microwave epoxidation

Ultrasound technology is used in innovative processes thanks to its ability to enhance mass transfer and kinetics. Ultrasound locally creates high temperature and pressure hot spots that can be useful to speed up processes. In this way, energy is produced inside the system in a more efficient way. This is the case of Chavan *et al* [7], [33].

In the field of innovative processes, MW heating is increasing its importance for its thermal and kinetic effect on reactive systems. In fact, MW field forces the orientation of polar molecules, that follows the rotating electric field lines. This causes two phenomena: heating of the system by dielectric losses and kinetic effects due to the field-coordinated rotation. These phenomena are relevant on polar species, and the kinetic effect is particularly effective with highly reactive systems such as peracids, as in the case of epoxidation. Few authors as Aguilera *et al.* [31] and Leveneur *et al.* [32] tried epoxidation under MW heating exploiting these effects. This is a quite important and innovative route, with still only a few published studies. Leveneur et al. [35] studied the epoxidation of oleic acid under MW heating, discovering that it speeds up kinetics of the process compared to conventional heating conditions. The authors used standard 2kW 2.45 GHz magnetrons. Epoxidation was carried out at 60°C using acetic acid and hydrogen peroxide with stirring velocity in the range 300-650rpm.

The authors found out that MW heating is effective when organic phase ratio is low (30%), because MW field targets especially the aqueous phase, thus leading to selective heating.

With 70% oil phase loading, the effect of MW field is negligible. In the case of conventional heating, the effect of stirring velocity is negligible between 400 and 650 rpm, since the dimension of the droplets is optimum. Stirring velocity is maintained above 300 rpm, the minimum stirring velocity for the formation of the suspension. In the case of MW heating, at 30% oil loading, the rate of conversion of double bonds is doubled, and the authors correlated it to a better dissipation of energy in the system.

Also Aguilera *et al.* [31] [36] studied MW process, using an experimental approach that included a batch reactor with an external MW loop, using acetic acid as oxygen carrier. The authors discovered that 300 rpm stirring velocity is the minimum to achieve complete mixing of the biphasic mixture. Above this threshold, the influence of the stirring velocity is negligible since interfacial area was optimal. In the case of MW heating, the enhancement of the rate of conversion was higher in the case of high stirring velocity. The authors explained this fact by the presence of higher temperature gradients that in turn increase mass transfer. Moreover, this gradient could modify partition coefficients, improving the epoxy yield.

1.1.5 Other methods

In addition to all these methods, other less relevant routes can be found in the literature. For this reason, these methods are only sketched and not explained. A first method consists in epoxidation in presence of silver as catalyst. This route is old and cheap, and leads to very low yield. An alternative route is epoxidation with halohydrines in presence of hypohalous acid [20] but this solution appears to be not environment-friendly. Another method was explained by Di Serio *et al.* [21] that uses Nb2O5-SiO2 catalysts in soybean oil epoxidation in presence of hydrogen peroxide. The catalyst is prepared by sol-gel technique. The catalyst showed a good activity in epoxidation but low selectivity. An alternative route for the epoxidation of soybean oil is reported by Jiang *et al.* [37]. The catalyst is based on methyltrioxorhenium that is immobilized with brushes of poly(4- vinylpyridine) grafted onto holloysite nanotubes by surface-initiated atom transfer radical polymerization.

Furthermore, epoxidation of vegetable oils has been attempted with a cumene-O2 system by Scotti *et al* [38]. With this route the epoxidation of esters of vegetable oil is carried out using cumene as oxygen carrier. Cumene firstly reacts with O2 generating cumene hydroperoxide, that reacts with the esters forming the epoxide. A catalyst is needed, and copper supported on alumina is used.

1.2 MW heating: the physics of dielectric losses heating

Dielectric losses heating is based on the thermal effect obtained when a material is in a high frequency oscillating field. This effect is made of two phenomena, the first created by the polarization of electric charges of the material that leads to rotation of the molecules, and the second caused by conduction currents of free charges. Dielectric losses heating is widespread among insulant materials because of its low electric conductivity, induction heating, and AC or DC direct heating is not possible. Moreover, dielectric losses heating is an efficient method for energy delivering in insulant materials with low thermal conductivity. In fact, in this case conventional heating processes (conduction heating) are slow and not efficient.
In a dielectric material where a vectorial E field is imposed, the displacement electric field is described as follows:

$$D = \varepsilon_0 E + P = \left(1 + \frac{P}{\varepsilon_0 E}\right) \cdot \varepsilon_0 E = (1 + \alpha) \cdot \varepsilon_0 E = \varepsilon \varepsilon_0 E \tag{1.1}$$

where polarization P is defined as

$$P = \alpha \varepsilon_0 E \tag{1.2}$$

and the electric permittivity ε_0 is equal to $8.86 \cdot 10^{-12}$ F/m and α is the electric susceptibility.
In a dielectric material, Ampère-Maxwell equation defines the magnetic field:

$$rotH = \sigma E + \frac{\partial D}{\partial t} \tag{1.4}$$

where:
H – magnetic field in the material
σ – electric conductivity of the material
G conduction current density
$\frac{\partial D}{\partial t}$ displacement current density.
A sinusoidal field E can be written in complex eulerian form $E = E \cdot e^{j\omega t}$, according to which Ampère-Maxwell equation can be written:

$$rotH = \sigma E + j\omega \varepsilon_0 \varepsilon E \tag{1.5}$$

and $rotH$ equal to the total current

$$G_t = \sigma E + j\omega\varepsilon_0\varepsilon E \tag{1.6}$$

that is the sum of the conduction and the polarization currents.

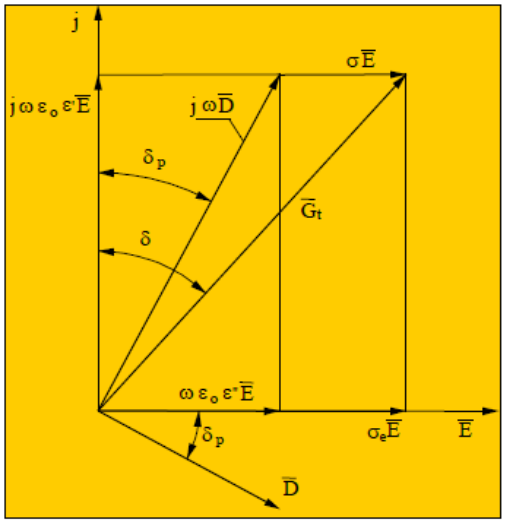

Figure 1.3. *Phasor diagram of a dielectric material under sinusoidal electric field* [39].

When a sinusoidal electric field is imposed, the polarisation process is not instantaneous, and it is phase-shifted because the electric field lags the polarisation vector. In these conditions, the electric displacement vector has a phase lag compared to the electric field vector by an angle δ_p, as shown in Figure 1.3. Hence, total current density is phase shifted by the polarisation term and also by the conduction current density, that is in phase with the electric field. In this way, the total current density is phase shifted by a total δ angle (loss angle), because of both conduction and polarisation.

Total current density can be expressed as a conduction current

$$G_t = (\sigma + j\omega\varepsilon_0\varepsilon) \cdot E = \sigma_t E \tag{1.7}$$

where $\varepsilon = \varepsilon'\text{-}j\varepsilon''$ is the complex dielectric permittivity and σ_t is the equivalent total complex conductivity.

Total current density can be expressed also as a displacement current:

$$G_t = j\omega\varepsilon_0\left(\varepsilon - \frac{j\sigma}{\omega\varepsilon_0}\right) \cdot E = j\omega\varepsilon_0\varepsilon'(1 - tg\delta) \cdot E \tag{1.8}$$

tgδ tangent of the loss angle.

The electrical representation of the equivalent circuit is shown in Figure 1.3. Capacitor C represent the ideal behaviour of the condenser whereas R_c and R_d represent conduction and polarisation currents respectively.

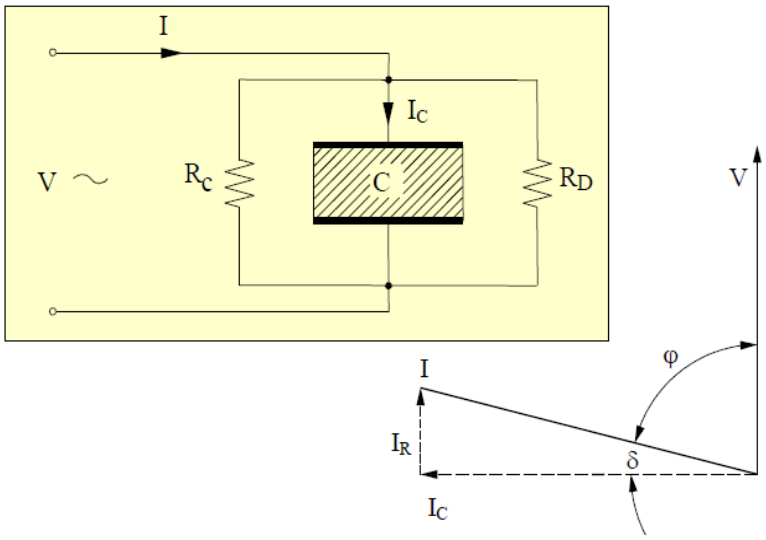

Figure 1.4. *Equivalent circuit of a dielectric material under sinusoidal electric field* [39].

Phasor diagram highlights that current has not a lead phase shift by 90° (ideal capacitor) but it is reduced by the loss angle δ.

From equation 1.8 conductivity σ_t can be expressed as:

$$\sigma_t = j\omega\varepsilon 0\varepsilon'(1 - tg\delta) \tag{1.9}$$

and the tangent of the total angle δ is an index of the amount of losses in the dielectric, due to both terms:

$$tg\delta = \frac{\varepsilon''}{\varepsilon'} + \frac{\sigma}{\omega\varepsilon_0\varepsilon'} = tg\delta_P + \frac{\sigma}{\omega\varepsilon_0\varepsilon'}. \tag{1.10}$$

Complex power per unit of volume generated in the dielectric is calculated as:

$$P + jQ = E \cdot G_t^* = \sigma_t^* \cdot E^2 \tag{1.11}$$

and * represents the conjugated complex. Complex power can be expressed as:

$$P + jQ = (\sigma + \omega\varepsilon_0\varepsilon'' - j\omega\varepsilon_0\varepsilon') \cdot E^2 = \omega E^2\varepsilon_0\varepsilon'(tg\delta - 1) \tag{1.12}$$

and this equation highlights the resistive-capacitive behaviour of the system. The thermal power

generated in the system is the real part of the complex power. Hence the active power *P* is equal to:

$$P = \omega E^2 \varepsilon_0 \varepsilon' tg\delta \quad (1.13)$$

that is the fundamental equation for dielectric heating processes that states that the power generated in the material is directly proportional to the frequency, the squared intensity of the field and to the loss factor $\varepsilon' tg\delta$. This equation is fundamental for the design of dielectric losses heating processes.

A dielectric material is different from a conductor for its capacity to be polarised under electric field. Different polarisation processes take place when an external field is imposed. For example, elastic polarisation (or electronic polarisation) is the elastic deformation of the electronic orbitals under an electric field. In this way, molecules can behave as dipoles and their electric moment is proportional to field intensity. The natural frequency of this process is in the order of 10^{14} – 10^{16} Hz. Since heating processes never use frequencies higher that 10^9 Hz, dipoles can strictly follow electric field, and electric losses are negligible. If dielectric molecules have a dipolar moment, dipolar polarisation (or relaxation polarisation) take place. In absence of electric field, dipoles are randomly distributed by thermal phenomena. Under electric field, dipoles spin around its axis, and they can be orientated along field lies. The orientation process is hindered by thermal agitation processes, and under step-wise electric field application polarisation is equal to:

$$P_r = P_{0r}\left(1 - e^{-\frac{t}{\tau}}\right) \quad (1.14)$$

where P_{0r} is the steady state relaxation polarisation, and τ is the characteristic time of the polarisation process.

For frequencies under 1 GHz, it can be assumed that elastic polarisation is instantaneous compared to the frequencies of the field, and under step-wise application of the field, equation 1.15 can be written:

$$P(t) = P_{el} \cdot \delta_1(t) \quad (1.15)$$

where $\delta_1(t)$ is step function, and its module is equal to 1.

Consequently, the total polarisation is equal to:

$$P(t) = P_{el} \cdot \delta_1(t) + P_{0r}\left(1 - e^{-\frac{t}{\tau}}\right) \tag{1.16}$$

Applying Laplace transform, the *operational dielectric constant* can be expressed as:

$$\varepsilon(s) = 1 + \frac{p(s)}{\varepsilon_0 E(s)} = \varepsilon_1 + \frac{\Delta\varepsilon}{1+s\tau} \tag{1.17}$$

and it can be expressed in the Laplace domain. The operational dielectric constant is made of a constant term (electric polarisation) and a variable term (relaxation polarisation).

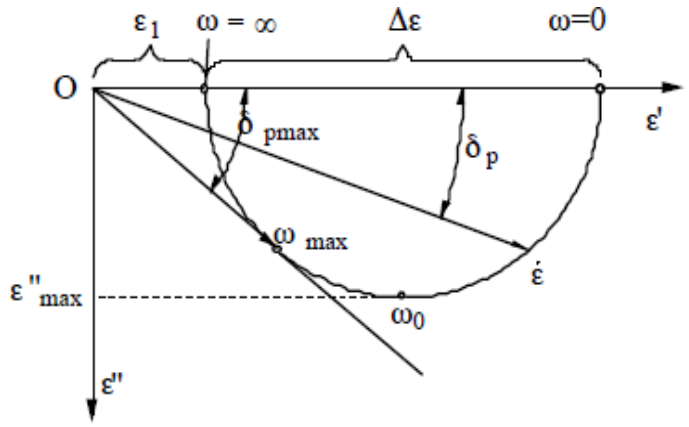

Figure 1.5. *Locus of complex dielectric constant in the complex plane* [39].

Figure 1.5 shows that at low frequencies, ε'' is low because the characteristic time of the relaxation polarisation is lower than the semi-period of the oscillation of the electric field. In this way, dipoles accurately follow field lines and lead time is negligible. Increasing the frequency, the relaxation time becomes comparable to the semi-period of the oscillation and the orientation of dipoles is delayed, producing energy losses in the dielectric. Imaginary dielectric constant ε'' increases up to a maximum, above which it decreases down to zero at very high frequency. In fact, at very high frequency, the characteristic time of the relaxation polarisation is higher than semi-period of the oscillation, so that dipoles have not enough time for the orientation process. For this reason, the plot in Figure 1.5 permits to determine the proper frequency at which a material have the maximum ε'' for maximum energy dissipation.
The previous relation can be expressed in time domain:

$$\varepsilon = \varepsilon' - j\varepsilon'' = \varepsilon_1 + \frac{\Delta\varepsilon}{1+j\omega\tau} \tag{1.18}$$

Thus, constants ε' and ε'' can be expressed as follows:

$$\varepsilon' = \varepsilon_1 + \frac{\Delta\varepsilon}{1+(1+\omega\tau)^2} \quad (1.19)$$

$$\varepsilon'' = \frac{\omega\tau\Delta\varepsilon}{1+(1+\omega\tau)^2} \quad (1.19)$$

From previous relations, it can be obtained that δ_p angle, that only considers the polarisation, can be obtained as:

$$tg\delta_P = \frac{\omega\tau\Delta\varepsilon}{\Delta\varepsilon+\varepsilon_1[1+(\omega\tau)^2]} \quad (1.20)$$

The frequency to obtain the maximum of $tg\delta_P$ can be obtained imposing equal to zero its derivative:

$$\omega_{max} = \omega_0\sqrt{1+\frac{\Delta\varepsilon}{\varepsilon_1}} \quad (1.21)$$

where $\omega_{max} = \frac{1}{\tau}$ and the maximum value of $tg\delta_P$ is equal to:

$$tg\delta_{p\,max} = \frac{\Delta\varepsilon}{2\sqrt{\varepsilon_1(\varepsilon_1+\Delta\varepsilon)}} \quad (1.18)$$

The locus of the complex vector ε is represented by the circle shown in Figure 1.4. Increasing the frequency, ε'monotonically decreases down to ε_1 at infinite frequency whereas the imaginary part ε'' increases up to $\Delta\varepsilon/2$ at $\omega = \omega_0$ and it decreases to zero for higher frequency.

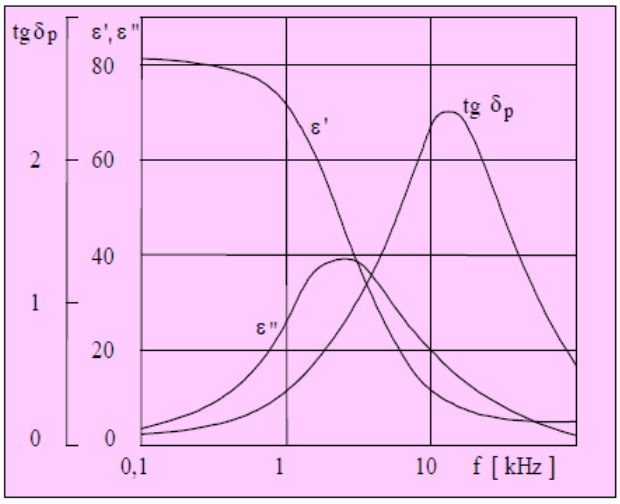

Figure 1.6. *Dielectric charactersitcs of ice obtained from distilled water at -10°C.*[39]

A typical example of the behaviour previously explained is the one of the ice (Figure 1.4).

Curves can be explained as follows:

- At low frequency, the semi-period of the oscillation is considerably higher than time τ, and relaxation polarisation has enough time to take place. The polarisation vector P and displacement vector are in phase with the electric field E.
  In this way $\varepsilon' = \varepsilon_1 + \frac{\Delta\varepsilon}{1+(1+\omega\tau)^2}$ and $tg\delta_P = 0$.
- Increasing the frequency, the semi period of the oscillation is comparable with the characteristic time of relaxation, thus lagging polarisation vector P. In fact, particles forced to move by the field are involved in thermal collisions that hinder this movement, leading to "molecular friction". These phenomena cause energy dissipation into heat. The maximum dissipative effect occurs at $\omega = \omega_{max}$.

In the most common materials, this description is qualitatively valid, but differences can be appreciated. In fact, in the material the relaxation time is not a univocally determined number, but rather a statistic distribution.
In the case of epoxidation process, oil and aqueous solution are employed. In the case of oil, ε'=2.8 and ε''=0.15. In the case of distilled water at 60°C, these values are equal to 64 and 4.9. Furthermore, for dissolving salts or acids, ε'' can increase up to 50-100 [39]. The aqueous phase is indeed made of acids and salts, hence they contribute to relaxation polarisation and conduction. Consequently, dielectric losses in the aqueous phase is much stronger than in the oil phase, promoting the formation of thermal gradients.

1.3 Microfluidic applications

The last part of this work deals with the epoxidation in a continuous reactor. That reactor was designed to work at the meso-scale, but the technology and the idea were taken from microfluidic systems for biological applications. The principle of this technology is of micro-scaling all the units of a process, for increased control and detail of the study. At the microscale, physics of the system changes, since inertial effects are negligible, and processes are controlled exclusively by viscous and diffusion phenomena [40] [41]. Moreover, microfluidic systems are usually made by PDMS and glass, therefore transparency permits visual analysis. Microfluidic systems can be used for an extremely wide range of applications, as static or rotary mixers, valves, reactors, separation units. About separation units, particular applications can be set up as membrane separation, osmosis, electrophoresis acoustic streaming. Furthermore, scaling

down to the characteristic size of microfluidic devices, permits to carry out a lot of application that could be hardly performed at larger scales. Among all, the two-phase controllable droplet flow is particularly interesting, since it allows to produce a series of water and oil droplets, with controlled dimension. This technique was also experimented in this work.

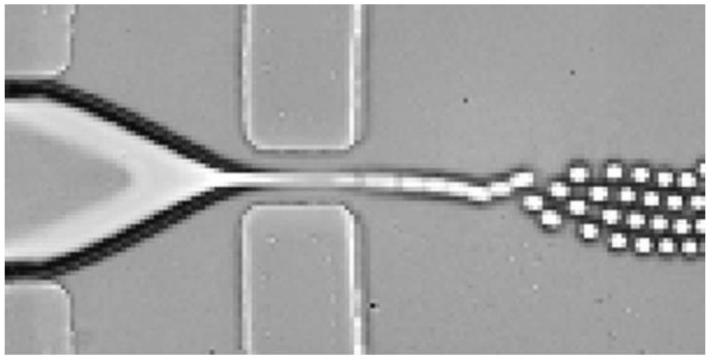

Figure 1.7. *A stream of water flows between streams of oil and is geometrically focused into a narrow cylindrical jet, generating monodispersed droplets. [42]*

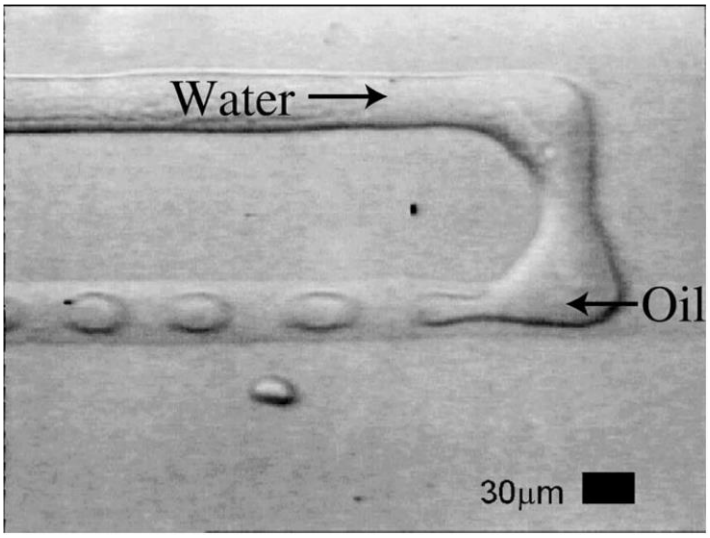

Figure 1.8. *Monodispersed microdroplet generation in a simple microfluidic device.* [43]

1.4 Kinetic and mass transfer modelling

Different approaches were implemented in the literature with different degrees of complexity and detail. In particular, models can be pseudo-homogeneus, or multiphase.

1.4.1 Pseudo-homogeneus models

Pseudo-homogeneus models assume that all the reactions take place in a single pseudo-phase. Under this assumption, a single pseudo-phase is considered having properties averaged on the constituent phases as in De Quadros *et al.* [14] and De Haro *et al* [44]. In this way, the model is strongly simplified, avoiding the use of the partition coefficient, that permits to calculate how the different species are distributed among phases. Moreover, since a single phase is considered, mass transfer is neglected since no interface is considered. In fact, this approach can be valid only under strong agitation, and if mass transfer limitation is negligible, and the process is kinetically-controlled. Even if this assumption is strongly limiting, several authors demonstrated that the process is kinetically controlled, thus this model can be considered [44]. Concerning the MW epoxidation, Aguilera *et al.* [36] proposed a pseudo-homogeneous model to study their process, made of a batch reactor with an external loop.

1.4.2 Multiphase model: kinetic and mass transfer

This approach is more complete than the previous one and considers the two phases and the mass transfer between them ,and is based on the Withman's two films theory. The model is made of mass balances for all the species in each phase. Each equation is made of kinetics and mass transfer terms. According to the literature, the partition coefficient can be modelled according to different approaches, or can be experimentally modelled. Several papers deal with the modelling of the biphasic epoxidation system thanks to its complexity and interest. One of the most complete models was made by Leveneur *et al.* [35], in which both mass and energy balances were solved with good accuracy. Wu et al. [45] studied the system not only on the base of correlations for the determination of the surface are of the droplets, but also using a high speed camera for an accurate experimental determination. In general, this multiphase approach is made of a kinetic scheme composed of:

- Perhydrolisis (formation of the peracid): direct and reverse reactions
- Decomposition of hydrogen peroxide
- Epoxidation
- Epoxy ring opening by hydroxonium
- Epoxy ring opening by carboxylic acid
- Epoxy ring opening by peracid.

Kinetic equations are usually assumed to be elementary. In some cases, hydrogen peroxide decomposition is assumed to have order 2.5 [46]. Moreover, sometimes dienes and trienes are modelled since they have different reactivity, as demonstrated by La Scala and Wool [47].

Mass transfer is described assuming that mass fluxes are obtained by product of the mass transfer coefficient and the interfacial area, and the concentration difference between bulk and interface of each phase [48]:

$$J = k \cdot A \cdot (C_i^{bulk} - C_i^{interface}) \tag{1.18}$$

where *k* is the mass transfer coefficient and *A* is the interfacial area.

Partition coefficients are modelled according to different approaches, in some cases UNIFAC approach was exploited, in other cases a more accurate modelling and sometimes experimental determination [46].

1.5 Conclusions

In conclusion, the importance of vegetable oils, in particular epoxidized soybean oil, has been increasing in the last decades for environmental reasons. Several ways to achieve epoxidation of oils are available in the literature, from the more traditional to the recent and innovative ones, such as the MW epoxidation. In fact, among different techniques, MW epoxidation is the most promising one, demonstrating a noticeable kinetics enhancement compared to traditional heating sources. In fact, MW heating in polar reactive systems has both thermal and kinetic effects, thanks to the field coordinated rotation of molecules. For these reasons, in this chapter the physic of MW heating was explained, for a better understanding of these phenomena. Finally, the main features and application of microfluidic systems are reported, because this particular method was employed for this work, thanks to the small dimensions and increased controllability. Finally, a short overview on mathematical modelling of reacting systems for V.O. epoxidation was illustrated.

Bibliographic references

[1] Statista website, https://www.statista.com/, accessed: 5/6/2018].

[2] "Palm oil research." [Online]. Available: http://www.palmoilresearch.org/statistics.html. [Accessed: 05-Jun-2016].

[3] M. R. Janković, S. V. Sinadinović-Fišer, and O. M. Govedarica, "Kinetics of the epoxidation of castor oil with peracetic acid formed in situ in the presence of an ion-exchange resin," *Ind. Eng. Chem. Res.*, vol. 53, no. 22, pp. 9357–9364, 2014.

[4] A. Adhvaryu and S. . Erhan, "Epoxidized soybean oil as a potential source of high-temperature lubricants," *Ind. Crops Prod.*, vol. 15, no. 3, pp. 247–254, May 2002.

[5] "Eni website." [Online]. Available: https://www.eni.com/it_IT/innovazione/piattaforme-tecnologiche/bio-refinery/green-diesel-eni.page. [Accessed: 13-Jun-2018].

[6] J. V. de Quadros and R. Giudici, "Epoxidation of soybean oil at maximum heat removal and single addition of all reactants," *Chem. Eng. Process. Process Intensif.*, vol. 100, pp. 87–93, 2016.

[7] A. P. Chavan and P. R. Gogate, "Ultrasound assisted synthesis of epoxidized sunflower oil and application as plasticizer," *J. Ind. Eng. Chem.*, vol. 21, pp. 842–850, 2015.

[8] T. Saurabh, dr.Patnaik M., Bhagat S.L., and Prof.Renge V.C, "Studies on Synthesis of Biobased Epoxide Using Cottonseed Oil," *J. Adv. Eng. Res. Stud.*, vol. 1, no. 2, pp. 279–284, 2012.

[9] H. Eierdanz, *Industrial fatty chemical raw materials, processes, products*. Weinheim, 1993.

[10] D. E. Terry and D. H. Wheeler, "Process of preparing epoxy derivatives form unsaturated aliphatic compounds.," 4,458,484, 1949.

[11] D. E. Therry and D. H. Wheeler, "Process of preparing epoxy derivatives form unsaturated aliphatic compounds," U.S. Patent 4,458,484, 1949.

[12] S. Dinda, A. V Patwardhan, V. V Goud, and N. C. Pradhan, "Epoxidation of cottonseed oil by aqueous hydrogen peroxide catalysed by liquid inorganic acids.,"

Bioresour. Technol., vol. 99, no. 9, pp. 3737–44, Jun. 2008.

[13] S. Leveneur, J. Zheng, B. Taouk, F. Burel, J. Wärnå, and T. Salmi, "Interaction of thermal and kinetic parameters for a liquid-liquid reaction system: Application to vegetable oils epoxidation by peroxycarboxylic acid," *J. Taiwan Inst. Chem. Eng.*, vol. 45, no. 4, pp. 1449–1458, 2014.

[14] J. V. de Quadros and R. Giudici, "Epoxidation of soybean oil at maximum heat removal and single addition of all reactants," *Chem. Eng. Process. Process Intensif.*, vol. 100, pp. 87–93, 2016.

[15] V. V. Goud, A. V. Patwardhan, and N. C. Pradhan, "Studies on the epoxidation of mahua oil (Madhumica indica) by hydrogen peroxide," *Bioresour. Technol.*, vol. 97, no. 12, pp. 1365–1371, 2006.

[16] N. Kim, Y. Li, and X. S. Sun, "Epoxidation of Camelina sativa oil and peel adhesion properties," *Ind. Crops Prod.*, vol. 64, pp. 1–8, 2015.

[17] J. Sepulveda, S. Teixeira, and U. Schuchardt, "Alumina-catalyzed epoxidation of unsaturated fatty esters with hydrogen peroxide," *Appl. Catal. A Gen.*, vol. 318, pp. 213–217, 2007.

[18] R. Mungroo, N. C. Pradhan, V. V Goud, and A. K. Dalai, "Epoxidation of Canola Oil with Hydrogen Peroxide Catalyzed by Acidic Ion Exchange Resin," *J. Am. Oil Chem. Soc.*, vol. 85, no. 9, pp. 887–896, 2008.

[19] W. Li, M. Tian, H. Du, and Z. Liang, "A new approach for epoxidation of fatty acids by a paired electrosynthesis," *Electrochem. commun.*, vol. 54, pp. 46–50, 2015.

[20] S. Guenter, R. Rieth, and K. T. Rowbottom, *Ulmann's Encyclopedia of Industrial Chemistry*, 6th ed., vol. 12. John Wiley and Sons, 2003.

[21] M. Di Serio, R. Turco, P. Pernice, A. Aronne, F. Sannino, and E. Santacesaria, "Valuation of Nb 2O 5-SiO 2 catalysts in soybean oil epoxidation," *Catal. Today*, vol. 192, no. 1, pp. 112–116, 2012.

[22] S. Dworakowska *et al.*, "Mesoporous molecular sieves containing niobium(V) as catalysts for the epoxidation of fatty acid methyl esters and rapeseed oil," *J. Clean. Prod.*, vol. 166, pp. 901–909, 2017.

[23] M. Farias, M. Martinelli, and D. P. Bottega, “Epoxidation of soybean oil using a homogeneous catalytic system based on a molybdenum (VI) complex,” *Appl. Catal. A Gen.*, vol. 384, no. 1–2, pp. 213–219, 2010.

[24] C. Chen, L. Cai, L. Li, L. Bao, Z. Lin, and G. Wu, “Heterogeneous and non-acid process for production of epoxidized soybean oil from soybean oil using hydrogen peroxide as clean oxidant over TS-1 catalysts,” *Microporous Mesoporous Mater.*, vol. 276, no. September 2018, pp. 89–97, 2019.

[25] P. D. Rangarajan, B., Havey, A., Grulke, E. A. and Culnan, “Kinetic parameters of a two phase model for in-situ epoxidation of soybean oil,” *J. Am. Oil Chem. Soc.*, vol. 72, no. 10, pp. 1161–1169, 1995.

[26] E. Santacesaria, R. Tesser, M. Di Serio, R. Turco, V. Russo, and D. Verde, “A biphasic model describing soybean oil epoxidation with H2O2 in a fed-batch reactor,” *Chem. Eng. J.*, vol. 173, no. 1, pp. 198–209, 2011.

[27] X. Zhao, T. Zhang, Y. Zhou, and D. Liu, “Preparation of peracetic acid from hydrogen peroxide. Part I: Kinetics for peracetic acid synthesis and hydrolysis,” *J. Mol. Catal. A Chem.*, vol. 271, no. 1–2, pp. 246–252, 2007.

[28] X. Zhao, K. Cheng, J. Hao, and D. Liu, “Preparation of peracetic acid from hydrogen peroxide, part II: Kinetics for spontaneous decomposition of peracetic acid in the liquid phase,” *J. Mol. Catal. A Chem.*, vol. 284, no. 1–2, pp. 58–68, 2008.

[29] S. Dinda, A. V. Patwardhan, V. V. Goud, and N. C. Pradhan, “Epoxidation of cottonseed oil by aqueous hydrogen peroxide catalysed by liquid inorganic acids,” *Bioresour. Technol.*, vol. 99, no. 9, pp. 3737–3744, 2008.

[30] L. K. Jia, L. X. Gong, W. J. Ji, and C. Y. Kan, “Synthesis of vegetable oil based polyol with cottonseed oil and sorbitol derived from natural source,” *Chinese Chem. Lett.*, vol. 22, no. 11, pp. 1289–1292, 2011.

[31] A. F. Aguilera, P. Tolvanen, K. Eränen, S. Leveneur, and T. Salmi, “Epoxidation of oleic acid under conventional heating and microwave radiation,” *Chem. Eng. Process. Process Intensif.*, vol. 102, pp. 70–87, 2016.

[32] S. Leveneur, A. Ledoux, L. Estel, B. Taouk, and T. Salmi, “Epoxidation of vegetable

oils under microwave irradiation," *Chem. Eng. Res. Des.*, vol. 92, no. 8, pp. 1495–1502, 2014.

[33] V. P. Chavan, A. V. Patwardhan, and P. R. Gogate, "Intensification of epoxidation of soybean oil using sonochemical reactors," *Chem. Eng. Process. Process Intensif.*, vol. 54, pp. 22–28, 2012.

[34] Piccolo D., "Epoxidation of soybean oil by conventional and non-conventional methods", *Master Degree Thesis in Chemical and Process Engineering,* University of Padova, 2016.

[35] S. Leveneur, J. Zheng, B. Taouk, F. Burel, J. Wärnå, and T. Salmi, "Interaction of thermal and kinetic parameters for a liquid-liquid reaction system: Application to vegetable oils epoxidation by peroxycarboxylic acid," *J. Taiwan Inst. Chem. Eng.*, vol. 45, no. 4, pp. 1449–1458, 2014.

[36] A. F. Aguilera *et al.*, "Kinetic modelling of Prileschajew epoxidation of oleic acid under conventional heating and microwave irradiation," *Chem. Eng. Sci.*, vol. 199, pp. 426–438, 2019.

[37] J. Jiang, Y. Zhang, D. Cao, and P. Jiang, "Controlled immobilization of methyltrioxorhenium(VII) based on SI-ATRP of 4-vinyl pyridine from halloysite nanotubes for epoxidation of soybean oil," *Chem. Eng. J.*, vol. 215–216, pp. 222–226, 2013.

[38] N. Scotti *et al.*, "Copper mediated epoxidation of high oleic natural oils with a cumene-O2 system," *Catal. Commun.*, vol. 64, pp. 80–85, 2015.

[39] Sergio Lupi, *Appunti di Elettrotermia*. 2005.

[40] T. M. Squires and S. R, "Quake: Micro uidics: Fluid physics at the nanoliter scale," *Electrophoresis*, vol. 22, no. July, p. 3902, 2005.

[41] N.-T. Nguyen and W. Steven, *Fundamental and applications of microfluidics*. London, 2006.

[42] T. Thorsen, R. W. Roberts, F. H. Arnold, and S. R. Quake, "Dynamic pattern formation in a vesicle-generating microfluidic device," *Phys. Rev. Lett.*, vol. 86, no. 18, pp. 4163–4166, 2001.

[43] S. L. Anna, N. Bontoux, and H. A. Stone, "Formation of dispersions using 'flow focusing' in microchannels," *Appl. Phys. Lett.*, vol. 82, no. 3, pp. 364–366, 2003.

[44] J. C. de Haro, I. Izarra, J. F. Rodríguez, Á. Pérez, and M. Carmona, "Modelling the epoxidation reaction of grape seed oil by peracetic acid," *J. Clean. Prod.*, vol. 138, pp. 70–76, 2016.

[45] Z. Wu *et al.*, "Macroscopic kinetics modelling of liquid–liquid reaction system: Epoxidation of fatty acid methyl esters," *Ind. Crops Prod.*, vol. 122, no. March, pp. 266–276, 2018.

[46] E. Santacesaria, R. Tesser, M. Di Serio, R. Turco, V. Russo, and D. Verde, "A biphasic model describing soybean oil epoxidation with H2O2 in a fed-batch reactor," *Chem. Eng. J.*, vol. 173, no. 1, pp. 198–209, 2011.

[47] J. La Scala and R. P. Wool, "Effect of FA composition on epoxidation kinetics of TAG," *JAOCS, J. Am. Oil Chem. Soc.*, vol. 79, no. 4, pp. 373–378, 2002.

[48] Z. Wu *et al.*, "Mass transfer and reaction kinetics of soybean oil epoxidation in a formic acid-autocatalyzed reaction system," *Can. J. Chem. Eng.*, vol. 94, no. 8, pp. 1576–1582, 2016.

Chapter 2

Materials, instrumentation and methods

This chapter reports the instrumentation and the methodologies applied for this work. Different reactors were used for different purposes. The calorimetric reactor is a batch, jacketed, stirred reactor used for batch conventional epoxidation. The microwave heating reactor and the glass conventional heating reactor were employed to compare the effect of the microwave field on the reacting system, with respect to the conventional heating system. The two reactors have the same geometry to ensure the same fluid dynamics conditions. The mesofluidic system was used to make the process continuous, an interesting development for industrial scale applications. The mesofluidic system was based on microfluidic chips for biological applications, and it was designed to optimize the volume of the reactor based on the residence time of the process. The RF heating mesofluidic system was used to study the effect of RF field on a continuous process in comparison with conventional heating. RF field is more controllable than MW, and the RF applicator is particularly suitable for devices with planar geometry, as in the case of mesofluidic chips. In addition to these reactors, this chapter describes other pieces of instrumentation that were designed and built *ad hoc*, such as the automatic power-controlled power supply and the RF generator and applicator. As regards the methods, the operation of each equipment is explained and the methods for the analysis of the samples, i.e. titrations and FTIR analysis.

2.1 Instrumentation

2.1.1 Calorimetric reactor

The calorimetric reactor is a batch jacketed stirred reactor by *BüchiGlasUster* (Figure 2.1). The thermal control of the reactor is achieved by a stream of silicone oil in the jacket, which temperature is controlled by a thermocryostat by *Huber*. To reduce the dispersion, the reactor was insulated with a micro-cell expanded insulator. The apparatus is equipped with three thermocouples to measure the temperature inside the reactor and at the inlet and at the outlet of the jacket. A pressure transducer, a manometer and a rupture disk monitor pressure and guarantee the safety of the system.

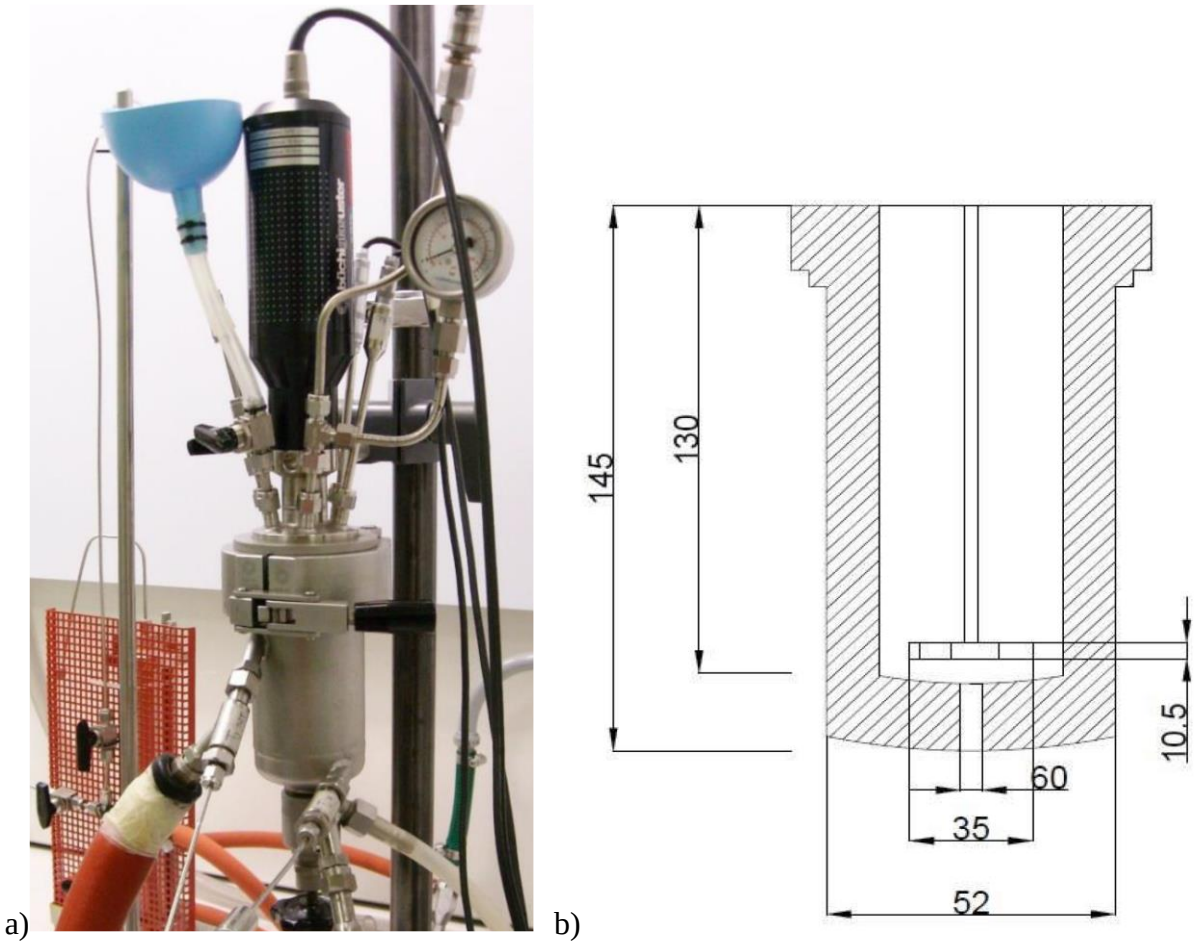

Figure 2.1. *Calorimetric reactor by BüchiGlasUster, a) picture of the reactor b) technical drawing*

Pressure and temperature data are acquired by a stack of DAQ modules by *National Instrument* and sent to a PC for visualization and storage. The agitation of the system is carried out thanks to a 35 mm Rushton turbine that is magnetically coupled to the motor to ensure perfect sealing of the system. The control of the impeller motor and the acquisition of the data are performed thanks to a custom made *Labview* script. The impeller control was accurately calibrated.

2.1.1.1 Creation of the software using *Labview*

The script for the automated control and data acquisition from the reactor was custom made using Labview software (Figure 2.2). In particular, the three temperatures and the pressure from the jacket and the reactor are displayed in real time both by an indicator and a plot that also shows the recent thermal history. The user interface allows setting the impeller velocity and, when executed, enables choosing the folder in which data can be saved. Data are saved in .csv format.

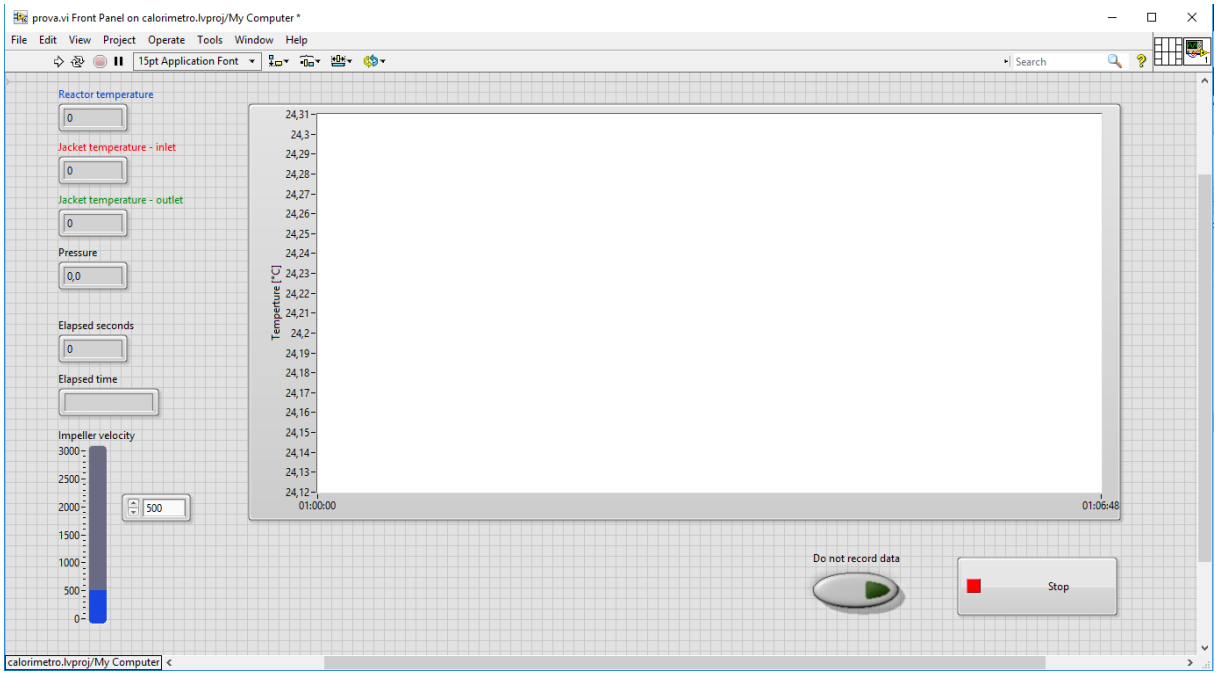

Figure 2.2. *Interface of the software created in Labview for the calorimetric reactor.*

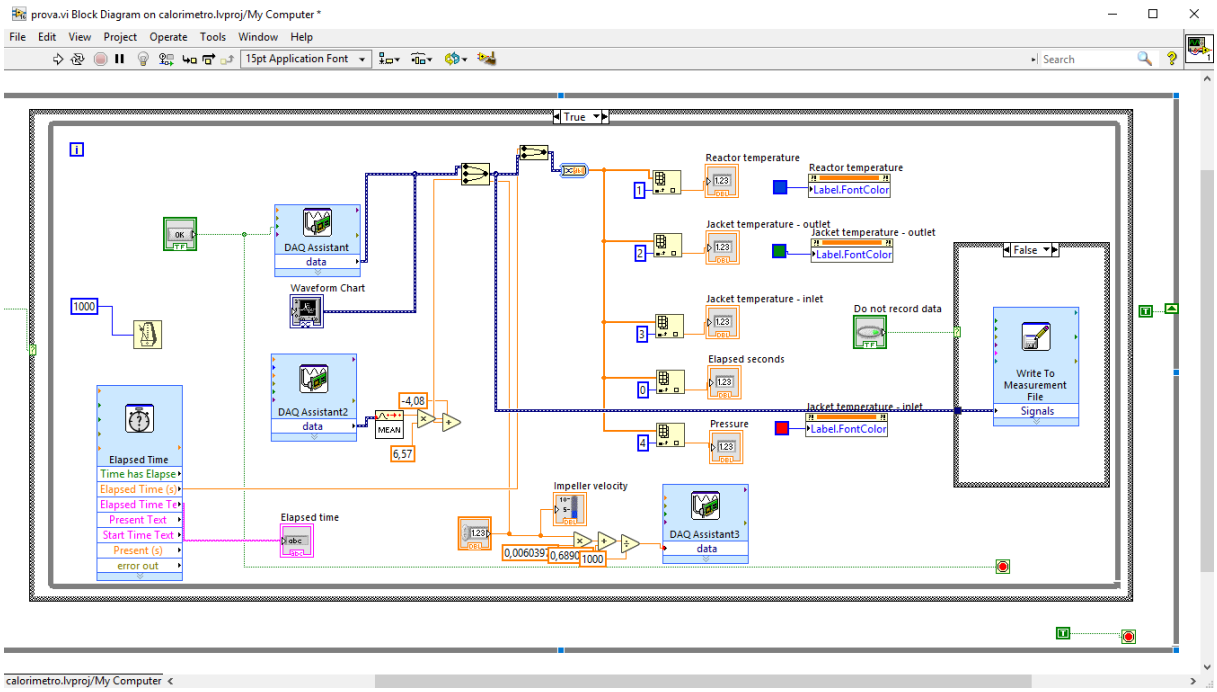

Figure 2.3. *Structure of the application made using Labview.*

The three temperatures are sampled by the DAQ modules that are compatible with the Labview interface. A single stream of data was created in order to obtain a vector with temperatures, pressure and elapsed time. The time was calculated using the “elapsed time” function and indicated in the interface. Data are displayed using both “numerical indicators” and “chart”.

Data are sampled each second thanks to an internal timer, displayed in the interface, and stored using a "Write to Measurement File" function. The impeller velocity was set using a numerical controller and displayed. The value of the impeller velocity was converted using a calibration curve previously determined and converted to a value of signal current. The software generates a digital signal to *NI* DAC that sends a 0-20 mA current signal to the impeller motor controller.

2.1.1.2 Instrumentation for the calibration of the impeller motor

The equation correlating the imposed current signal and the stirring velocity is fundamental for the correct operation of the reactor, and it must be set on the software controlling the impeller (and acquiring data). In order to carefully determine this equation, data were collected imposing a known current signal to the controller of the motor, and measuring the resulting stirring velocity. To measure the real stirring velocity, an optical system was designed and built *ad hoc* (Figure 2.4).

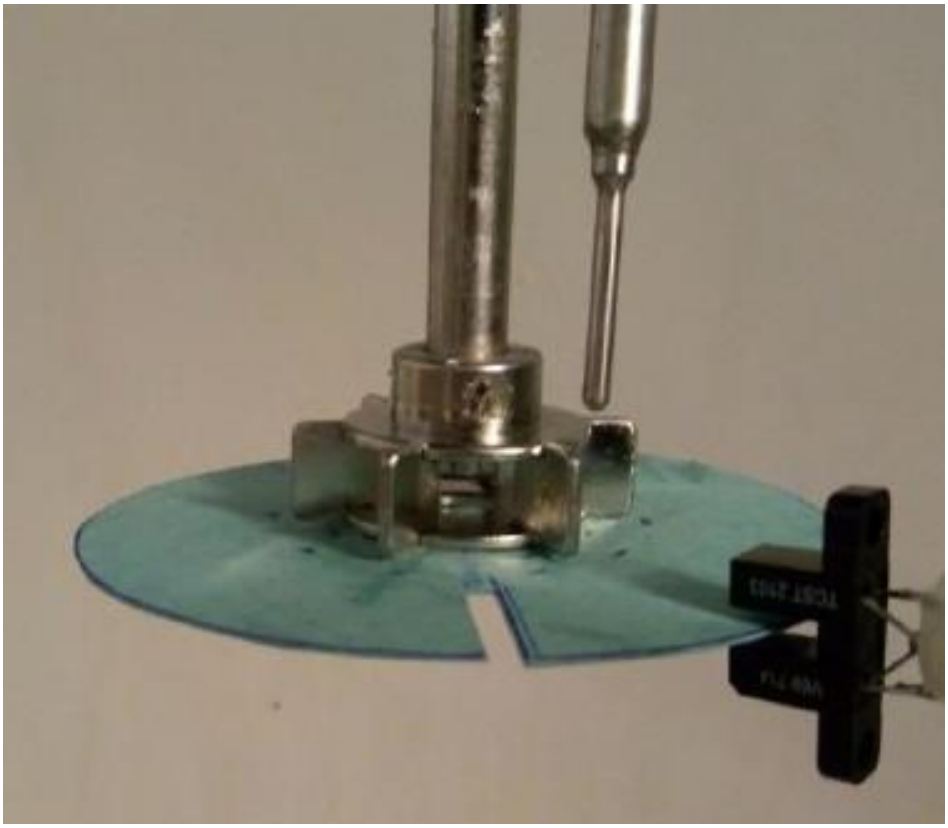

Figure 2.4. *Infrared fork and paper shutter used for the calibration of the mixing motor.*

The system was composed of an infrared optocoupler fork (TCST 2103) and a paper shutter with two holes located at 180°. The shutter was hold in place to the bottom of the impeller so that the infrared beam could pass the shutter twice at every turn of the impeller. In this way,

thanks to the detector of the fork (a phototransistor), it was possible to collect a signal composed of repetitive peaks which period was directly correlated to the rotating velocity of the mixer. The signal was sent to an oscilloscope *HAMEG*, model HM 205-3, for the visualization and the calculation of the period. The oscilloscope was analogic, and in order to achieve signal readings with maximum possible accuracy, particular attention had to be focused on carefully triggering it and on properly setting the time and voltage scales.

2.1.1.3 Instrumentation for the determination of the heat exchange coefficient

To determine the heat exchange coefficient, the characteristic time and the effective heat capacity, a stable and accurately controlled thermal power must be generated inside the reactor. The power was generated using a ceramic resistor, used as a heater for 3D plastics printers (Figure 2.5). This resistor was fed by a power-controlled power supply (Figure 2.6) guaranteeing that the generated power was accurately maintained near a setpoint, independently from the variation of resistivity due to variation of temperature or other disturbances. This device was designed, created and built *ad hoc*.

Figure 2.5. *Ceramic heater for 3D printers.*

Figure 2.6. *Power controlled power supply for the calibration of the calorimetric reactor.*

Once the user sets the desired temperature, the device properly manages the voltage in order to control power. This device was based on switching technology, and it was controlled by an Atmel SAM3X8E ARM Cortex M3 microcontroller (Arduino Due platform) in which a software was stored. The voltage was applied to the ceramic heater by means of a buck converter based on a p-channel Mosfet IRF9540 switch, ultrafast diode, and a LC filter that resonates at 25 Hz. The mosfet switch was controlled by a 1kHz PWM signal from the microcontroller which duty cycle regulates the output average voltage. In the circuit (Figure 2.7), a NPN BC547 transistor interfaces the microcontroller to the mosfet. The LC low pass filter smooths the output voltage and reduces the harmonic by about 3 orders of magnitude since it was tuned at a frequency noticeably lower (25 Hz) than the working frequency of the PWM.

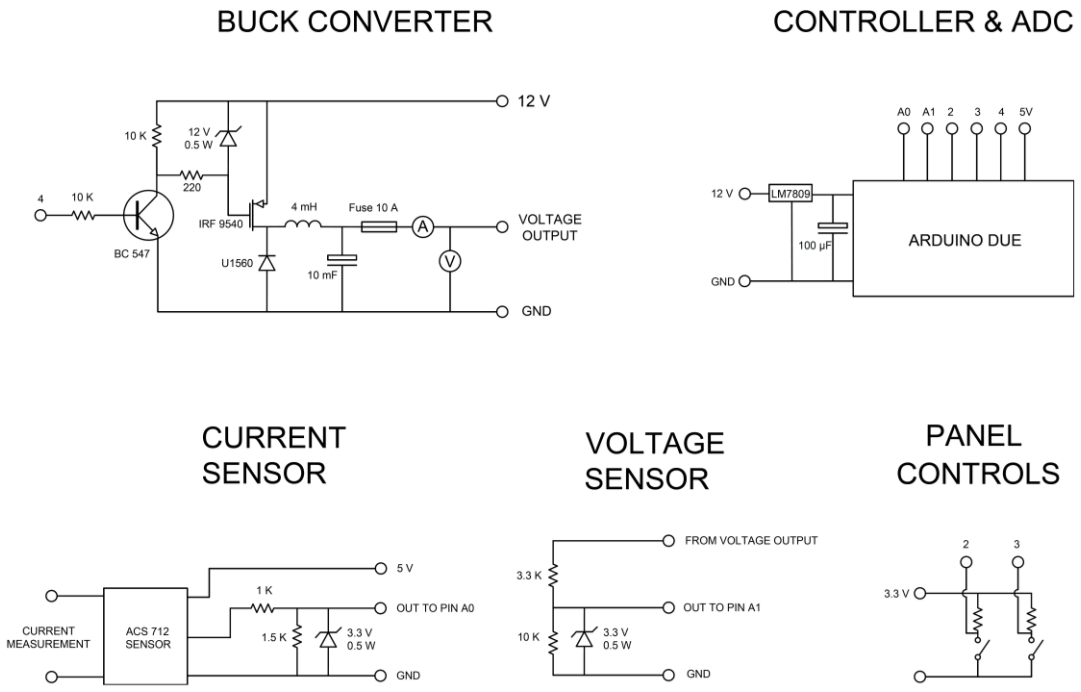

Figure 2.7. *Schematic of the power-controlled power supply.*

The microcontroller has an internal 12 bit analog to digital converter that converts the analog signal to a number from 0 to 4095, with a maximum input voltage of 3.3V (that is the internal reference of the ADC). In order to measure the dissipated power, the voltage applied to the ceramic heater was applied to a voltage divider to down scale the signal. The current was measured using a 0-5A sensor sending a voltage signal to a microcontroller that converts and collects it. The microcontroller software permits to collect the digital value of both signals and to calculate both current and voltage thanks to a calibration curve previously obtained from a fitting by means of a Matlab® code based on several data points (50 each). Once the microcontroller calculates the real voltage, current and power, the algorithm reads the setpoint

value set by the user. If the real power was lower than the setpoint, the controller increases the PWM duty cycle to increase the voltage output and *vice versa* if the real power was higher. The controller does not act if the error is lower than 0.3% to avoid instability.

2.1.2 Microwave reactor

The microwave reactor (Mileston, mod. Mycrosynth, Figure 2.8) is a microwave multimodal oven with a rotating plate that can accommodate up to 12 beakers. The beakers are made of teflon because it is chemically stable, and does not absorb radiation. The beakers have 36mm internal diameter, are equipped with a 20 mm magnetic stirrer and a lid that can be screwed so that sealing is ensured. One beaker was equipped with a IR optic fiber temperature sensor and a pressure transducer. The internal controller can maintain the setpoint conditions only in the monitored beaker. Consequently, since the MW field is strongly non-homogeneous, the temperature in the other beakers can vary sensibly so all the tests are performed in the sensed beaker. The plate was normally load with three beakers, the sensed one and 2 more that are used as controls and as counterweight to balance the rotating plate.

Figure 2.8. *Microsynth microwave reactor*[1].

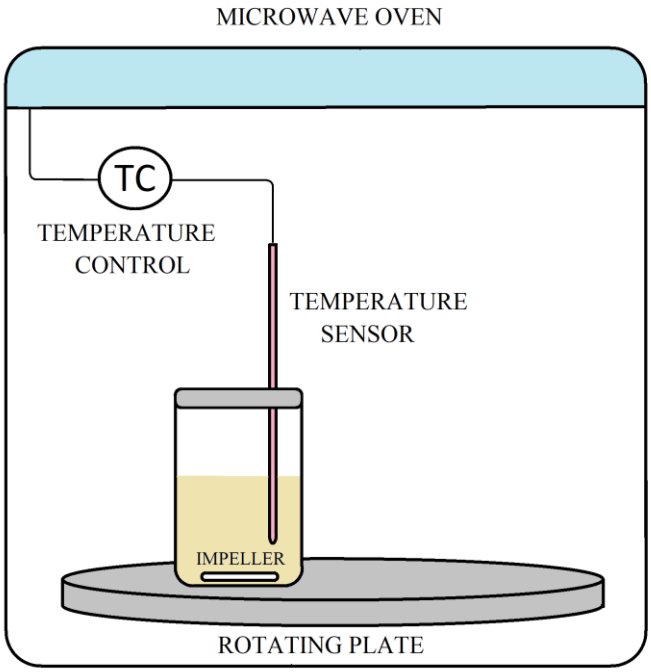

Figure 2.9. *Schematic representation of the MW reactor by Mileston*

2.1.3 Conventional glass reactor

In order to perform a rigorous comparison between the epoxidation process under microwave and conventional heating, another reactor was set up with the same geometric characteristics and impeller to have the same fluid dynamics conditions. This apparatus was simply made by a glass beaker (internal diameter 36 mm) with a 20 mm magnetic stirrer placed in a thermostatic bath heated by a magnetic mixer heater (Figure 2.10). The temperature of the bath was monitored using a thermocouple and the internal controller of the heater. The liquid used for the bath was diethylene glycol.

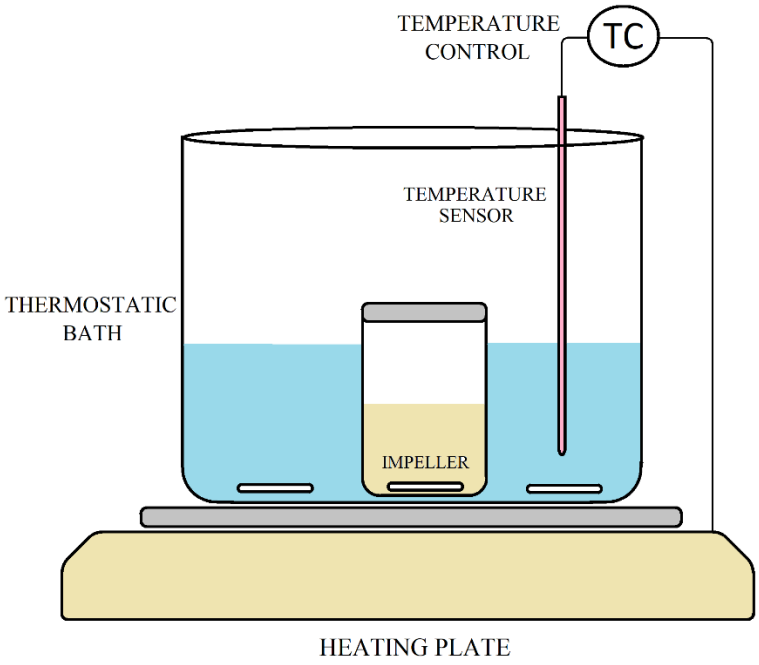

Figure 2.10. *Schematic representation of the conventional heating glass reactor.*

2.1.4 Mesofluidic reactor – conventional heating

This reactor was made of mesofluidic platforms connected in series to obtain a tubular reactor. These units were designed based on microfluidc chips for biological applications but in a larger scale (1-2 millimeters). Each unit is equipped with a thin thermocouple (0.5 mm diameter) and a thermoregulator that displays the monitored temperature and the setpoint value. Each unit was heated thanks to a 12V electric heater activated by the thermoregulator.

The reactor was designed with a modular configuration with one mixer and a number of tubular reactors in which the residence time can be 10-30 minutes, depending on the flow rate. This modularity enables an accurate control of the residence time and extends the range of operative conditions. These units are produced by means of two aluminum molds, one for the mixer, the other one for the tubular reactor. The two molds were obtaining by CNC milling from aluminum blocks (Figure 2.11-2.13).

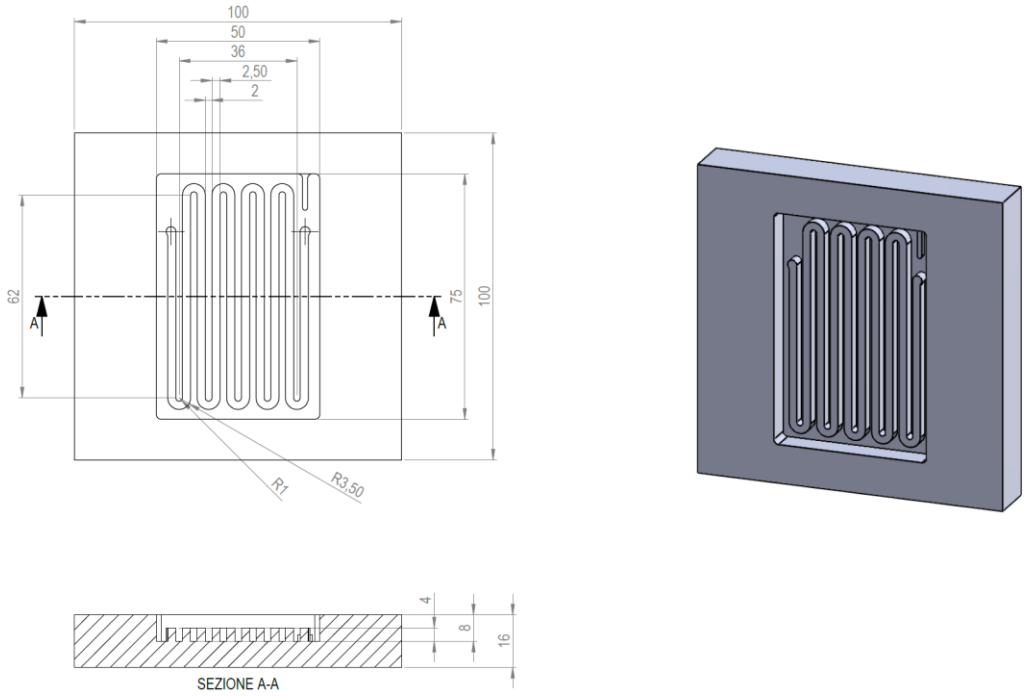

Figure 2.11. *Technical drawing of the reactor.*

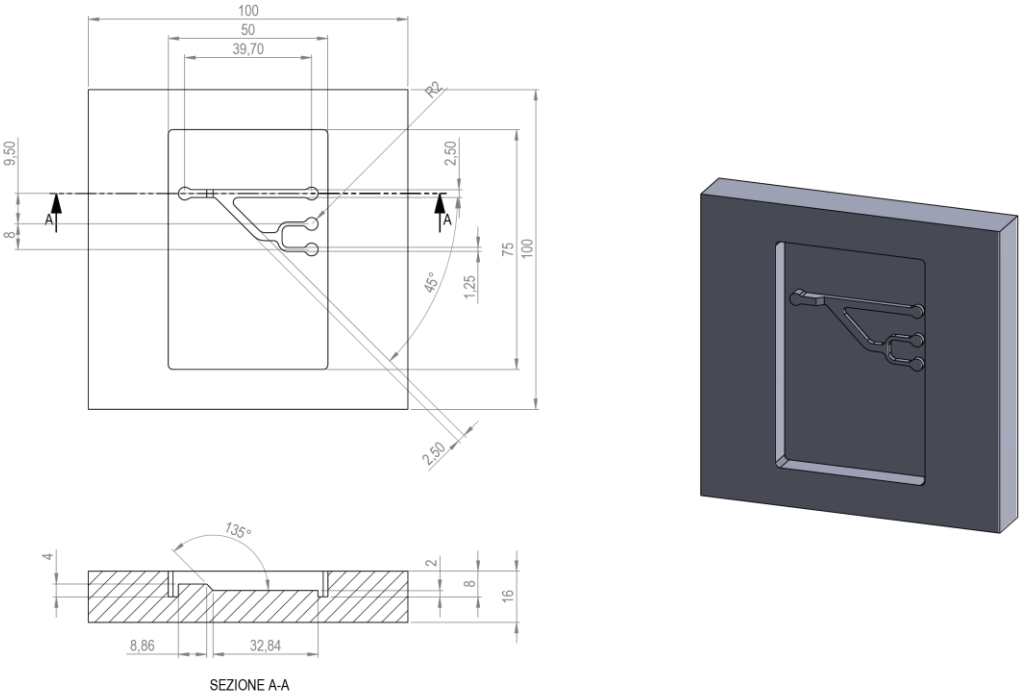

Figure 2.12. *Technical drawing of the mixer.*

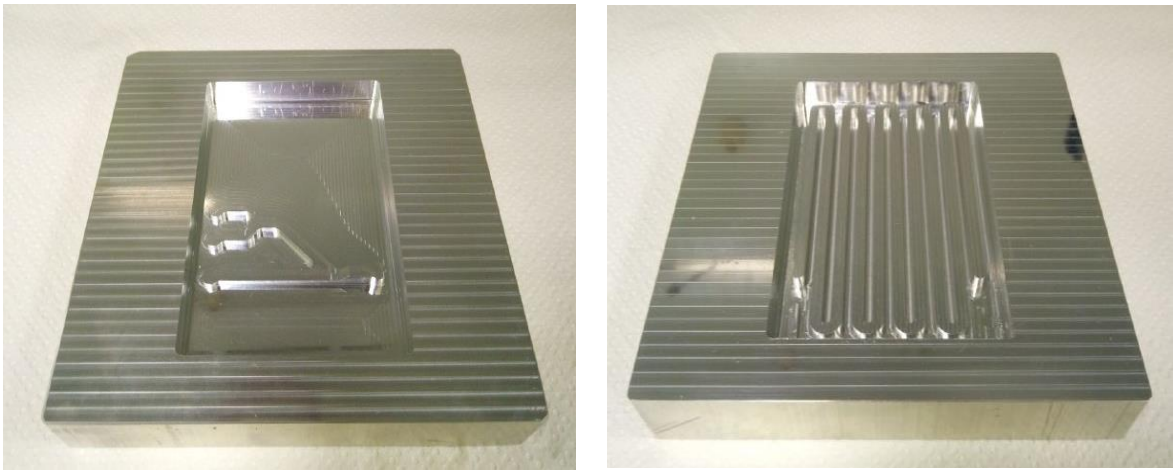

Figure 2.13. *Aluminum molds for the mixer (left) and the reactor (right).*

The units were obtained by polimerisation of Crystal 15 silicon resin in the molds. The chips must be closed by a lid, made of a silicon sheet of 1.5-2 mm thickness. After 12-18 hours the resin was peeled from the mold, and the silicon sheet accurately cut. The chips were irreversibly bound using a special glue. After several tests, it was found that the best binding method was using the same silicon resin as a glue. The resin was accurately spread using a brush on both sides, the pieces placed in contact and binding was complete after 18-24 hours. Crystal 15 resin is a resin used for artistic purposes for the production of molds, it costs 5 times less than PDMS, is strongly more resistant to cracks and elongation, and more anti-adherent. Although not as optically transparent as PDMS, its optical properties are sufficient for our purpose (Figure 2.14).

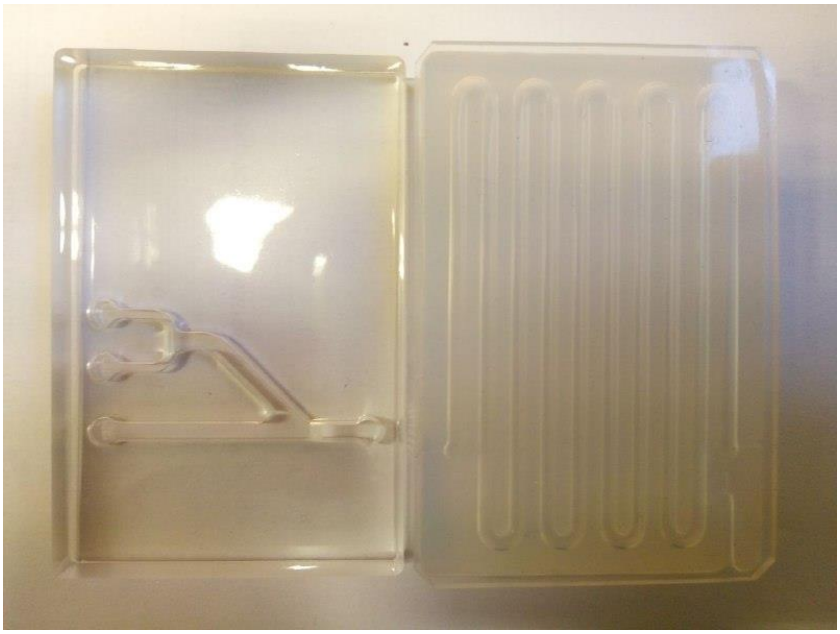

Figure 2.14. Mixer and reactor units made by Crystal 15 silicon resin.

The reactor section was made by adding or removing multiple tubular units in series. This approach strongly simply the production of the modules. This feature, and a three-way mixer permits to operate with great flexibility.

The optimized configuration was composed of (Figure 2.15):

- high shear mixer. These piece of equipment permits to create a stable emulsion made of oil, surfactant, acetic acid and hydrogen peroxide at very high velocity (25.000-30.000 rpm).
- two syringe pumps. These pumps send two streams to the mixer. One for the emulsion, and the other for the catalyst solution, i.e. sulfuric acid in hydrogen peroxide.
- heated mixer unit. The three-way mixer unit was used only with two inlets (one was unused). In this module, the two streams from the pumps were preheated and mixed. Temperature is controlled by means of a thermocouple, a resistive heater and a thermoregulator.
- heated reactor unit. This unit is the reactor in which the process is carried out. Temperature is controlled by means of a thermocouple, a resistive heater and thermoregulator.
- emulsion breakage unit. The product is collected in an agitated beaker, with hexane to break the emulsion. The pH is manually maintained around 7 injecting NaOH solution to stop the reactions.
- Separation unit. The organic phase is washed, neutralised and separated using a centrifuge and a separation funnel; hexane is removed by evaporation.

In our studies, one reactor unit was used, and variations of the residence time were set only changing the flow rate, without affecting the size of the micelles since the emulsion was obtained using a surfactant before entering the mixer-reactor modules.

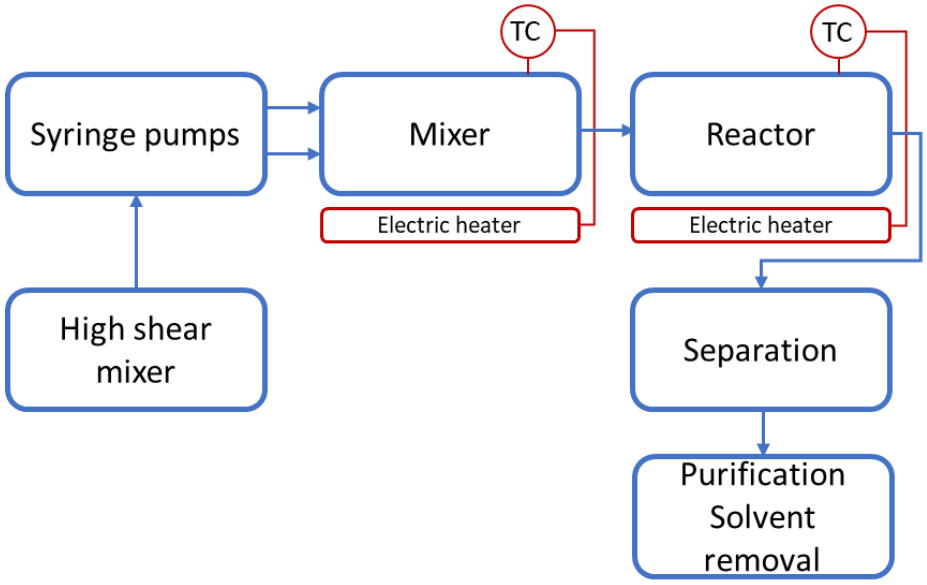

Figure 2.15. *Block diagram of the mesofluidic experimental setup*

2.1.4 Mesofluidic reactor – radiofrequency heating

The experimental setup for the mesofluidic reactor (§ 2.1.3) was also adapted for R.F. heating. The system was almost identical to the previous case except for the reactor, that was modified to apply the R.F. field. The reactor unit was employed as a dielectric between two copper sheets, to make a condenser. This condenser was the applicator of the R.F. field, and it was placed in an aluminum shielded box, to avoid dispersion of the field (Figure 2.17). The shielded applicator was linked to the R.F. power generator through a pi-match impedance adapter, to adapt the impedance of the load to the one of the generators (Figure 2.16). The impedance adapter is needed to reduce as much as possible the reflected power that could damage the generator. A Vector Network Analyzer (VNA) was used to characterize the quality of the load, studying its real and imaginary parts. This apparatus is fundamental to calculate the right value of the inductor of the impedance adapter, that was built ad-hoc using 5mm copper rod (9 turns equally spaced on 15 cm, 5 cm i.d.) (Figure 2.18).

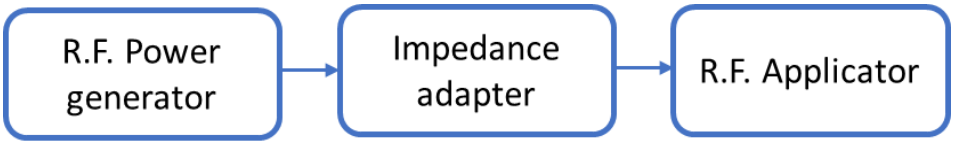

Figure 2.16. *Block diagram of the circuit for the application of the R.F. power*

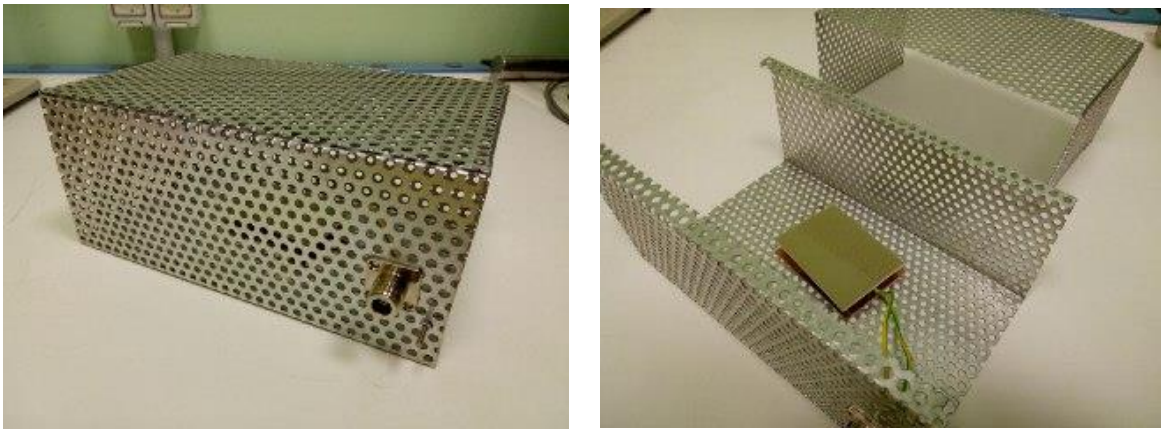

Figure 2.17. *Shielded R.F. applicator. The box is completely closed and R.F. power can be applied through a N-connector.*

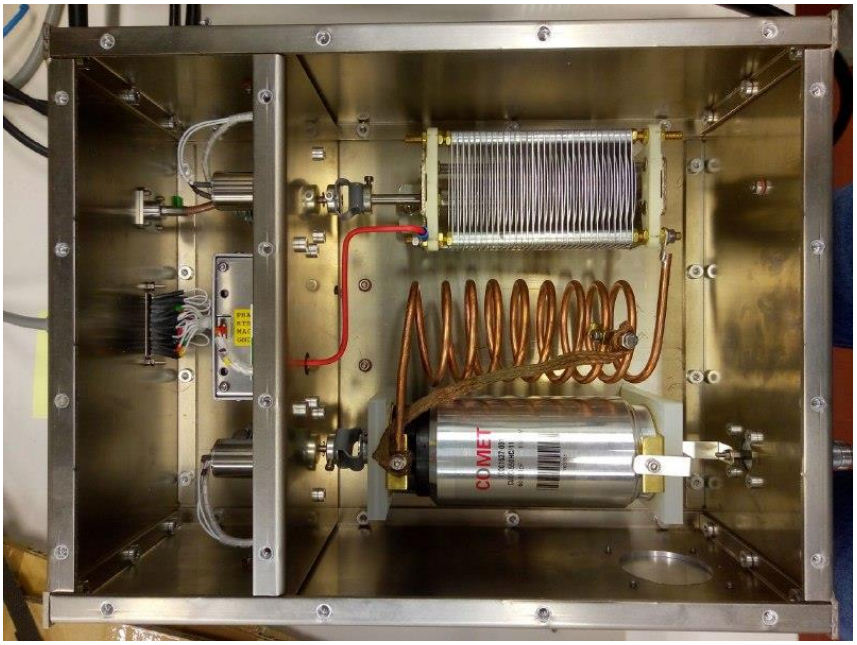

Figure 2.18. *Pi-match impedance adapter, with the two variable capacitor and the copper coil.*

The temperature was measured with an optical fiber and a portable infrared measurement equipment. In presence of R.F: electric field, it is not possible to use thermocouples.

2.1.6 Auxiliary instrumentation

- Syringe pumps: two syringe pumps PHD ULTRA by Harvard apparatus were used. They allow mounting several models of syringes with a large span of flow rate available with high accuracy;
- vacuum pump by KNF, model N86: it is a small vacuum pump for the removal of the solvent from the oil;
- Julabo thermostatic bath, it was used for the heating of the solvent-oil mixture for rapid solvent removal;
- Thermo-Fisher centrifuge, it was used for rapid separation of water-oil supspension/emulsion.
- Ika magnetic stirrer, it was used during titrations, collecting of the product of the mesofluidic process and other operations.

2.2 Materials

Acetic acid >99%, hydrogen peroxide 35wt.%, hydrogen sodium carbonate 99%, diethyl ether 98%, hydrobromic acid in acetic acid 45wt.%/wt., potassium hydrogen phthalate and crystal violet were purchased from Alfa Aesar (Thermo Fischer GmbH). Sulfuric acid was purchased from Carlo Erba Reagents srl. Soybean oil is food grade and it wa purchased from a supermarket.

2.3 Methods

For all the tests, oil and aqueous solution were used at 1:1 weight ratio. The aqueous solution was made of 16.6wt.% acetic acid, 80.4wt.% hydrogen peroxide 35wt.%, 3wt.% sulfuric acid. The total amount was equal to 20 grams for MW and glass conventional reactor and 90 grams for the conventional reactor.

2.3.1 Use of the calorimetric reactor

The mixture was made of 45 g of soybean oil, 7.70 g of glacial acetic acid, 37.30 g of hydrogen peroxide aqueous solution 35wt.% and 1.35 grams of sulfuric acid. First, the oil, the acetic acid and 27.30 g of hydrogen peroxide solution were charged inside the reactor and the application

for the data acquisition and the impeller control was executed. Then, the thermocryostat was switched on and the desired temperature was set. Once the thermal steady state was reached, a solution made of 10 g of hydrogen peroxide and 1.35 g of sulfuric acid was poured inside the reactor. This moment was considered as the “time zero” instant.
To shut down the process, the thermocryostat was set at 40°C to reduce the temperature. Once the temperature was reached, the impeller was switched off and the valve at the bottom of the of the reactor was opened to allow the reactor to empty.

2.3.2 Use of the microwave reactor

Three beakers were used, to keep the rotating plate well balanced. The reactor beaker was loaded with 10 g of soybean oil and 10 g of aqueous solution (16.6wt.% acetic acid, 80.5wt.% hydrogen peroxide 34wt.%, 2.9wt.% sulfuric acid). Once the temperature and pressure sensors were installed, the temperature program was set to perform a preliminary temperature ramp (10 minutes) up to the setpoint value, and then the temperature was maintained for the desired time.

2.3.3 Use of the glass conventional reactor

First, the thermostatic bath was set to desired temperature. The reactor beaker was loaded with 10 g of oil and 10 g of aqueous mixture (total 20 g) and placed in the thermostatic bath (16.6wt.% acetic acid, 80.5wt.% hydrogen peroxide 34wt.%, 2.9wt.% sulfuric acid). The beaker was sealed with a rubber plug covered with a teflon film. The amount and the composition of the reactant was identical to the previous case.

2.3.4 Use of the mesofluidic reactor with conventional heating

In a first step, an emulsion of soybean oil, acetic acid and hydrogen peroxide was prepared. A mixture of surfactants Span 80 (75wt.%) and Tween80 (25wt.%) was prepared. The surfactant (0.25wt.%) was dispersed in an acetic acid (17.1wt.%) hydrogen peroxide solution (84.9wt.%). The surfactant was dispersed using a high shear mixer at 25.000-30.000 rpm for 120 seconds. The soybean oil was added (5wt.%) and dispersed using the mixer at the same velocity for 150 seconds. This procedure resulted in a uniform and stable emulsion . The emulsion was loaded in a 50 mL plastic syringe, that was mounted on the pump.

The catalyst solution was made of sulfuric acid 16.7wt.% and 83.3wt.% hydrogen peroxide. This solution was loaded in a 20 mL syringe and mounted on another pump. The reactor, the mixer and the connecting pipes were filled with water, to avoid that some air was trapped in the circuit, and heating was switched on. Once the thermal steady state was reached, the syringe pumps were connected and switched on. The first part of the product (few milliliters) was discharged.

2.3.5 Use of the mesofluidic reactor with RF heating

The operation was identical to the previous case except for the operation of the R.F. heating system. In a first step, the impedance of the reactor (loaded with the reaction mixture) was analysed by means of the VNA to guarantee that the real part is at least 2 ohms (minimum value for the system to operate correctly). After this check, the generator and the impedance match adapter were connected and switched on. The adapter was adjusted to achieve the best coupling (minimum reflected power).

2.3.6 Post process treatment

The biphasic mixture was separated and washed in a separating funnel using diethyl ether to improve separation, and 0.02M sodium hydroxide solution to neutralize acids and discarding the aqueous phase. Normally three washings are sufficient, and the pH is checked at the end of the treatment to verify that the value is around 7. The oil-ether solution was heated in a thermostatic bath (by Julabo) under vacuum conditions and strong mixing to promote nucleation. In such a way, ether can be removed and only oil can be obtained. The epoxidised oil was stored at 4°C and it was analysed as soon as possible (max 24 hours).

2.3.7 Post process treatment for mesofluidic process

In the case of the mesofluidic process, post-process treatment was a little different, because of the use of a surfactant and the continuous process. In fact, the product obtained by the reactor was collected in a beaker strongly agitated by a magnetic stirrer. The product was dissolved in n-hexane to break the emulsion. The pH was continuously checked by litmus paper tests and maintained around 7 injecting 1M NaOH aqueous solution and the solvent was added to compensate the evaporation. At the end of the process, the biphasic mixture was strongly mixed

for 90 seconds using the high shear mixer to ensure the optimal contact between solvent and the emulsion. The mixture was placed in the centrifuge at 3000 rpm for 3 minutes, then the oil phase was collected and washed in a separation funnel with 0.02 M $NaHCO_3$ water solution for two times. After discarding the aqueous phase, the oil phase was centrifuged at 3000 rpm for 2 minutes. The organic phase was collected, and the solvent was removed. Solvent removal was carried out in a 50 mL falcon tube, connected to a vacuum pump and heated in the thermostatic bath (65-70°C) under vigorous stirring to promote the nucleation of the bubble. Complete removal of the hexane was achieved in 10-15 minutes. Because of the presence of a surfactant, diethyl ether was not a good choice as a solvent for separation, since it is not completely non-polar and a lot of residual water can be solubilized in the oil. Consequently, hexane was used because it is a completely non-polar solvent, and allows a much easier phase separation. The final product was completely anhydrous. However, even though density is a little lower in the case of the hexane (655 vs 713 kg/m^3), the boiling point is considerably higher (68 vs 34.6°C), so solvent removal is a bit more difficult.

2.3.8 FTIR analysis

Infrared technique was used for preliminary analysis of the product. FTIR spectrum permits to evaluate the presence of double bonds (3010 cm^{-1}), epoxides (825 cm^{-1}) or glycols (3500 cm^{-1}) [2]. This is a user friendly, very fast qualitative and semi-quantitative technique that permits to rapidly check a sample of the process. For accurate measurements, titrations were used. The spectrometer is from Thermo-Fischer (model Nicolet, figure 2.19), and samples were analysed using NaCl disks washed with chloroform.

Figure 2.19. *FTIR Nicolet by Thermo-Fisher IS50* [3].

The scanned wavenumber window is 4000-550 cm^{-1} whereas lower values are not feasible because of sodium chloride absorption. Atmospheric water and carbon dioxide correction was enabled to reduce interference errors. Typical spectra of virgin and epoxidised soybean oil are reported in Figure 2.20.

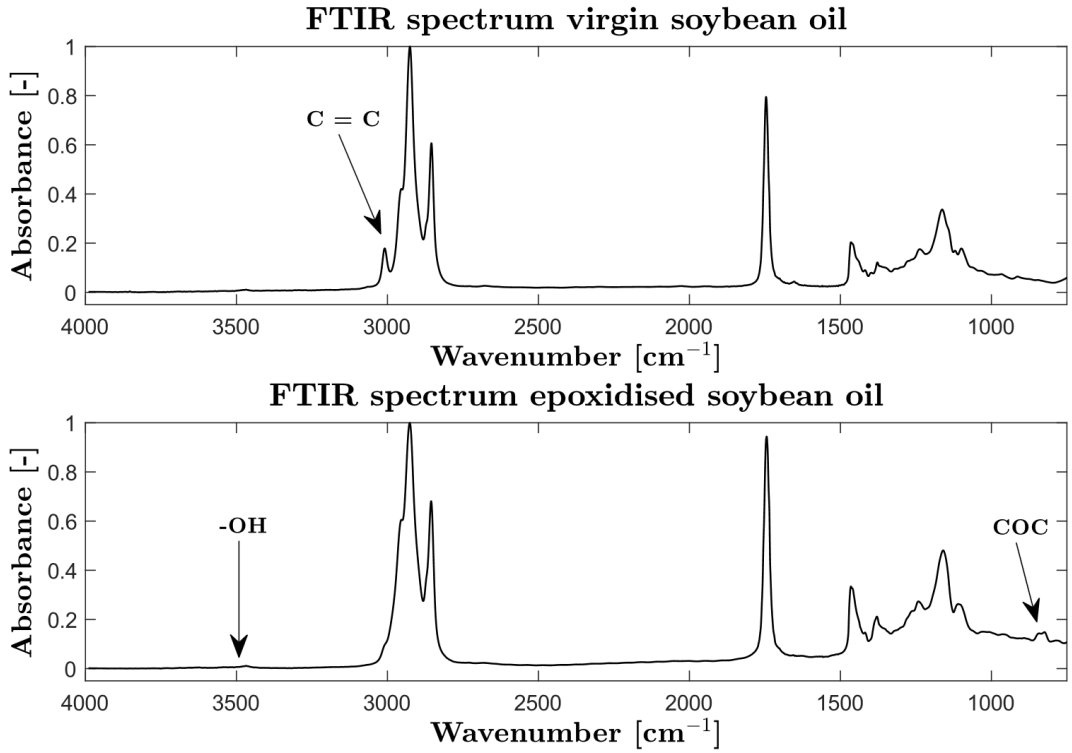

Figure 2.20. *FTIR spectra of virgin soybean oil and epoxidized soybean oil*

Figure 2.20 shows the peak of the unreacted double bonds in the virgin soybean oil (3010 cm^{-1}). In the case of the ESBO, the spectrum shows that almost all the double bonds are converted and that epoxides are present (825 cm^{-1}). Moreover, a minimal quantity of glycols is detected since the peak of the -OH group is fairly low (3450 cm^{-1}). In the case of the epoxy groups and double bonds, the sensibility of this IR technique is not very high, whereas the sensibility on the -OH group is noticeable. For these reasons, the analytical method via titrations was preferred for a more accurate analysis. However, FTIR technique is exploited in several papers also for quantitative analysis, as the case of Leveneur [4].

2.3.8 Epoxides titrations AOCS 9-57 method

AOCS 9-57 method was used to obtain the percentage of oxirane oxygen, i.e. the percentage of the weight of the epoxy oxygen on the total weight of the molecule. Other methods are available as for example hydrochloric acid or other standards with hydrobromic acid [5]. The most recent and commonly used protocol is the AOCS 9-57 method, according to which the titration is carried out using hydrobromic acid in glacial acetic acid 0.1N. The titrant is normalized using potassium hydrogen phthalate to determine the exact concentration of the titrant. Once the oxirane oxygen percentage is known, the yield of epoxides can be calculated as follows:

$$Yield\ [\%] = \frac{OO_{exp}[\%]}{OO_{th}[\%]} \cdot 100\% \tag{2.1}$$

where OO_{exp} is the experimental oxirane oxygen and OO_{th} is the maximum oxirane oxygen theoretically achievable. This can be calculated knowing the iodine number as follows:

$$OO_{th} = \left[\frac{IN/MW_{I_2}}{100+\left(\frac{IN}{MW_{I_2}}\right)\cdot MW_O}\right] MW_O \cdot 100\% \tag{2.2}$$

whereas IN is the iodine number of the virgin soybean oil, MW_{I_2} is the weight of the molecular iodine, and MW_O is the molecular weight of the atomic oxygen. This equations are in line with the literature, and they are considered a standard for this process [6]. For a typical soybean oil, the iodine number is around 125-127 and consequently the OO_{th} is around 7.3-7.4%.

2.3.9 Acetic and peracetic acid titrations

To determine the acetic and peracetic acid concentrations in the aqueous phase, several methods are available in the literature [7], [8], [9]. These methods are intended to be used for acetic, peracetic, hydrogen peroxide and water solutions using a standardized sodium hydroxide aqueous solution. The analysis can be performed using an automatic titrator and the pH curve can be obtained. The two inflection points are at about at pH 7 (acetic acid) and 9.5 (peracetic acid). To better highlight these points, the derivative of the curve can be obtained, obtaining two peaks at which the volume of titrant can be calculated. Since an automatic titrator was not available, a two pH indicators titration was used. Red phenol and phenolphthalein are respectively used for the two turning points of acetic and peracetic acid. Phenol red was available in powder and it should be prepared dissolving 0.1g of indicator in 14.20 ml of 0.02N NaOH and diluted to 250 ml with deionized water, as suggested by Sigma-Aldrich [10].
The protocol that was followed used 2 g of sample diluted to 40 g with deionized water. Two diluted solutions were prepared, and pH indicator was added, phenol red in a case, phenolphthalein in the other one. Titration were performed in both cases using standardized 0.5M NaOH solution. The titration performed with phenol red determines the volume of titrant to neutralize the acetic acid. The other titration, gives the volume of titrant to neutralize both the acetic acid and peracetic acid. To calculate the concentrations of both acids, the peracetic acid must be obtained by difference. The calculations must consider the fact that sulfuric acid is present in the reacting system and it is the first acid to be neutralized during the titration.

Bibliographic references

[1] Milestone website, https://www.milestonesrl.com/, accessed 10/6/2019.

[2] K. Saremi, T. Tabarsa, A. Shakeri, and A. Babanalbandi, "Epoxidation of Soybean Oil," *Sch. Res. Libr. Ann. Biol. Res.*, vol. 3, no. 9, pp. 4254–4258, 2012.

[3] Thermo Fisher website, https://www.thermofisher.com/it/en/home.html, accessed 10/6/2019.

[4] S. Leveneur, A. Ledoux, L. Estel, B. Taouk, and T. Salmi, "Epoxidation of vegetable oils under microwave irradiation," *Chem. Eng. Res. Des.*, vol. 92, no. 8, pp. 1495–1502, 2014.

[5] A. J. Durbetaki, "Direct Titration of Oxirane Oxygen with Hydrogen Bromide in Acetic Acid," *Anal. Chem.*, vol. 28, no. 12, pp. 2000–2001, 1956.

[6] V. V. Goud, A. V. Patwardhan, and N. C. Pradhan, "Studies on the epoxidation of mahua oil (Madhumica indica) by hydrogen peroxide," *Bioresour. Technol.*, vol. 97, no. 12, pp. 1365–1371, 2006.

[7] Hach, "Application Note Determination of Peracetic Acid (Paa) and Hydrogen Peroxide (H 2 O 2) in Water," no. 1, pp. 2–4.

[8] F. Sode, "Simultaneous determination of peracetic acid and acetic acid by titration with NaOH," *Anal. Methods*, vol. 6, no. 7, pp. 2406–2409, 2014.

[9] L. Domínguez-Henao, A. Turolla, D. Monticelli, and M. Antonelli, "Assessment of a colorimetric method for the measurement of low concentrations of peracetic acid and hydrogen peroxide in water," *Talanta*, vol. 183, no. December 2017, pp. 209–215, 2018.

[10] Sigma Aldrich website, *Preparation red phenol solution*. https://www.sigmaaldrich.com/content/dam/sigma-aldrich/docs/.../p0290pis.pdf accessed 10/6/2019

Chapter 3

Calibration of the calorimetric reactor

This chapter details the calibration of the calorimetric reactor. In particular, the calibration of the stirring system was achieved by means of an infrared optocoupler. Furthermore, a comprehensive approach was implemented *ad hoc* for the experimental determination of the heat exchange coefficient. This method that enables a complete study of the thermal parameters, including effective heat capacity and thermal losses.

3.1 Calibration of the stirring system

For the correct operation of the calorimetric reactor, the software for data acquisition and the control of the impeller must work with the equation correlating the imposed current signal control and the stirring velocity. For this purpose, the experimental set up shown at §2.1.1.2 was implemented, based on a TCST2103 optocoupler [1] and a paper shutter. A representative resulting signal is shown in Figure 3.1.

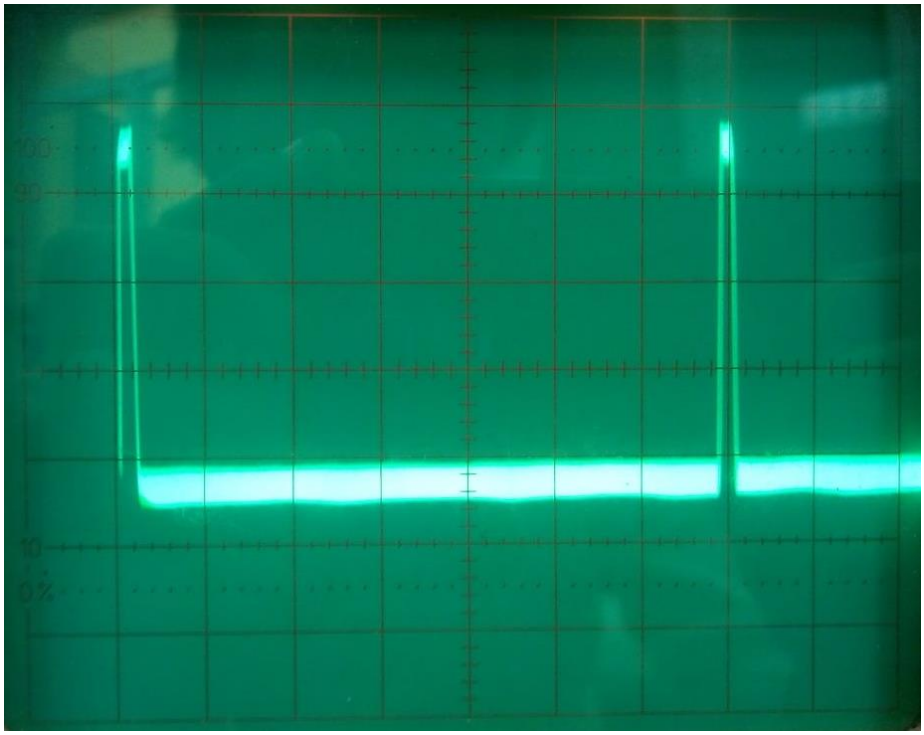

Figure 3.1. *Visualization of the signal generated by the system for the measurement of the impeller velocity.*

The time between two peaks is the semi-period of rotation of the impeller, since the shutter has two holes placed at 180°. The time of the semi-period can be read by counting the divisions on the x-axis and multiplying the number by the time per division ratio of the internal clock of the oscilloscope. The velocity of the impeller, expressed as revolutions per minute, can be calculated as follows:

$$\omega\ [rev/min] = \frac{1}{2 \cdot T[sec] \cdot 60}. \qquad 3.1$$

Once the acquisition of the data was completed, a linear fitting was performed, and the calibration curve was determined (Figure 3.2). Data were collected and elaborated performing a linear fitting using a Matlab® code.

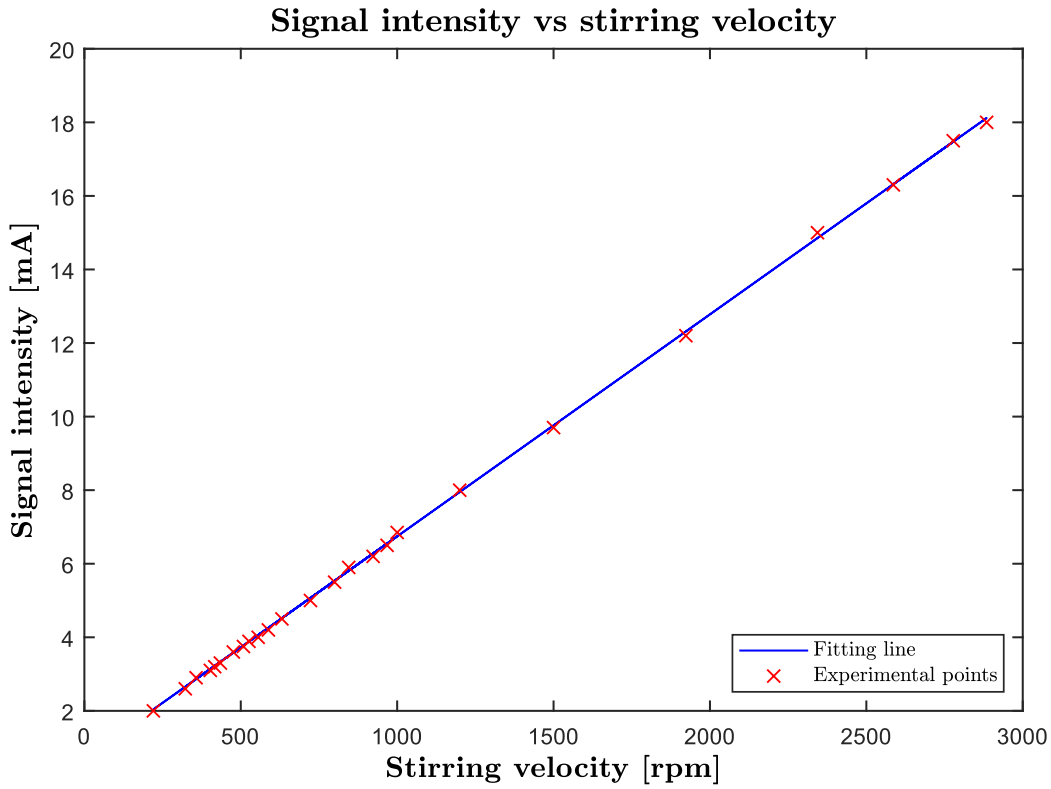

Figure 3.2. *Linear fitting of the experimental data signal intensity – stirring velocity.*

The result of the fitting has good accuracy, and represents a linear calibration line (3.2)

$$Signal\ \ output\ [mA] = 0.00604\ \cdot Stirring\ velocity\ [rpm] + 0.708\ . \qquad 3.2$$

Knowing this, once the desired impeller velocity is set, the software calculates the intensity of signal output to be sent to the motor interface.

3.2 Determination of the heat exchange coefficient

In this paragraph, the approach the determination of the heat exchange coefficient of the calorimetric reactor is described. In the literature there are different approaches for this purpose, as reported by Debab *et al.* [2], Nassar *et al.* [3] and De Quadros *et al.* [4].
The approach proposed by Debab *et al.* deals with a batch jacketed reactor agitated by a turbine and thermo-regulated by a liquid-flow in a closed loop. The general balance is:

$$m \cdot cp \cdot \frac{dT}{dt} = -U \cdot A \cdot \left(T - T_J\right) + \dot{Q}_s + \dot{Q}_r \qquad 3.3$$

where $m \cdot cp$ is the heat capacity of the loaded mixture, U is the heat exchange coefficient, A is the exchange area, $T - T_J$ is the temperature difference between the reactor and the jacket, $\dot{Q}_s$ and $\dot{Q}_r$ are the power dissipated by the stirrer, and the heat power generated by the reaction, respectively. For the determination of the heat exchange coefficient, the heat power generated by the reaction is zero (reaction stopped) and $\dot{Q}_s$ is assumed to be zero.
According Debab, the differential term is discretized:

$$m \cdot cp \cdot \frac{dT}{dt} \sim m \cdot cp \cdot \frac{(T_r^{end} - T_r^{initial})}{\Delta t}. \qquad 3.4$$

The heat exchange coefficient can thus be written as follows:

$$U \sim \frac{(T_r^{end} - T_r^{initial})}{\Delta t \cdot (T_r - T_J) \cdot A} \cdot m \cdot cp. \qquad 3.5$$

In this way, once the reactor is heated by the jacket, the heating transient is linearized as in Figure 3.3.
However, the linearization of the transient is a rough simplification, that can lead to significant errors. This approach was considered over-simplified for the aim of this work, even if the idea is valid.

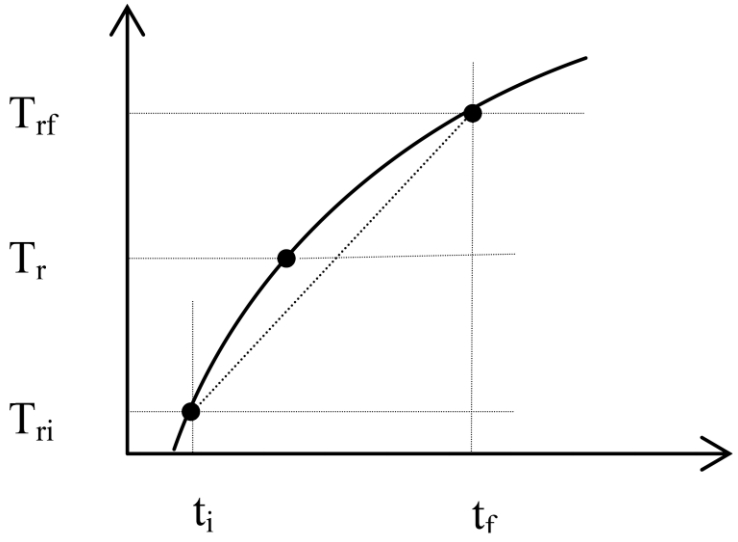

Figure 3.3. *Thermal transient of the reactor linearized profile* [4].

In the case of De Quadros et al. [4], the reactor is loaded and heated by means of an electric heater. Heating and cooling transients profiles were obtained and fitted using the integrated differential balance:

$$\ln\big(T(t) - T_J\big) = -\frac{U \cdot A}{m \cdot cp}(t - t_0) + \ln\big(T(t_0) - T_J\big). \qquad 3.6$$

The transient is thus transformed in logarithmic scale and the slope of the fitted straight line is $-\frac{U \cdot A}{m \cdot cp}$ (Figure 3.4).

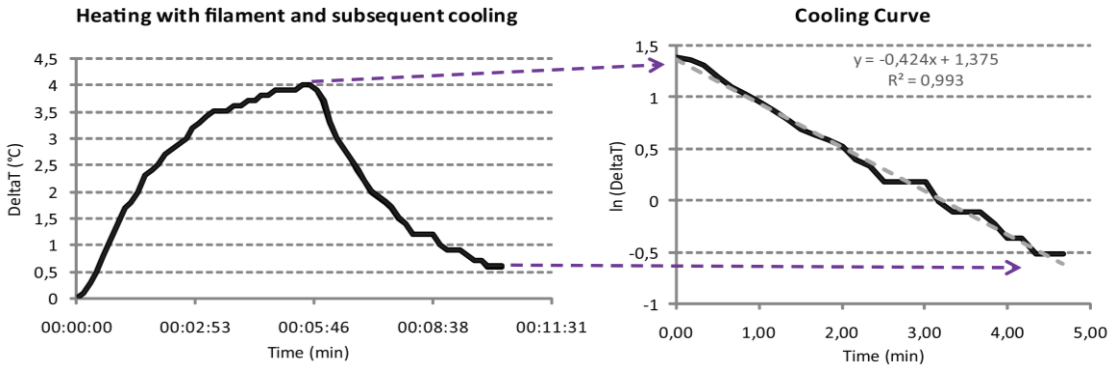

Figure 3.4. *Heating and cooling transients and logarithmic fitting* [4].

Once the slope of the of the line is determined, and the heat capacity $m \cdot cp$ is calculated, the product $U \cdot A$ can be determined. The heat capacity is determined considering the $m \cdot cp$ of the

sole reaction mixture, neglecting the capacity of the instrumentation of the reactor, i.e. thermocouples and metallic impeller. It should however be noted that the metallic instrumentation has a noticeable heat capacity that cannot be neglected without committing a large mistake.

In this work, the determination of the heat exchange coefficient was carried out in more complex and accurate manner.

Well determined thermal power is generated in the reactor using an electrical heater, and the resulting thermal profile is elaborated. The reactor is loaded with the same reaction mixture to achieve the same conditions, but the acid catalyst is not added so the reaction does not take place. This means that no thermal power is provided by the process, and variations of temperature are only due to the generation of power by the heater. Moreover, the impeller velocity is 500 rpm, the same set in the process. The electrical power is generated for 17 minutes and then the heater is switched off for another 17 minutes. The test is repeated different times applying 5, 10, 15, 20 and 25 watts. This test is further repeated for all the three temperatures set for the epoxidation runs, i.e. 40, 55 and 70°C. The typical plot of generated power vs time and the resulting thermal profile are shown in Figure 3.5.

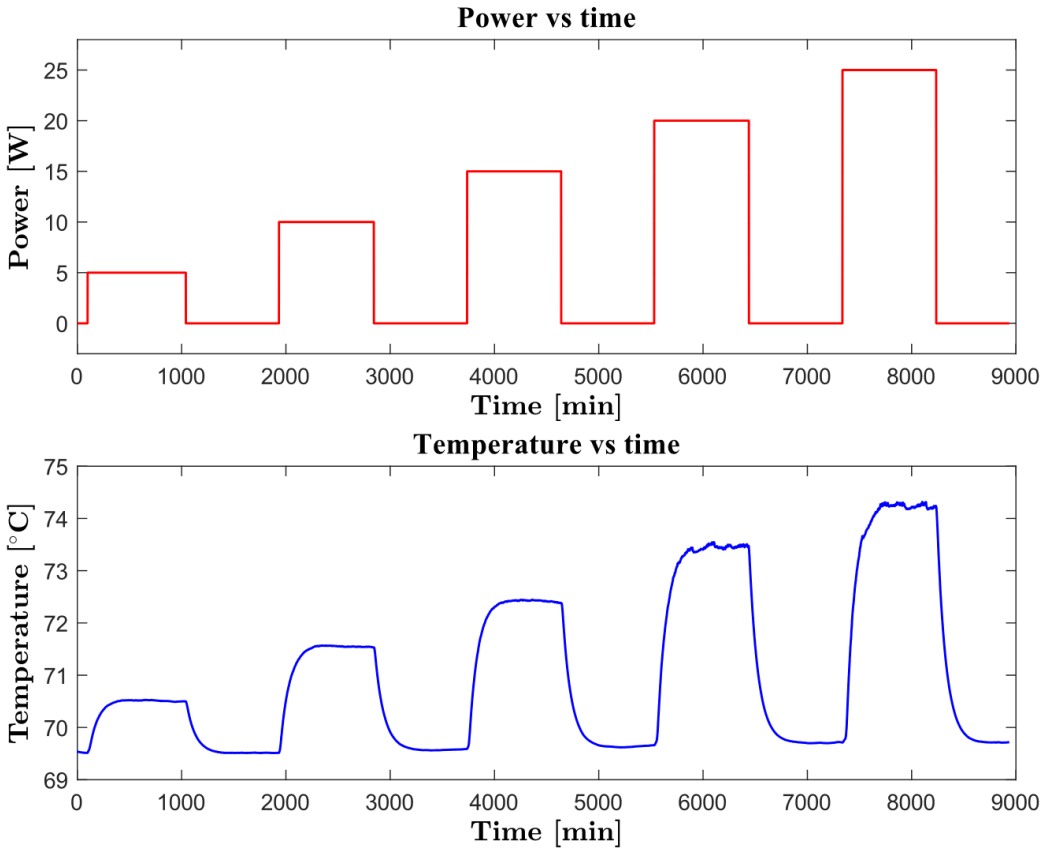

Figure 3.5. *Plot of the power generated by the electrical heater vs time and its effect on the temperature.*

From this study, several different information can be obtained as heat exchange coefficient, the effective heat capacity and the time constant of the system. Only the thermal steady state and the cooling transient are considered. The heating transient is discharged because its dynamics are affected by that of the controller.

3.2.1 Cooling transient analysis

From the cooling transient, the enthalpy balance gives equation 3.7:

$$m \cdot cp \cdot \frac{dT}{dt} = -U \cdot A \cdot (T - T_J) \tag{3.7}$$

In which $m \cdot cp$ is the effective heat capacity obtained considering that of the reaction mixture and all the metallic instrumentations such as the steel impeller. The effective heat capacity is totally different from the one of the reaction mixture alone, highlighting the importance of considering all the other pieces of instrumentation in order to avoid large errors. The product between the heat exchange coefficient and the exchange area is indicated by $U \cdot A$, whereas $\frac{dT}{dt}$ indicates the time derivative of the temperature of the reactor; $T - T_J$ indicates the difference between the temperature of the reactor and the one of the jacket. Equation 3.1 can be arranged as:

$$\frac{dT}{T - T_J} = -\frac{U \cdot A}{m \cdot cp} \cdot dt \tag{3.8}$$

Which, properly integrated, leads to equation 3.9

$$\frac{T(t) - T_J}{T(t_0) - T_J} = e^{-\frac{U \cdot A}{m \cdot cp}(t - t_0)} = e^{-\frac{t - t_0}{\tau}} \tag{3.9}$$

Once equation 3.9 is written in logarithmic form, equation 3.10 can be obtained:

$$\begin{aligned} \ln\big(T(t) - T_J\big) &= -\frac{U \cdot A}{m \cdot cp}(t - t_0) + \ln(T(t_0) - T_J) \\ &= -\frac{t - t_0}{\tau} + \ln(T(t_0) - T_J). \end{aligned} \tag{3.10}$$

Equation 3.10 has now the form of a straight line as equation 3.11:

$$y = -\frac{1}{\tau}x + b \qquad 3.11$$

Consequently, a linear fitting of the cooling transients can be performed if expressed in logarithmic form.

Figure 3.6 reports an exemplifying plot of the experimental data fitting for the case of 10 W power and 70°C.

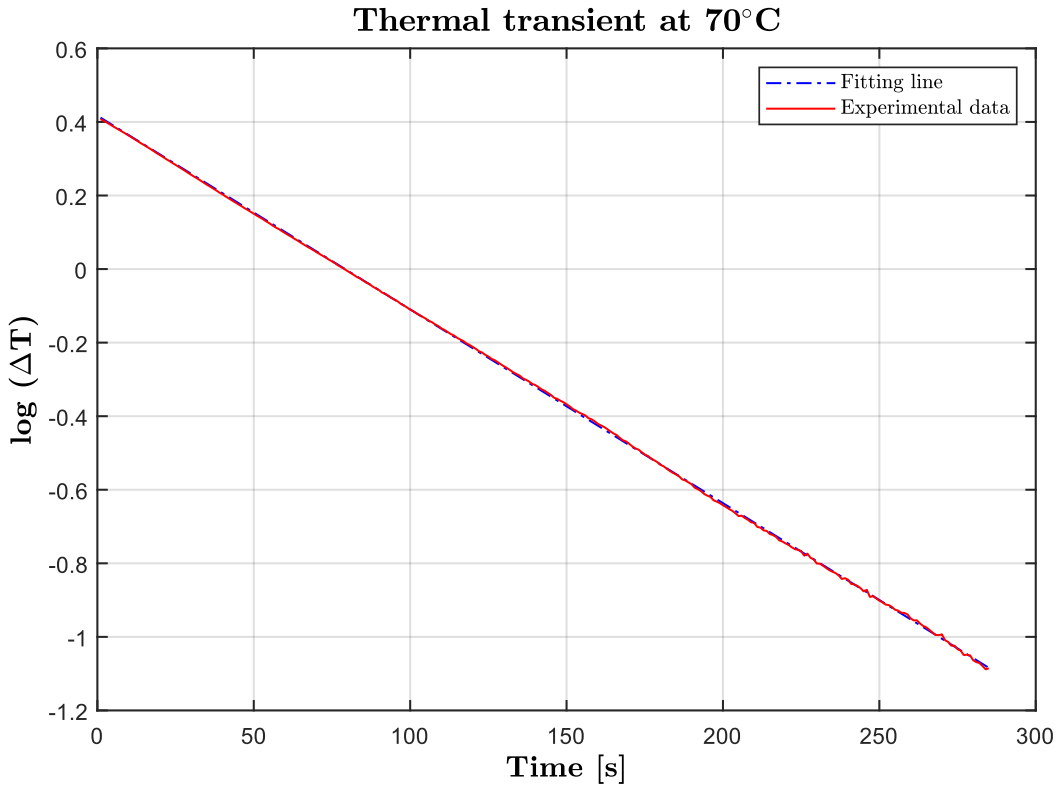

Figure 3.6. *Plot of the experimental data in logarithmic form of the cooling transient (red) at 70°C after generating 10 W by an electrical heater. Linear fitting (blue).*

All the others 14 tests are not reported for sake of brevity. All the results are indicated in Table 3.1.

Table 3.1. *Results of the linear fitting of the experimental data obtained from the cooling transient at 40°C.*

Temperature [°C]	Power [W]	τ^{-1} [min^{-1}]	τ [min]	τ^{-1} [s^{-1}]= $\frac{U \cdot A}{m \cdot cp}$	τ [s]= $\frac{m \cdot cp}{U \cdot A}$
40°C	5	0.184	5.44	0.00307	326
	10	0.157	6.36	0.00262	381
	15	0.159	6.28	0.00265	377
	20	0.161	6.20	0.00269	372
	25	0.160	6.24	0.00267	374

Mean value		**0.164**	**6.10**	**0.00274**	**366**

Table 3.2. *Results of the linear fitting of the experimental data obtained from the cooling transient at 55°C.*

Temperature [°C]	**Power [W]**	τ^{-1} **[min^{-1}]**	τ **[min]**	τ^{-1} **[s^{-1}]]=** $\frac{U \cdot A}{m \cdot cp}$	τ **[s]** $= \frac{m \cdot cp}{U \cdot A}$
55°C	5	0.207	4.82	0.00346	289
	10	0.200	4.99	0.00334	300
	15	0.197	5.09	0.00328	305
	20	0.194	5.17	0.00323	310
	25	0.200	5.00	0.00333	300
Mean value		**0.200**	**5.02**	**0.00333**	**300**

Table 3.3. *Results of the linear fitting of the experimental data obtained from the cooling transient at 70°C.*

Temperature [°C]	**Power [W]**	τ^{-1} **[min^{-1}]**	τ **[min]**	τ^{-1} **[s^{-1}]]=** $\frac{U \cdot A}{m \cdot cp}$	τ **[s]** $= \frac{m \cdot cp}{U \cdot A}$
70°C	5	0.184	5.44	0.00306	326
	10	0.208	4.81	0.00346	289
	15	0.195	5.12	0.00325	307
	20	0.192	5.21	0.00320	312
	25	0.198	5.05	0.00330	303
Mean value		**0.195**	**5.13**	**0.00326**	**307**

For all tests, the coefficient of determination R^2 is greater than 0.997, proving the quality of the fitting. In conclusion, the mean value of the characteristic time is equal to 366, 300 and 307 seconds for 40, 55 and 70°C. This is the time needed to reach 63.2% of the transient, if the system is assumed to be first order. This means that after 4τ-5τ (approximately 20-25 minutes) the transient can be considered extinguished. The characteristic time is a little higher in the case of 40°C because of the greater viscosity, translating into slower heat transfer.

3.2.2 Steady state analysis

The thermal profiles previously obtained were also studied to gather information regarding the steady state. In order to do that, the mean temperature of each peak was considered. According the equation of the steady state:

$$(T - T_J) = \frac{Q}{U \cdot A} \qquad 3.12$$

Knowing that the power Q is the net power generated inside the reactor, it can be explicated as the difference between the power generated by the electrical heater P and the power dissipated by heat dispersion Q_d. In fact, not the whole surface of the reactor is covered by the jacket (for example the bottom) and this is a source of heat dissipation. Moreover, the metallic impeller is cooler than the other parts of the reactor because it is held by the motor that is not temperature-controlled. The equation can be arranged gicing a straight line as follows:

$$T = \frac{(P - Q_d)}{U \cdot A} + T_j \qquad 3.13$$

Data of the steady states were fitted according to this approach. The fitting was repeated for the three temperatures of 40, 55 and 70°C. The generated plot is represented in Figure 3.7, only showing data obtained at 70°C, for sake of brevity.

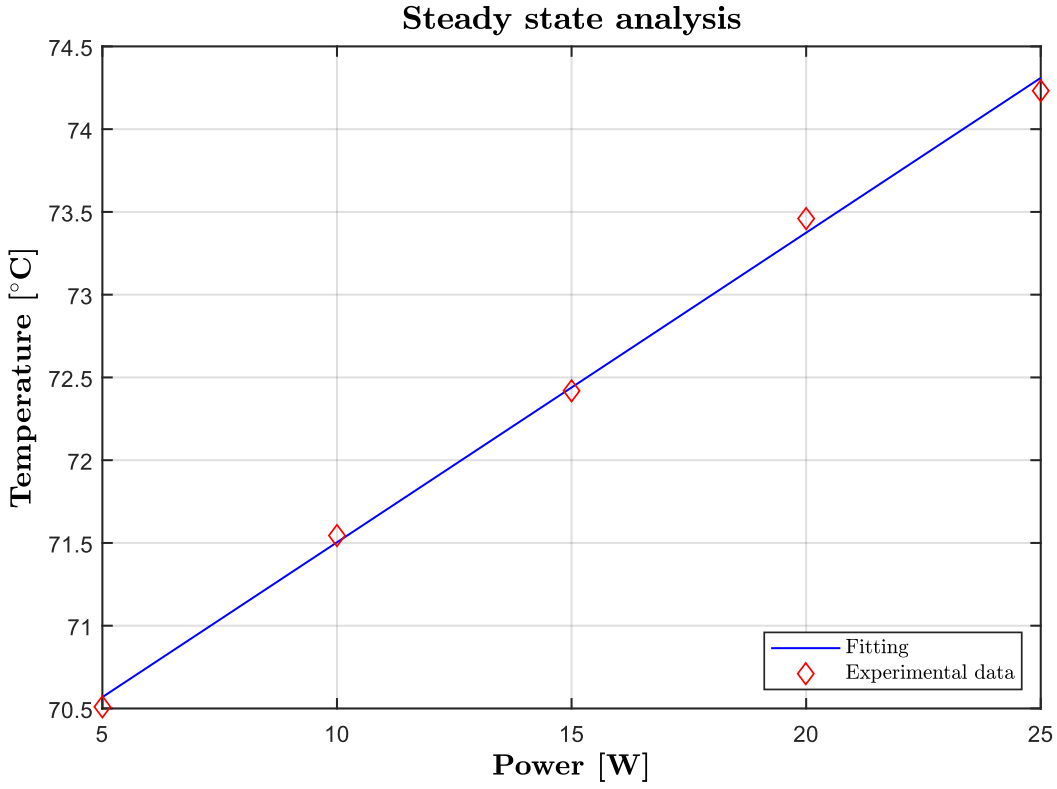

Figure 3.7. *Analysis of the thermal steady state at 70°C. Experimental points are indicated in red whereas the linear fitting is shown in blue.*

The quality of the fitting is again very high, with a coefficient of determination always higher than 0.99. The results are indicated in table 3.4.

Table 3.4. *Results of the linear fitting of the experimental data obtained from the steady state.*

Temperature [°C]	$\boldsymbol{U \cdot A}$ $\boldsymbol{[W/K]}$	$\boldsymbol{Q_d}$ $\boldsymbol{[W]}$	$\boldsymbol{R^2}$ $[-]$
40	2.22	0.8	0.991
55	2.87	0.8	0.992
70	2.77	0.8	0.998
Mean value	**2.62**	**0.8**	

From Table 3.4, the difference of the $U \cdot A$ between 40 and 55°C is only about 3%, that is quite negligible. At 40°C the coefficient is sensibly lower, a result in perfect agreement with the findings detailed in the previous paragraph, and confirming that heat transport is sensibly slower at low temperatures.

Once coefficient $U \cdot A$ and the characteristic time are found, the effective heat capacity can be detemined, from the data in tables 3.1-3.3.

Table 3.5. *Determination of the effective heat capacity at different temperatures.*

$\boldsymbol{\tau}$ **[s]** $= \frac{m \cdot cp}{U \cdot A}$	$\boldsymbol{U \cdot A}$ $\boldsymbol{[W/K]}$	$\boldsymbol{m \cdot cp}$ $\boldsymbol{[J/K]}$
366	2.22	813
300	2.87	861
307	2.77	855
Mean value		**843**

The calculated effective heat capacity is 843 kJ/K, with a maximum variation from the mean value of 3.5%. Considering that the heat capacity of soybean oil is around 2 J/g, and that of the aqueous solution is assumed to be similar to the one of the water, i.e. 4.2 J/g, the theoretical

heat capacity is roughly equal to 300 J/K. This value is strongly different from what previously obtained because the metallic instrumentation (impeller, thermocouples…) have a large impact on it. This demonstrates that the capacity of the instrumentation cannot be neglected, despite what assessed by De Quadros *et al.* [4].

Bibliographic references

[1] V. Semiconductors, “Vishay Semiconductors Transmissive Optical Sensor with Phototransistor Output.”

[2] A. Debab, N. Chergui, K. Bekrentchir, and J. Bertrand, “An investigation of heat transfer in a mechanically agitated vessel,” *J. Appl. Fluid Mech.*, vol. 4, no. 3, pp. 43–50, 2011.

[3] N. N. Nassar and A. K. Mehrotra, “Design of a laboratory experiment on heat transfer in an agitated vessel,” *Educ. Chem. Eng.*, vol. 6, no. 3, pp. e83–e89, 2011.

[4] J. V. de Quadros and R. Giudici, “Epoxidation of soybean oil at maximum heat removal and single addition of all reactants,” *Chem. Eng. Process. Process Intensif.*, vol. 100, pp. 87–93, 2016.

Chapter 4

Kinetic and mass transfer modelling

This chapter details the modelling approach that was exploited to study the different systems. A biphasic mathematical model was implemented to perform a fitting on the experimental data and enable a complete understanding of kinetics and mass transfer. As mentioned in Chapter 1 (§1.4), in the literature there are many approaches for the modelling of this kind of this system, and several authors based their work on a pseudo-homogeneous approach [1],[2],[3] that deals with a single pseudo phase in which properties are averaged on the constituent phases. This model is strongly simplified, and does not permit to fully study the system. For this reason, in this work a higher accuracy, complete biphasic approach was implemented, partially based on the works of Rangarajan *et al.* [4], Leveneur *et al*.[5] and Santacesaria *et al* [6]. These authors presented two works with biphasic approaches, with strong assumptions imposed to simplify the complex nature of the system. Other more detailed models, as for example droplets population models, were discarded because the higher accuracy of the results does not justify the noticeably higher complexity of the implementation.

4.1 Mechanism of the process

The model implemented in this work considers both mass transfer between phases and reactions in each phase. As previously mentioned in Chapter 1, the main reactions are the formation of the peroxyacetic acid in the aqueous phase and the epoxidation in the organic one. The continuous migration of peroxyacetic acid in the organic phase and of acetic acid occurs according to the mechanism sketched in Figure 4.1

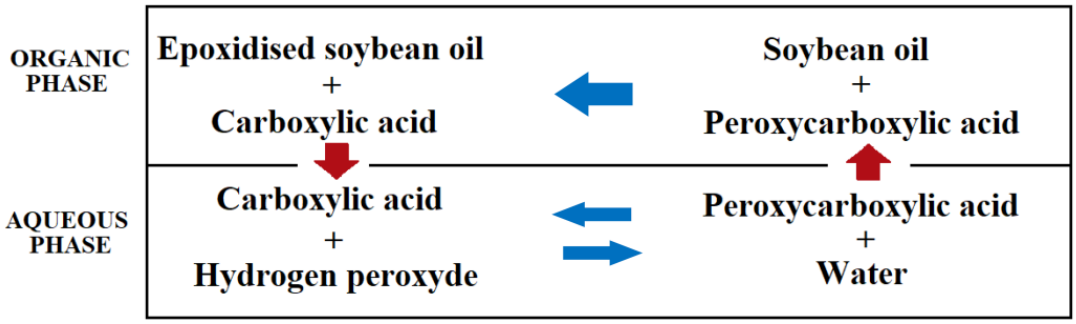

Figure 4.1. *Graphical representation of the reacting system.*

The concentration profiles can be represented as in Figure 4.2. For each species, the concentration is higher in the phase in which they are more soluble. The discontinuity in the concentration profile at the interface is due to the difference of affinity of each species between different phases.

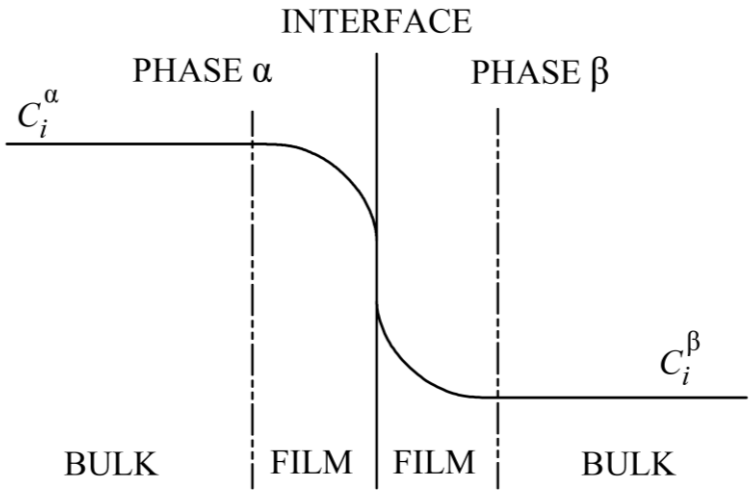

Figure 4.2. *Profiles of concentration in the two phases according the two films theory.*

4.2 Reaction scheme

The reaction system is quite complex because of the compresence of several substances, reactions and mass transfer between phases. Moreover, the desired product can be degraded to quite a large number of by-products. In fact, epoxides can be easily attacked in several ways because of their quite high reactivity, and can react with water, hydrogen peroxide, acetic acid, peracetic acid and other compounds. However, according to the literature, it is reasonable to

simplify the system and assume that epoxides can be attacked only by acetic and peracetic acids. Furthermore, according La Scala and Wool [7], the model should take into account the composition of the oil because of the higher reactivity of dienes and especially trienes compared to monounsaturated fatty acids. However, since it was not possibile to analyse the composition of the oil, and since the most reactive component (alpha-linolenic acid) is usually lower than 7%, the model was structured assuming that all the unsaturations have the same reactivity. In this way, the model considers the unsaturation as a reacting group, without distinguishing between the number of unsaturations of the chains. This assumption is in line with the literature[8].

In addition, some assumptions on the solubility of the substances were posed. It was hypothesized that water and hydrogen peroxide are not soluble in the organic phase, and that oil is not soluble in the aqueous phase, whereas only acetic and peracetic acid are soluble in both phases, as in Leveneur *et al*.[5]. This implies that some reactions take place only in the aqueous phase, and others only in the oil phase, even though all the reactions could be possible in both phases. This simplification is very useful to simplify the model. These assumptions are very reasonable, and do not represent a limitation to the accuracy of the model.

The reacting system is reported in the following equations.

Reactions in the water phase:

1. Direct reaction of the production of peracetic acid

$$CH_3COOH + H_2O_2 \overset{k_1}{\rightarrow} CH_3COOOH + H_2O \qquad 4.1$$

2. Inverse reaction of the decomposition of peracetic acid

$$CH_3COOOH + H_2O \overset{k_2}{\rightarrow} CH_3COOH + H_2O_2 \qquad 4.2$$

3. Degradation of hydrogen peroxide

$$H_2O_2 \overset{k_3}{\rightarrow} H_2O + {}^1/_2\, O_2 \qquad 4.3$$

Reactions in the oil phase:

4. Epoxidation reaction

$$R_1 - C = C - R_2 + CH_3COOOH \overset{k_4}{\rightarrow} R_1 - CHOCH - R_2 + CH_3COOH \qquad 4.4$$

5. Oxirane ring opening by acetic acid

$$R_1 - CHOCH - R_2 + CH_3COOH \xrightarrow{k_5} EG_{AA} \quad 4.5$$

6. Oxirane ring opening by peroxyacetic acid

$$R_1 - CHOCH - R_2 + CH_3COOOH \xrightarrow{k_6} EG_{PAA} \quad 4.6$$

For sake of simplicity, from now on, epoxides are indicated as *EP*, double bonds as *DB*, acetic acid as *AA*, peroxyacetic acid as *PAA*, glycols as *EG*, hydrogen peroxide as *HP*, water as *W*, virgin oil as *DB*.

Since virgin oil is soluble only in the organic phase, water and hydrogen peroxide are soluble only in the aqueous phase, only acetic and peracetic acid are soluble in both phases, so they are the only two species that can migrate from a phase to another one.

For this reason, it is useful to define the partition coefficients:

$$K_i = {C_i^w}/{C_i^o} \quad 4.7$$

were K_i is the partition coefficient of the *i-th* species, C_i^w and C_i^o stands for the concentration of the *i-th* species in the aqueous and organic phase respectively.

Table 4.2 *Partition coefficient of the main species involved in the epoxidation process*

Chemical species	K_i**[-]**
AA	3.8
PAA	27
HP	→∞
DB	→0
EP	→0
W	→∞
EG	→0

Thanks to the assumptions on the solubility in the phases and according to the literature, the partition coefficient are equal to zero for oil, epoxidised oil and glycols, whereas those of

hydrogen peroxide and water are very large (so they tend to infinite). The partition coefficients are summarized in Table 4.2.

4.3 Kinetic equations

The kinetic system is made of six reactions. The formation of the peroxyacetic acid was studied in the literature but there are no clear and univocal references about the kinetic mechanism, so the reaction is assumed as elementary. The formation of the peroxyacetic acid is an equilibrium reaction, which constant can be found in the literature. The equilibrium constant is defined as:

$$K_{eq} = {k_1}/{k_2} \tag{4.8}$$

and consequently, in order to exploit this constraint, the kinetic constant of the reversed reaction can be expressed as follows. In this way, k_2 is not a parameter of the model because it is expressed in function of k_1.

$$k_2 = {k_1}/{K_{eq}} \tag{4.9}$$

About the decomposition of the hydrogen peroxide, according to Santacesaria *et al.* [8] . the reaction is not elementary, but the order of the reaction is assumed to be equal to 2.5.

$$R_1 = k_1 C_{AA}^w C_{HP}^w \tag{4.10}$$

$$R_2 = \frac{k_1}{K_{eq}} C_{PAA}^w C_W^w \tag{4.11}$$

$$R_3 = k_3 (C_{HP}^w)^{2.5} \tag{4.12}$$

$$R_4 = k_4 C_{DB}^o C_{PAA}^o \tag{4.13}$$

$$R_5 = k_5 C_{EP}^o C_{AA}^o \tag{4.14}$$

$$R_6 = k_6 C_{EP}^o C_{PAA}^o \tag{4.15}$$

Moreover, it is assumed that all the reactions take place in the bulk and no reactions take place at the interface.

4.4 Mass transfer

Mass transfer is modelled according the two films Whitman's theory. The mass transfer rate for the component *i* from the aqueous phase to the organic one is expressed as:

$$J_i^{\alpha} = \beta_i^{\alpha}\left(C_i^{\alpha,bulk} - C_i^{\alpha,int}\right) \quad 4.17$$

where α is a generic phase, and the difference of concentration is calculated between the bulk and the interface. The mass transfer rate has the dimensions of $[mol/(l \cdot min)]$ when the concentrations are expressed in $[mol/l]$ and β_i^{α} is expressed in $[min^{-1}]$.
Moreover, β_i^{α} is defined as:

$$\beta_i^{\alpha} = h_{m,i}^{\alpha} \cdot A^{\alpha/\beta} \quad 4.18$$

where $h_{m,i}^{\alpha}$ is the mass transfer coefficient of the species *i* in the generic phase α and $A^{\alpha/\beta}$ is the interfacial area between phases α and β. The parameter β_i^{α} gives an indication of the mass transfer efficiency.
According to the definition of the partition coefficient K_i, the interfacial concentrations can be expressed as follows:

$$C_i^{w,int} = K_i \cdot C_i^{o,int} \quad 4.19$$

Considering that the only the two species that can migrate acetic and peroxyacetic acid, mass transfer rate can be written:

$$J_{AA}^{w} = \beta_{AA}^{w}\left(C_{AA}^{w,b} - K_{AA} \cdot C_{AA}^{o,int}\right) \quad 4.20$$

$$J_{PAA}^{w} = \beta_{PAA}^{w}\left(C_{PAA}^{w,b} - K_{PAA} \cdot C_{PAA}^{o,int}\right) \quad 4.21$$

$$J_{AA}^{o} = \beta_{AA}^{o}\left(C_{AA}^{o,int} - C_{AA}^{o,bulk}\right) \quad 4.22$$

$$J_{PAA}^{o} = \beta_{PAA}^{o}\left(C_{PAA}^{o,int} - C_{PAA}^{o,bulk}\right) \quad 4.23$$

In this way, interfacial concentration can be easily obtained, once it is reminded the constraint that holds the mass transfer between phases:

$$V^o \cdot J_i^o = V^w \cdot J_i^w \quad 4.24$$

that is valid for the batch case. Instead, for the continuous case:

$$Q^o \cdot J_i^o = Q^w \cdot J_i^w \quad 4.25$$

and Q is volumetric florate.

Consequently, the concentration of acetic and peracetic acid can be derived:

$$C_{AA}^{o,int} = \frac{V^o \cdot \beta_{AA}^o \cdot C_{AA}^{o.bulk} + V^w \cdot \beta_{AA}^w \cdot C_{AA}^{w.bulk}}{V^w \cdot \beta_{AA}^w \cdot K_{AA} + V^O \cdot \beta_{AA}^o} \quad 4.26$$

$$C_{PAA}^{o,int} = \frac{V^o \cdot \beta_{PAA}^o \cdot C_{PAA}^{o.bulk} + V^w \cdot \beta_{PAA}^w \cdot C_{PAA}^{w.bulk}}{V^w \cdot \beta_{PAA}^w \cdot K_{PAA} + V^O \cdot \beta_{PAA}^o} \quad 4.27$$

that is valid for the batch case. Instead, for the continuous case:

$$C_{AA}^{o,int} = \frac{Q^o \cdot \beta_{AA}^o \cdot C_{AA}^{o.bulk} + Q^w \cdot \beta_{AA}^w \cdot C_{AA}^{w.bulk}}{Q^w \cdot \beta_{AA}^w \cdot K_{AA} + Q^O \cdot \beta_{AA}^o} \quad 4.28$$

$$C_{PAA}^{o,int} = \frac{Q^o \cdot \beta_{PAA}^o \cdot C_{PAA}^{o.bulk} + Q^w \cdot \beta_{PAA}^w \cdot C_{PAA}^{w.bulk}}{Q^w \cdot \beta_{PAA}^w \cdot K_{PAA} + Q^O \cdot \beta_{PAA}^o} \quad 4.29$$

where all the terms of volume of the two phases are replaced with the volumetric flowrates of the phases.

For sake of simplicity, it is assumed that $h_{m,AA}^w$ and $h_{m,PAA}^w$ are equal, as well as $h_{m,AA}^o$ and $h_{m,PAA}^o$. This assumption notably simplifies the system, but is still quite reasonable since acetic and peroxyacetic acid have a very similar structure. Since the interfacial area is independent from species, the same relation can be extended to coefficient β_{AA}^o and β_{PAA}^o, β_{AA}^o and β_{PAA}^o.

4.5 Balances

A generic mass or mole balance can be written as follows:

$$A = IN - OUT + P - C \tag{4.30}$$

in which A stands for accumulation term, IN and OUT the inlet and outlet terms, P and C the production and consumption terms, respectively.

4.5.1 Batch

Even if the considered system is batch, the balance on a single phase is not batch. According to this approach, molar balances were written for each phase and for each species. Considering two phases α and β:

$$\frac{dN_i^\alpha}{dt} = V^\alpha \cdot \left(J_i^{\alpha/\beta} + \sum_j \nu_{ij} R_j\right) \tag{4.31}$$

where N_i is the number of moles of species *i,* α is a generic phase, R_j is a generic reaction, ν_{ij} is the stoichiometric matrix for all the species and all the reactions and $J_i^{\alpha/\beta}$ is the mass transfer from phase α to β. The balance for the i *–th* species and the phase α can be repeated for the other phase β. The accumulation term can be expressed in terms of concentration and volume:

$$\frac{dN_i^\alpha}{dt} = \frac{d(C_i \cdot V^\alpha)}{dt} = V^\alpha \frac{dC_i^\alpha}{dt} + C_i \frac{dV^\alpha}{dt}. \tag{4.32}$$

Assumed that the volume of each phase is constant (that is reasonable), the derivative of the volume is equal to zero. In this way, equation 4.32 can be written as:

$$\frac{dC_i^\alpha}{dt} = J_i^{\alpha/\beta} + \sum_j \nu_{ij} R_j. \tag{4.33}$$

For this biphasic system, it is considered that mass transfer rates of a phase are positive when entering in that phase. The general balances for the two phases are:

$$\frac{dC_i^w}{dt} = J_i^w + \sum_j \nu_{i,j} R_j \tag{4.34}$$

$$\frac{dC_i^o}{dt} = J_i^o + \sum_j \nu_{i,j} R_j \tag{4.35}$$

Developing the balances for all the species, the following balances can be written.

Aqueous phase:

$$\frac{dC_{AA}^{W}}{dt} = -R_1 + R_2 - J_{AA}^{W} \quad 4.36$$

$$\frac{dC_{H_2O_2}^{W}}{dt} = -R_3 \quad 4.37$$

$$\frac{dC_{PAA}^{W}}{dt} = R_1 - R_2 - J_{PAA}^{W} \quad 4.38$$

$$\frac{dC_{H_2O_2}^{W}}{dt} = R_3 \quad 4.39$$

Organic phase:

$$\frac{dC_{AA}^{O}}{dt} = R_4 + J_{AA}^{o} \quad 4.40$$

$$\frac{dC_{PAA}^{O}}{dt} = -R_4 + J_{PAA}^{o} \quad 4.41$$

$$\frac{dC_{DB}^{O}}{dt} = -R_4 \quad 4.42$$

$$\frac{dC_{EP}^{O}}{dt} = R_4 - R_5 \quad 4.43$$

$$\frac{dC_{EG}^{O}}{dt} = R_5 + R_6 \quad 4.44$$

4.5.1 PFR

In the case of continuous reactor, if conditions of axial segregation and radial perfect homogeneity are valid, a PFR model can be assumed. Balances are similar to the case of batch model, but the time derivative does not consider the reaction time but the residence time instead. In this case, the general balance on each phase can be written as:

$$\frac{dN_i^{\alpha}}{d\tau} = V^{\alpha} \cdot \left(J_i^{\alpha/\beta} + \sum_j \nu_{ij} R_j\right) \quad 4.45$$

Hence, under the assumption of negligible volume variations:

$$\frac{dC_i^{\alpha}}{d\tau} = v\frac{dC_i^{\alpha}}{dz} = J_i^{\alpha/\beta} + \sum_j \nu_{ij} R_j. \quad 4.46$$

where *v* is the superficial velocity and *z* is the axial coordinate. For the two phases:

$$\frac{dC_i^{w}}{d\tau} = J_i^{w} + \sum_j \nu_{i,j} R_j \quad 4.47$$

$$\frac{dC_i^{o}}{d\tau} = J_i^{o} + \sum_j \nu_{i,j} R_j \quad 4.48$$

For these reasons, balance equations from 4.36 to 4.44 (valid for the batch case) can be written considering the residence time instead of the reaction time.

Aqueous phase:

$$\frac{dC_{AA}^{w}}{d\tau} = -R_1 + R_2 - J_{AA}^{w} \quad 4.49$$

$$\frac{dC_{H_2O_2}^{w}}{d\tau} = -R_3 \quad 4.50$$

$$\frac{dC_{PAA}^{w}}{d\tau} = R_1 - R_2 - J_{PAA}^{w} \quad 4.51$$

$$\frac{dC_{H_2O_2}^{w}}{d\tau} = R_3 \quad 4.52$$

Organic phase:

$$\frac{dC_{AA}^{O}}{d\tau} = R_4 + J_{AA}^{o} \quad 4.53$$

$$\frac{dC_{PAA}^{O}}{d\tau} = -R_4 + J_{PAA}^{o} \quad 4.54$$

$$\frac{dC_{DB}^{O}}{d\tau} = -R_4 \quad 4.55$$

$$\frac{dC_{EP}^{O}}{d\tau} = R_4 - R_5 \quad 4.56$$

$$\frac{dC_{EG}^{O}}{d\tau} = R_5 + R_6 \quad 4.57$$

4.6 Modelling of the calorimetric reactor

The process carried out in the calorimetric reactor was modelled according to the approach exposed for the batch case. The overall system was considered isothermal, even though the reactor was isoperibolically controlled (so the temperature of the jacket is maintained constant). This assumption is quite reasonable since thermal overshoots occur, but are not so large (max. 2-3°C).

The batch assumption is reasonably valid for the calorimetric reactor since it is well stirred, segregation does not take place, and the volume does not sensibly vary during the reaction, hence it can be considered constant.

4.7 Modelling of the conventional heating and MW reactors

Kinetic and mass transfer modelling of the conventional heating reactor is similar to the previous case, since it is a batch stirred isothermal reactor. Hence, for this case a batch approach was followed.

In the case of the microwave heating system, the only work of MW modelling was by Aguilera *et al.* [9], which system was made by two batch systems and a pseudo-homogeneous approach was implemented.

There is no information in the literature regarding the effect of the MW field on mass transfer, or on its potential promotion of a different kinetic path in the reacting system. This information requires a very complex study, on the physics of the MW field on the molecules and its kinetic effect. This approach is over-detailed, and the results would not be in line with the objective of this work.

For these reasons, modelling of MW heating reactor was maintained identical to the case of conventional heating. In fact, the system is assumed to be batch, and no terms related to MW contribution are considered in the mass balance. In this way, the model was intended to capture how mass transfer and kinetics terms change under MW field, compared to conventional heating. In this way, a direct comparison allows to evaluate in which steps MW field is more effective, and how it could be useful at the industrial scale.

4.8 Modelling of the continuous reactor

The continuous reactor was modelled according to a PFR approach, explained in §4.5.1. In fact, the continuous reactor was modelled under the hypothesis of plug flow reactor, as in the case of Santacesaria *et al*. [6].

However, experiments were carried out at different residence times, with constant reactor volume. Each test has a different residence time, and for this purpose the total volumetric flowrate was changed, fixing the aqueous to organic phases ratio. For this reason, equations 4.28 and 4.29 can be written as follows:

$$C_{AA}^{o,int} = \frac{Q^o/Q^w \cdot \beta_{AA}^o \cdot C_{AA}^{o.bulk} + \beta_{AA}^w \cdot C_{AA}^{w.bulk}}{\beta_{AA}^w \cdot K_{AA} + Q^O/Q^w \cdot \beta_{AA}^o} \quad 4.58$$

$$C_{PAA}^{o,int} = \frac{Q^o/Q^w \cdot \beta_{PAA}^o \cdot C_{PAA}^{o.bulk} + \beta_{PAA}^w \cdot C_{PAA}^{w.bulk}}{\beta_{PAA}^w \cdot K_{PAA} + Q^O/Q^w \cdot \beta_{PAA}^o}. \quad 4.59$$

and the interface concentrations are expressed parametrically to the flowrates' ratio.

Bibliographic references

[1] J. V. de Quadros and R. Giudici, "Epoxidation of soybean oil at maximum heat removal and single addition of all reactants," *Chem. Eng. Process. Process Intensif.*, vol. 100, pp. 87–93, 2016.

[2] M. R. Janković, S. V. Sinadinović-Fišer, and O. M. Govedarica, "Kinetics of the epoxidation of castor oil with peracetic acid formed in situ in the presence of an ion-exchange resin," *Ind. Eng. Chem. Res.*, vol. 53, no. 22, pp. 9357–9364, 2014.

[3] J. C. de Haro, I. Izarra, J. F. Rodríguez, Á. Pérez, and M. Carmona, "Modelling the epoxidation reaction of grape seed oil by peracetic acid," *J. Clean. Prod.*, vol. 138, pp. 70–76, 2016.

[4] P. D. Rangarajan, B., Havey, A., Grulke, E. A. and Culnan, "Kinetic parameters of a two phase model for in-situ epoxidation of soybean oil," *J. Am. Oil Chem. Soc.*, vol. 72, no. 10, pp. 1161–1169, 1995.

[5] S. Leveneur, J. Zheng, B. Taouk, F. Burel, J. Wärnå, and T. Salmi, "Interaction of thermal and kinetic parameters for a liquid-liquid reaction system: Application to vegetable oils epoxidation by peroxycarboxylic acid," *J. Taiwan Inst. Chem. Eng.*, vol. 45, no. 4, pp. 1449–1458, 2014.

[6] E. Santacesaria, A. Renken, V. Russo, R. Turco, R. Tesser, and M. Di Serio, "Biphasic model describing soybean oil epoxidation with H2O2 in continuous reactors," *Ind. Eng. Chem. Res.*, vol. 51, no. 26, pp. 8760–8767, 2012.

[7] J. La Scala and R. P. Wool, "Effect of FA composition on epoxidation kinetics of TAG," *JAOCS, J. Am. Oil Chem. Soc.*, vol. 79, no. 4, pp. 373–378, 2002.

[8] E. Santacesaria, R. Tesser, M. Di Serio, R. Turco, V. Russo, and D. Verde, "A biphasic model describing soybean oil epoxidation with H2O2 in a fed-batch reactor," *Chem. Eng. J.*, vol. 173, no. 1, pp. 198–209, 2011.

[9] A. F. Aguilera *et al.*, "Kinetic modelling of Prileschajew epoxidation of oleic acid under conventional heating and microwave irradiation," *Chem. Eng. Sci.*, vol. 199, pp. 426–438, 2019.

Chapter 5

Epoxidation in the calorimetric reactor

The system was studied under conventional heating in the calorimetric reactor at different temperatures. For each temperature, the yield vs time curves were obtained collecting several samples at different times. Points at different intermediate times were acquired performing the process up to the desired time. In this way each curve was obtained not by a single experimental run but by as much experiments as the points of the curve. This choice was motivated by the unfeasibility of intermediate samplings, since the volume of the sample was not negligible compared to the total volume. This was a high demanding procedure both in terms of time and materials, but the obtained results were most accurate. In this chapter, the results of soybean oil epoxidation in the calorimetric reactor are presented, both as regards the experimental and the modelling. The mathematical model enabled a complete understanding of kinetic and mass transfer phenomena.

5.1 Effect and choice of the process variables

The choice of the process variables was based on the previous work carried out in my master thesis research [1]. Based on these results, the concentration of reactants and other parameters were set. For sake of clarity, a brief overview of the previous results, obtained in the safety study in a *Thermal Screening Unit*, are here recalled. Moreover, the system was studied in the calorimetric reactor, and the effect of the concentration of the different reactants was assessed. Furthermore, the use of an acid ion exchange resin as a catalyst was tested (instead of the sulfuric acid) and additional tests on the importance of mixing were carried out [2], [3].

5.1.1 Onset temperature of runway decomposition of the hydrogen peroxide

The reaction mixture was tested in a *Thermal Screening Unit*, an apparatus the permits to perform thermal tests (ramped or isothermal) on the desired mixture. The system made of hydrogen peroxide and acetic acid was screened by means of a ramped test (2°C/min) and a noticeable exothermal peak was detected, with thermal peaks up to 250°C and pressure over 40 bars. The pressure peaks highlighted the rapid decomposition of the hydrogen peroxide that occurs at 100-110 °C. This can be considered a threshold temperature that should be taken into account in an industrial process for safety purposes. Considering a mass sample of 1.6 g, the rate of decomposition at 70°C was determined equal to 0.0058 mmol/min whereas at 90°C this rate is ten time higher, 0.049 mmol/min.

Furthermore, other tests were carried out using acetic acid, hydrogen peroxide and oil, with oil stabilising the system because of its thermal inertia. In these conditions, performing isothermal tests up to 8 hours, the pressure increase is limited to maximum 2.5 bars at 70°C. For these reasons, safety problems due to decomposition of hydrogen peroxide are largely reduced.

From these preliminary tests, the process presents strong safety problems due to the exothermal decomposition of the hydrogen peroxide, but the conditions are less severe thanks to the presence of the oil.

5.1.2 Effect of the concentration of the sulfuric acid

Sulfuric acid is sometimes used as catalyst. Tests were carried out in the calorimetric reactor at 500 rpm stirring for 4 hours in absence of sulfuric acid, using acetic acid : hydrogen peroxide : double bonds molar ratio equal to 0.5:1.5:1, according to what exposed in Chapter 1 (1.1.1). Tests highlighted that this process is totally infeasible, and conversion is negligible. Adding 3wt.% sulfuric acid, a noticeable thermal overshoot is detected, and the conversion is nearly complete in 3-4 hours. Tests were carried out also at 2 and 4wt.%. It was proved that sulfuric acid has a great catalytic effect on the system, and its increase affects the selectivity. For these reasons, the concentration of sulfuric acid was maintained at 3wt.%. Other researchers studied the effect of the sulfuric or phosphoric acid, demonstrating the high catalytic activity of these acids. [4] Nevertheless, in the literature some work were carried out without any acid catalyst as De Quadros *et al.* [5], thus using highly concentrated hydrogen peroxide and formic acid.

5.1.3 Effect of the concentration of the acetic acid

Tests were carried with 0.5:1 and 1:1 acetic acid : double bonds molar ratio for 4 hours. Increasing the acetic acid concentration, the reactivity is higher, but the selectivity decreases noticeably. For this reason, the acetic acid : double bonds molar ratio was maintained to 0.5:1, also because a larger use of acetic acid is not justified. Large amounts of acetic acid increase the amount of peracid in the aqueous phase, boosting the epoxidation. Nevertheless, acetic acid and peracid are involved in the epoxy degradation because of the acid attack of the oxirane rings.

5.1.4 Ion exchange resin as acid catalyst

Feasibility tests using Amberlite IR-120 as acid catalyst were carried out. This resin is made of sulfonated polystyrene pellets, and was intended to substitute sulfuric acid. At the end of the process, the resin was separated by simple filtration. Loadings of 10wt.%, 25wt.% and 40wt.% in oil were tested for 4 hours. The process was feasible, and epoxidized oil was obtained. Despite 10wt.% loading showed a very low conversion of double bonds (about 25%), 25wt.% and 40 wt.% loading achieved conversion higher tan 60-70%. The feasibility of carrying out the process using ion exchange resin was demonstrated, even with lower efficiency than sulfuric acid. If the process is used with this catalyst, a 25wt.% could be a good compromise between reactivity and economy of used catalyst.

5.1.5 Mixing program

The reactor used a Rushton turbine to obtain a good mixing between phases. However, the reactor geometry is not particularly indicated for this kind of impeller, since the height of the reactor is about 3 times the diameter. For this reason, axial segregation takes place. One solution was to increase the velocity of the impeller up to 1500-2000 rpm, to improve mixing. In these conditions, mixing is so strong that oil can be easily degraded in presence of acids. A proposed solution was based on the implementation of a mixing program, alternating 20 minutes at 500 rpm and 1500 rpm for 30 seconds. It was noticed that when the mixture was strongly mixed, a new thermal overshoot was detected thanks to contact between unreacted oil on the top of the

reactor and unreacted peracid on the bottom. The implementation of a proper mixing program allowed to increase both conversion and selectivity.

5.1.6 Epoxidation in the calorimetric reactor: choice of the process variables

For all the tests carried in this work, the acetic acid : hydrogen peroxide : double bonds proportion was fixed to 0.5:1.5:1, based on the literature (§1.1.1) and on our previous findings. These values could be further optimised, also considering the composition of the oil and the temperature, but were considered a good compromise for this work. Consequently, this ratio was fixed whereas other parameters were varied during the process, as for example temperature and time. The use of ion exchange resin can be a good solution especially for the microwave heating process, but for sake of simplicity this method was discarded. In fact, despite microwave field could be particularly effective on acid wet solids, polymer melting and hot spots could be an issue and the mathematical model to describe the system should consider three phases, thus remarkably complicating the approach.
To avoid segregation issues, the loading of the calorimetric reactor was considered. In fact, the loading was calculated so that the height of the liquid is about equal to the reactor diameter, as suggested by the literature [6]. In this way, axial segregation problems are solved.

5.2 Experimental results

On the base of the preliminary results, epoxidation in the calorimetric reactor was carried out. The quantities of the reactants are indicated in Table 5.1.

Table 5.1. *Table of the quantities of all the reactants.*

Reactant	Mass [g]
Soybean	45
Acetic acid	7.695
Hydrogen peroxide	37.305
Sulfuric acid	1.351

The total amount is 90 grams and the stirring velocity is 500 rpm and the Reynolds number is about $2 \cdot 10^4$, hence the turbulent regime is completely developed. This quantity was determined so that the height of the liquid is equal to the diameter of the reactor. In this way, the amount of liquid is sufficiently low to avoid axial segregation of the biphasic mixture. This issues require particular attention since the Rushton turbine can generate a radial flow field, and axial segregation could easily take place. On the other hand, the thermocouple is sufficiently immersed in the liquid so that the measurement is affordable. To prevent as much as possible a double loop flow pattern instead of a single loop one, the impeller clearance was set at 5 mm from the bottom. To verify that no dead zones were present, and segregation did not occur, a homogeneity test was performed. A glass beaker with the same diameter of the reactor was used to perform a visual analysis of mixing. From Figure 5.1, no dead zones were observed, and the impeller was able to involve the whole mass of fluid, thus creating a uniform suspension. The composition of the mixture used for this preliminary test is the one used for the epoxidation (Table 5.1).

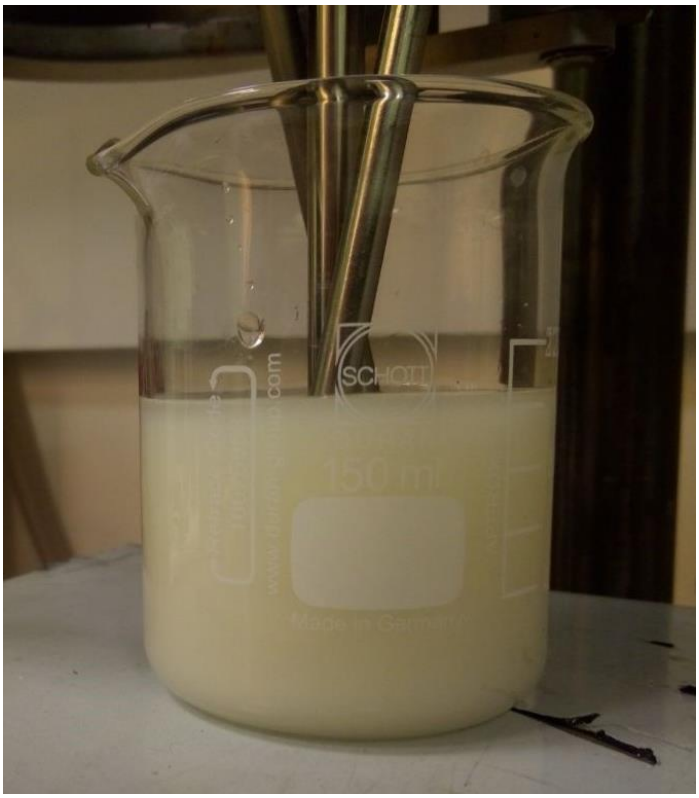

Figure 5.1. *Homogeneity test to evaluate the presence of dead volumes using a Rushton turbine and glass becher with the same diameter of the reactor. Stirring velocity is 500 rpm.*

Therefore, the homogeneity test demonstrated that the height of the liquid and the speed velocity were appropriated, so that the whole mass was involved by the impeller thus obtaining a fully homogenized mixture.

The process was carried out at 40, 55 and 70°C at 500 rpm. Figure 5.2 indicates the yield vs time curves parametric to the temperature.
Intermediate sampling was not feasible since samples volume was not negligible compared to total volume; thus each point was obtained performing the process up to the desired time. In this way, several experimental runs were carried out, as much as the points. This was a high demanding procedure, both in terms of time and chemicals but it ensured the obtainment of rigorous results.

Figure 5.2 shows that kinetics are strongly influenced by the temperature, since the time to maximum yield decreases from 25 (40°C) to 7 (55 °C) and 3 hours (70°C). It is possible to notice that the maximum yield is about 90%, and it is quite constant for all the cases. However, at 70°C the acid attack is very fast, and epoxides are rapidly degraded to glycols. For an industrial application, since the maximum yield does not greatly vary with temperature, the temperature of 70°C could be the optimal choice, but it must be ensured that the process is stopped exactly at the maximum. In other cases, it could be convenient to slightly decrease it to slow down the degradation of the epoxides.

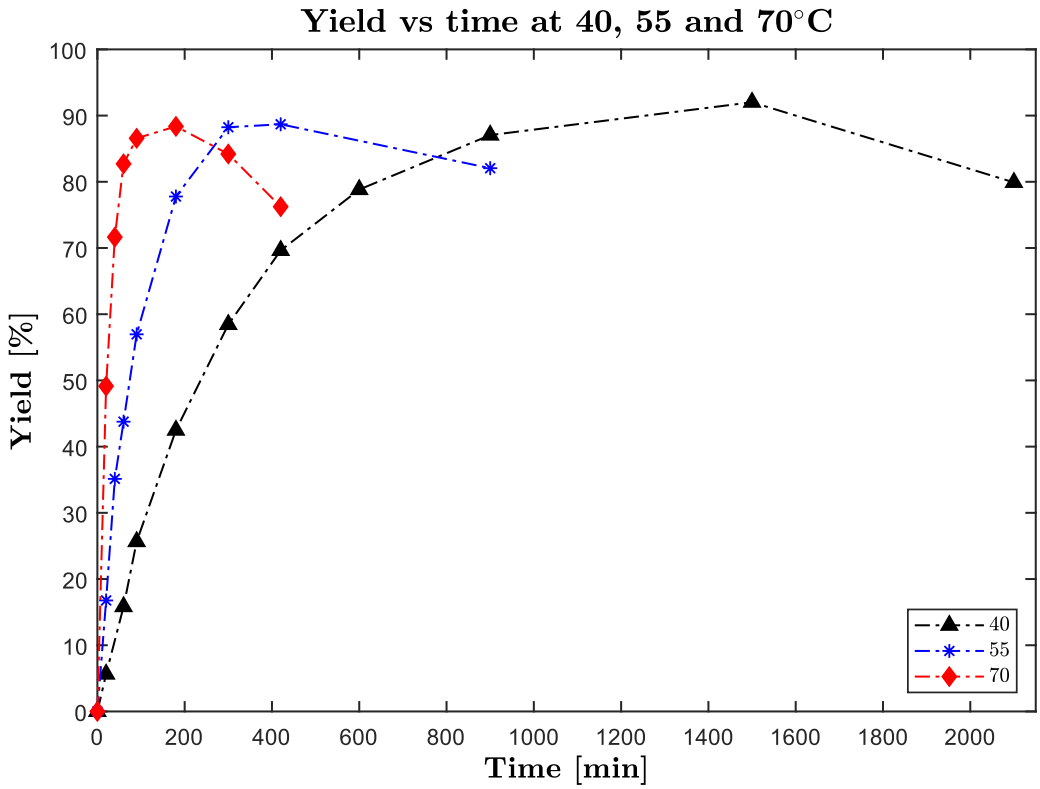

Figure 5.2. *Yield vs time curves of the epoxidation process in the calorimetric reactor. Temperatures 40°C (black triangles), 55°C (blues stars), 70°C (red diamonds). Points are joint only for clarity purposes.*

The system was modelled using a mathematical model in Matlab®, according to the approach exposed in Chapter 4.

Thermal profiles were collected for each test, hence as much as the points. However, the profiles considered for the thermal study are only the ones that describe the whole process, up to a value of conversion approximatively 100%. For this reason, this study considered tests at 70°C for 7 hours, 55°C for 15 hours and 40°C for 35 hours.

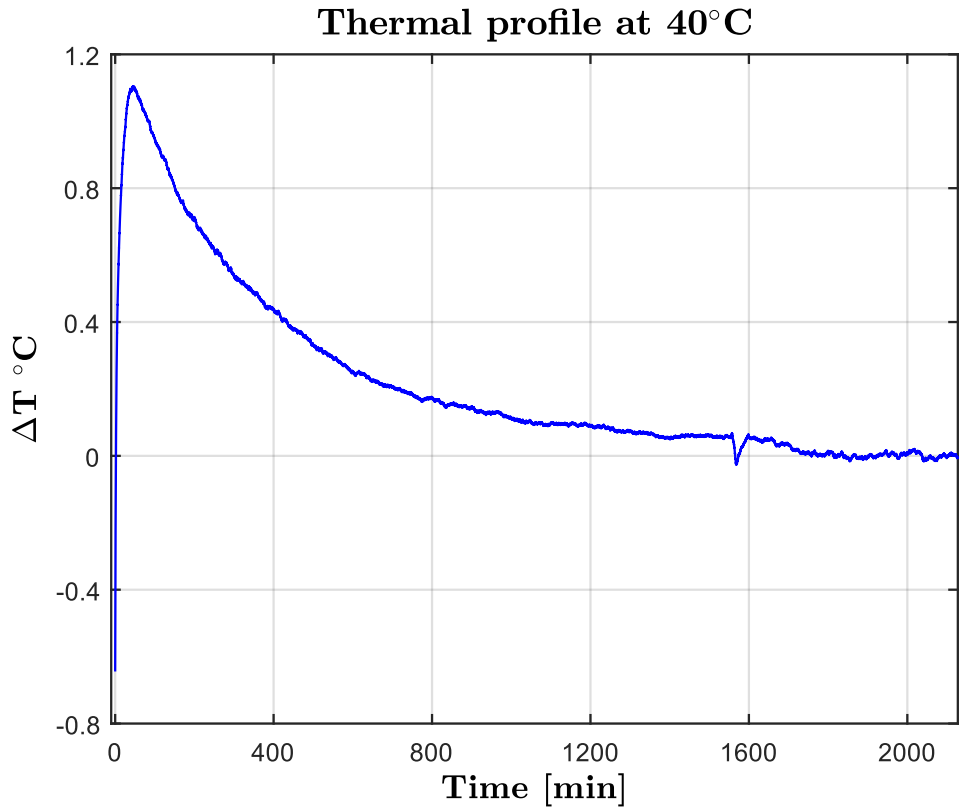

Figure 5.3. *Thermal profile vs time of a test at 40°C displayed as difference between the temperature of the reactor and the no-reaction thermal steady state.*

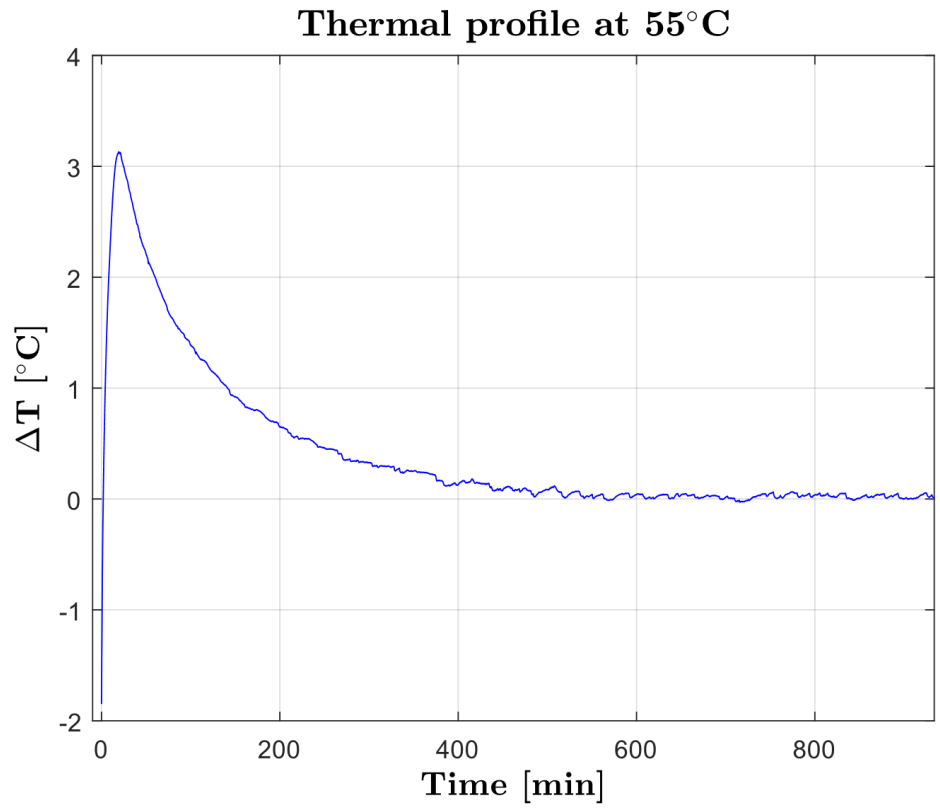

Figure 5.4. *Thermal profile vs time of a test at 55°C displayed as difference between the temperature of the reactor and the no-reaction thermal steady state.*

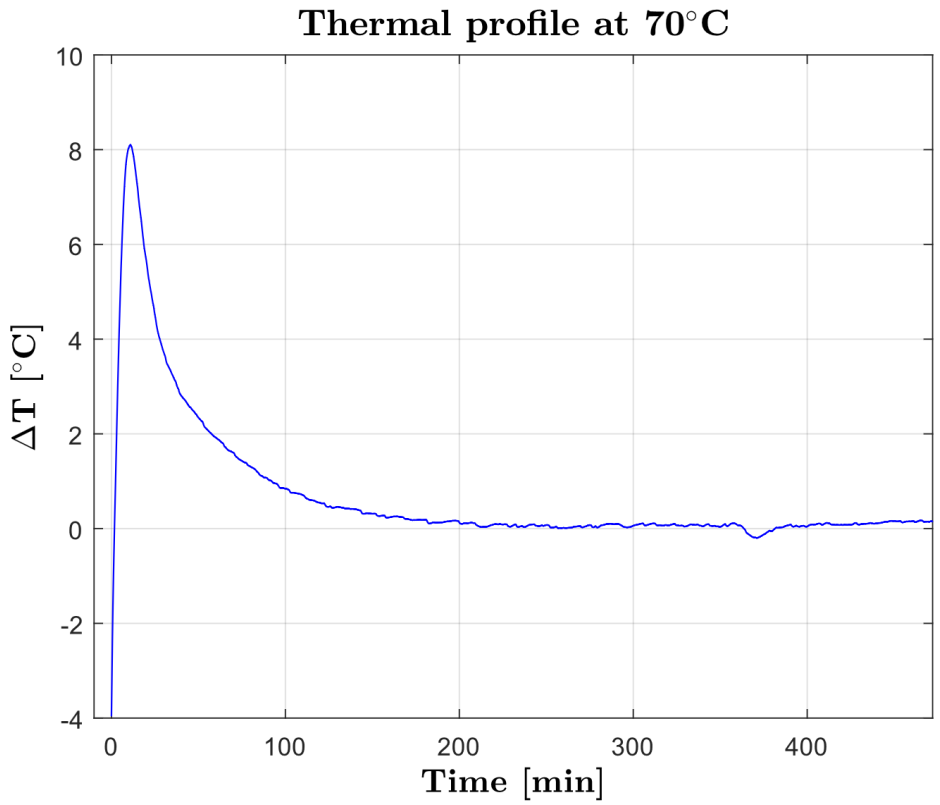

Figure 5.5. *Thermal profile vs time of a test at 70°C displayed as difference between the temperature of the reactor and the no-reaction thermal steady state.*

Thermal profiles in Figure 5.3-5.5 are displayed as difference between the temperature of the reactor and the no-reaction thermal steady state. Initial thermal overshoots highlight the strong exothermicity of the process, and pass from 1.1°C to 3.1°C and 8°C increasing the setpoint temperature from 40°C to 55°C and 70°C. This is due the increased kinetics, hence increased generated thermal power. Increasing the setpoint, temperature kinetics become faster, hence the generated thermal power is higher but the thermal overshoot extinguish faster because of the rapid consumption of the double bonds. The quality of the thermal profiles is good, and the shape of the curves is smooth, without excessive noise.

5.3 Kinetic and mass transfer modelling results

The mathematical system developed in §4.1 was implemented in Matlab®. Performing a multivariable fitting on experimental data, the kinetic parameters and mass transfer coefficient can be estimated. The fitting is performed minimising the residual error based on the concentration of epoxides, between experimental points and calculated ones, according to equation 5.1:

$$Err = \sum\left(C_{EP}^{experimental} - C_{EP}^{calculated}\right)^2 \quad 5.1$$

In particular, after optimisation, all the kinetic constants ($k_1, k_2, k_3, k_4, k_5, k_6$) and the two mass transfer coefficients β^w, β^o, can be determined. It is recalled that β^w, β^o are the product between the mass transfer coefficient and the interfacial area. To initialise the model, the initial concentration of the substances must be known, hence the concentration matrix C_i^j is reported in Table 5.2. The volume of the oil phase is 0.049 l whereas the aqueous phase is 0.042 l.

Figure 5.6 reports the experimental yield vs time curves, compared to the calculated profiles. Figure 5.7-5.9 report the concentration profile along the process time. The considered species in these plots are: acetic and peracetic acid in both phases, water in aqueous phase, hydrogen peroxide in aqueous phase, double bonds and epoxides in organic phase.

Table 5.2. *Concentrations of species in the organic and aqueous phases.*

Substance	Concentration aqueous phase [mol/l]	Concentration organic phase [mol/l]
Hydrogen peroxide	9.38	0
Acetic acid	3.13	0
Peroxyacetic acid	0	0
Water	32.90	0
Double bonds	0	4.54
Epoxides	0	0

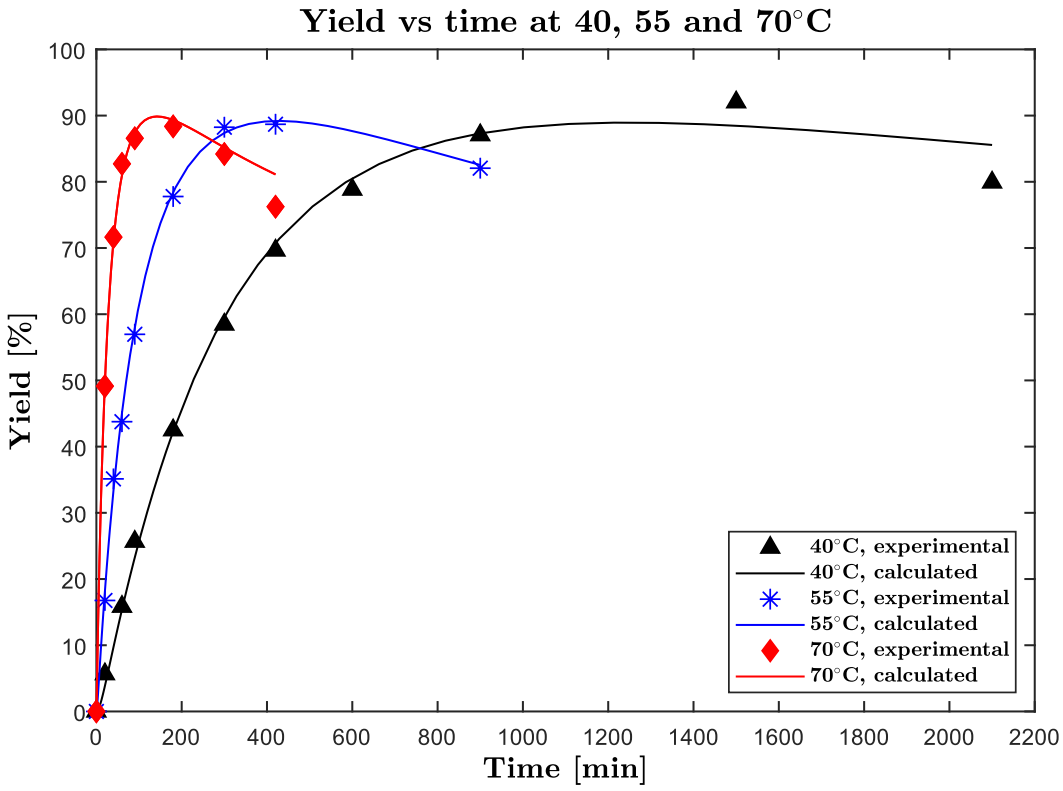

Figure 5.6. *Yield vs time curves (experimental and calculated) of the epoxidation process in the calorimetric reactor at different temperatures.*

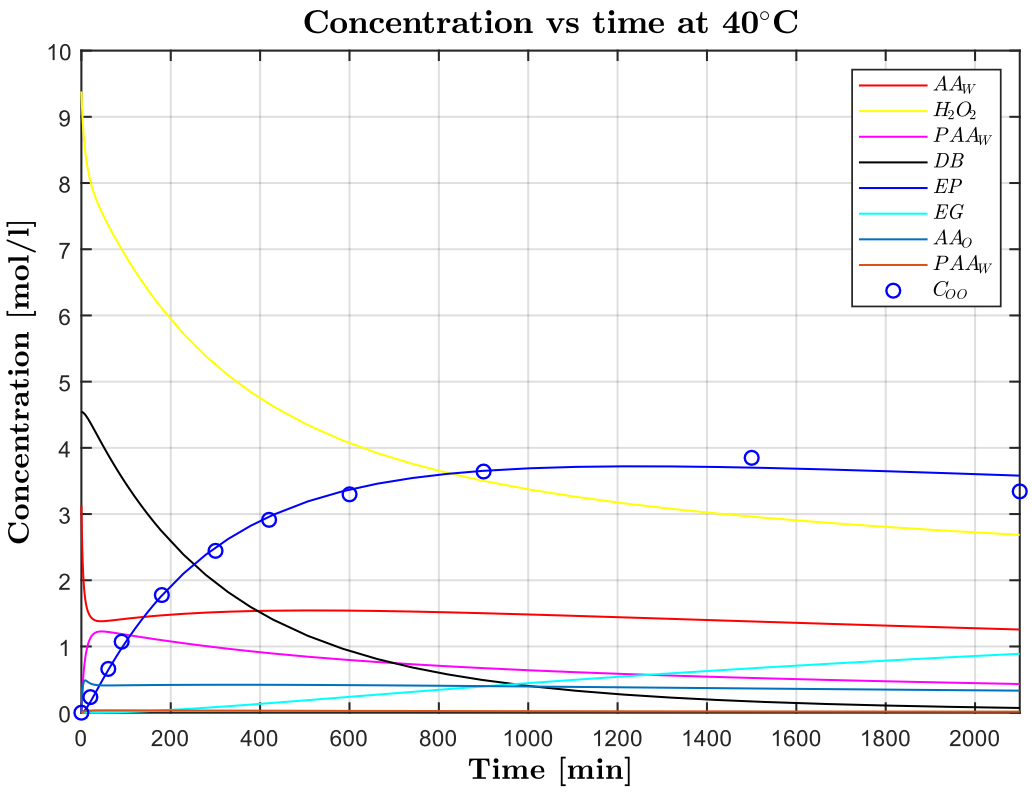

Figure 5.7. *Profile of concentration of the different species involved in the process at 40°C. The concentration of water is neglected.*

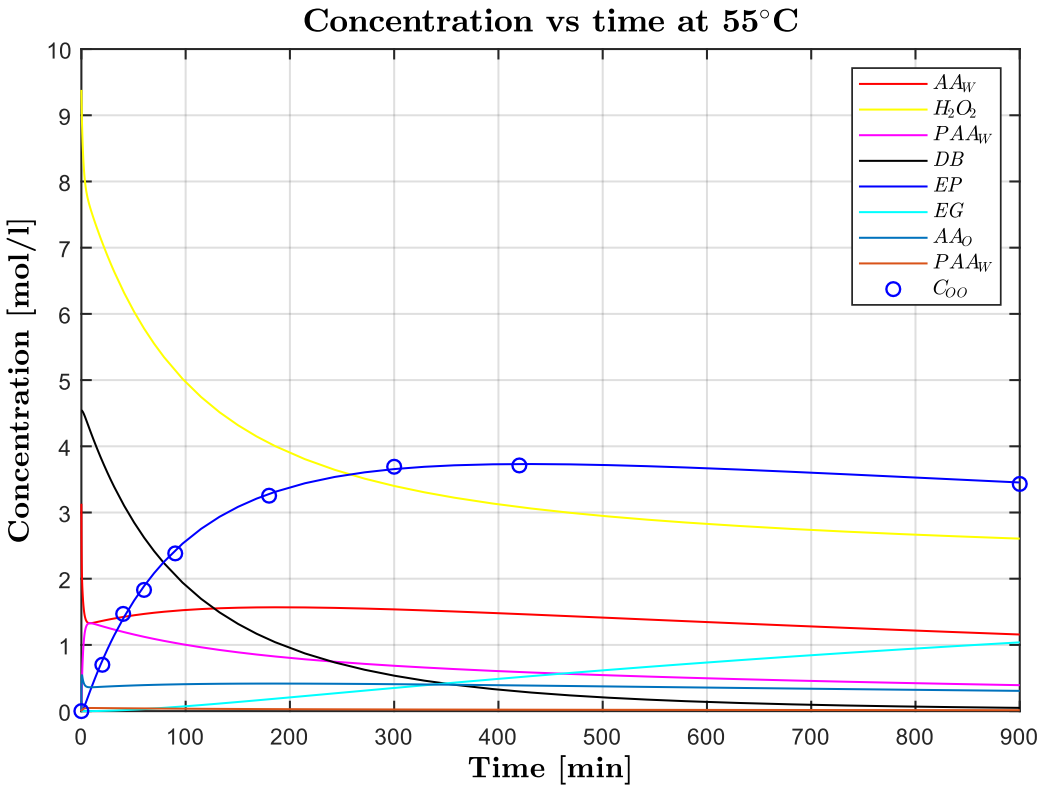

Figure 5.8. *Profile of concentration of the different species involved in the process at 55°C. The concentration of water is neglected.*

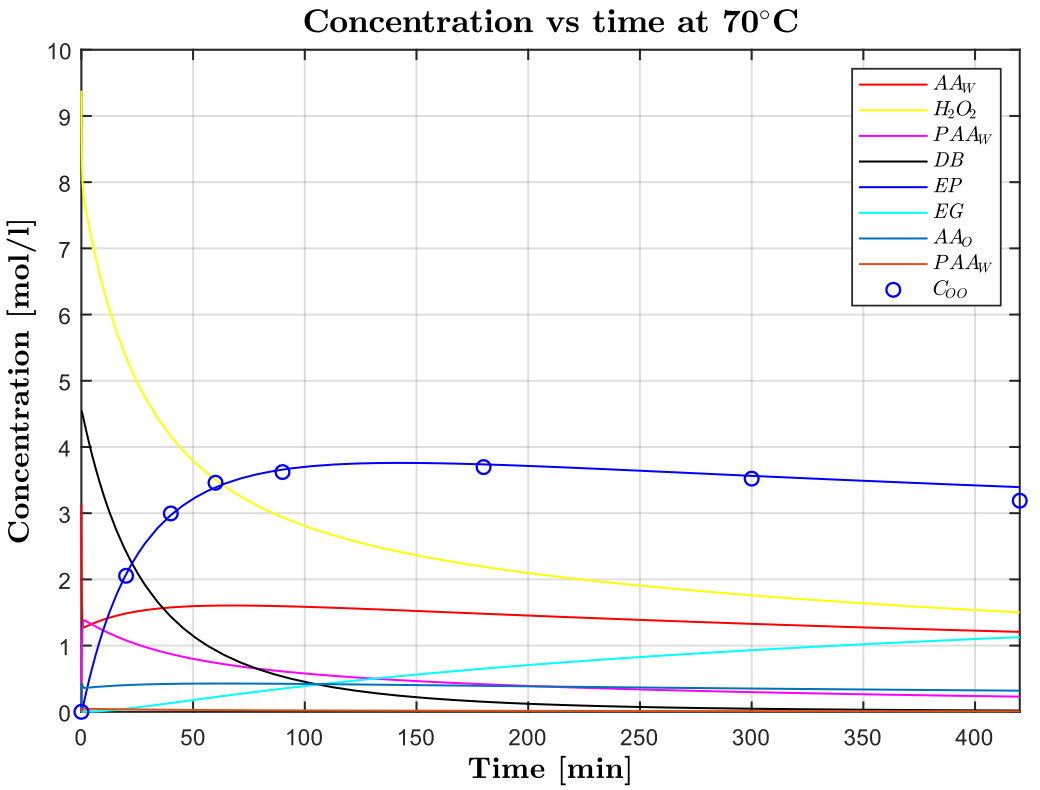

Figure 5.9. *Profile of concentration of the different species involved in the process at 70°C. The concentration of water is neglected.*

As can be seen from the experimental modelling, in all the three cases the fitting was performed with a very high accuracy and the coefficient of determination is very high, as indicated in Table 5.3.

Table 5.5. *Coefficient of determination of the fitting performed on the experimental data at 40, 55, 70°C.*

Temperature [°C]	Coefficient of determination R^2 [-]
40	0.996
55	0.999
70	0.999

In the three cases, the maximum yield was comparable (over 90%), whereas the time to reach the maximum strongly decreases from 25 to 3 hours simply increasing the temperature from 40 to 70°C. Since the selectivity is not strongly affected, the convenience to operate the process at high temperature is evident.

Figures 5.10-5.12 show that the difference of concentration of acetic and peracetic acid between bulk and interface is negligible at 40, 55 and 70°C, both in organic and inorganic phase. These are calculated results obtained by means of the model. Only at 40°C, in the early stages of the process the difference in concentration is a little higher (about 8%) than the previous cases, probably because at low temperature viscosity is higher, diffusivity is lower and so mass transport is more difficult.

Since the difference of concentration between bulk and interface is low, spatial gradients are low. Therefore, there are no mass transfer limitation and hence the process is kinetically controlled. This is an important result, since the process can be sped up changing the stirring velocity or improving mass transfer. This result is in line with Wu *et al.* [7], Santacesaria *et al.* [8]. Other authors simply assumed no mass transfer limitation, based on the Hatta number or other considerations, but without experimental validation [5], [9].

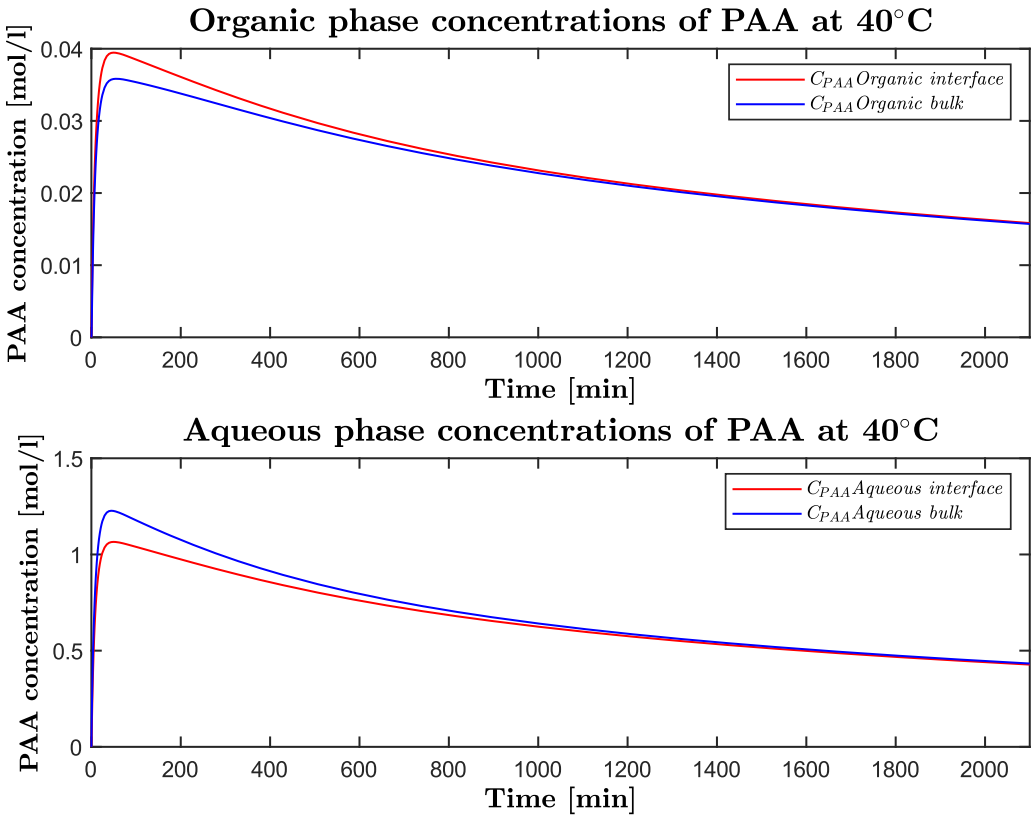

Figure 5.10. *Profiles of concentration of the peracetic acid in organic and aqueous phases at 40°C*

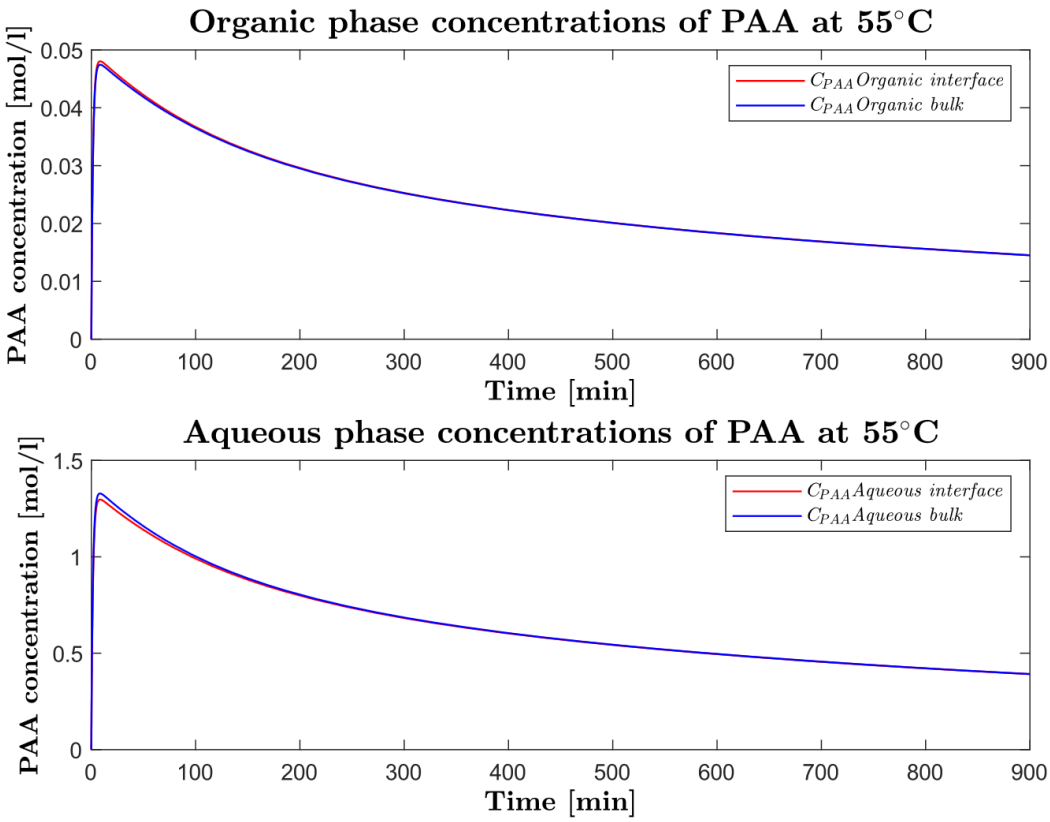

Figure 5.11. *Profiles of concentration of the peracetic acid in organic and aqueous phase at 55°C.*

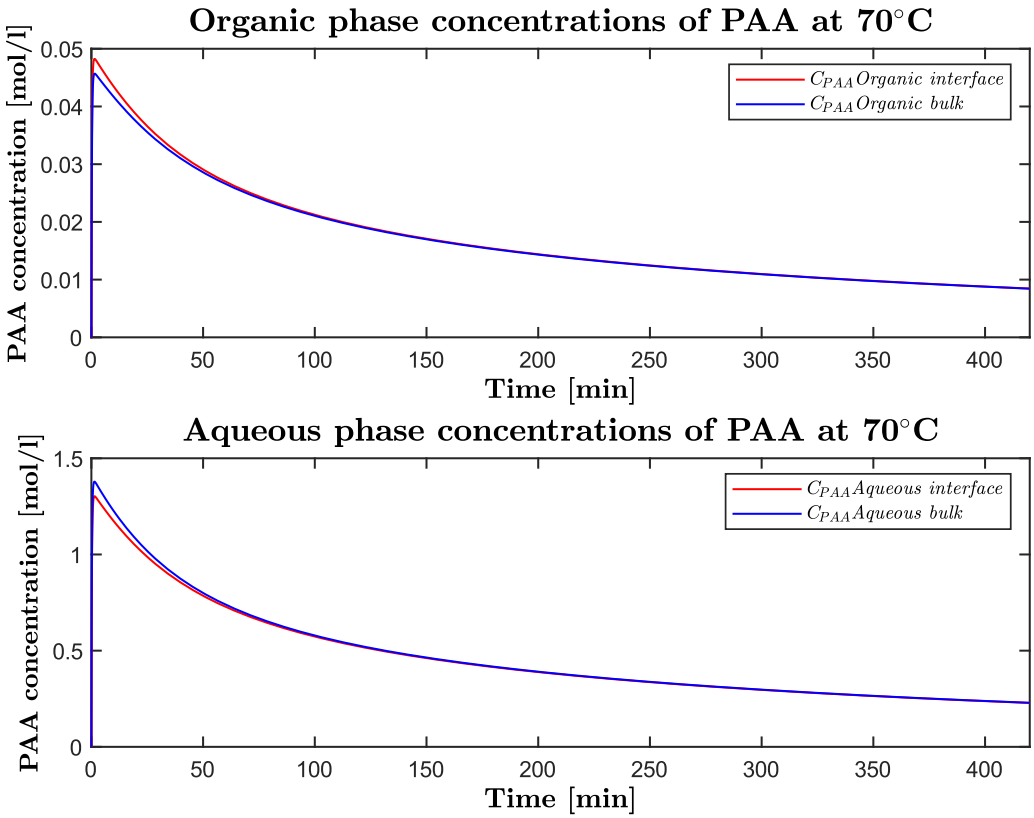

Figure 5.12. *Profiles of concentration of the peracetic acid in organic and aqueous phases at 70°C*

Since the control is kinetic, it is useful to understand which reaction is the rate determining step of the process. Figures 5.13-5.15 show the rate of reaction of formation of peracetic acid and epoxidation for all the three cases.

It is strongly evident that the rate determining step is the epoxidation of the double bonds. In fact, the formation of the peracetic acid is roughly 50 times faster than epoxidation. In all three cases, the formation of the peracetic acid at the early stages of the process is very fast and rapidly reaches equilibrium. In fact, as the concentration of the peracid increases, the inverse reaction becomes faster and faster. The equilibrium can be never reached because the peracid is continuously subtracted from the organic phase, in which it diffuses since it is continuously consumed by the epoxidation reaction.

This result is totally in contrast with the literature, excepts for Santacesaria *et al* [8] and Wu *et al.* [7]. The process can be simply sped up increasing the amount of acid catalyst (sulfuric acid), but this would also strongly promote the oxirane ring opening. Moreover, the post-process purification to wash the oil and bring the pH to neutrality would be more complex. For this reason, the amount of sulfuric acid was considered a best compromise, also according a previous work and other authors that can be found in the literature.

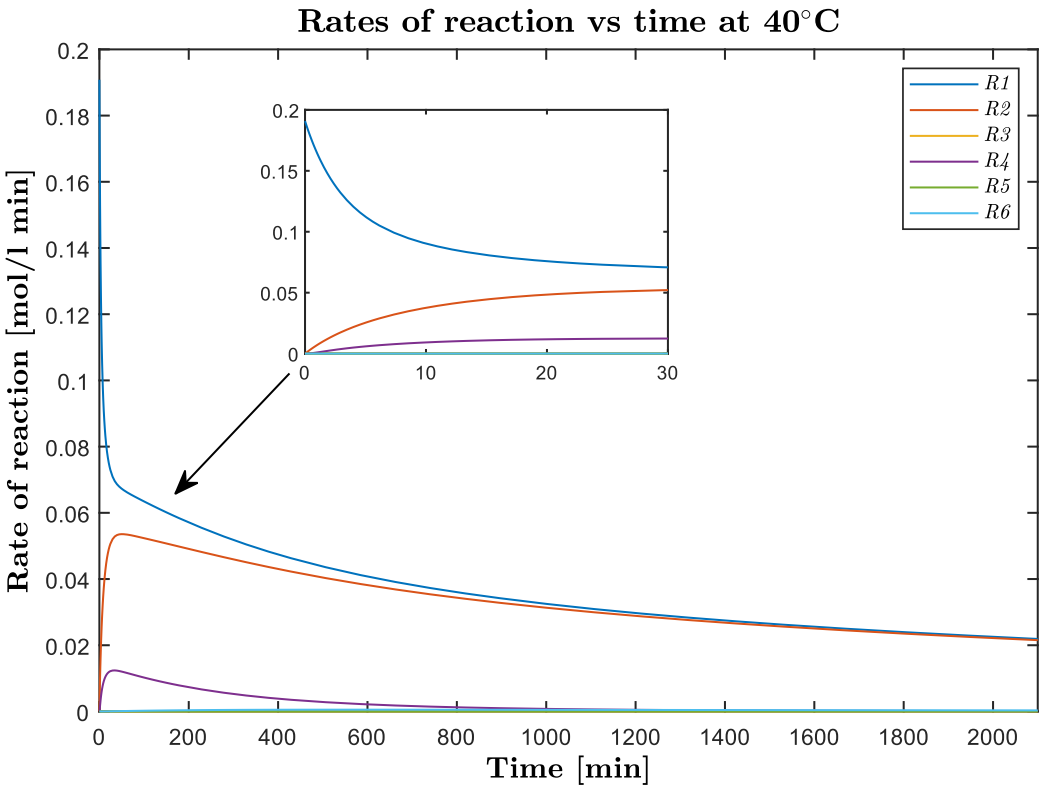

Figure 5.13. *Rate of reactions at 40°C.*

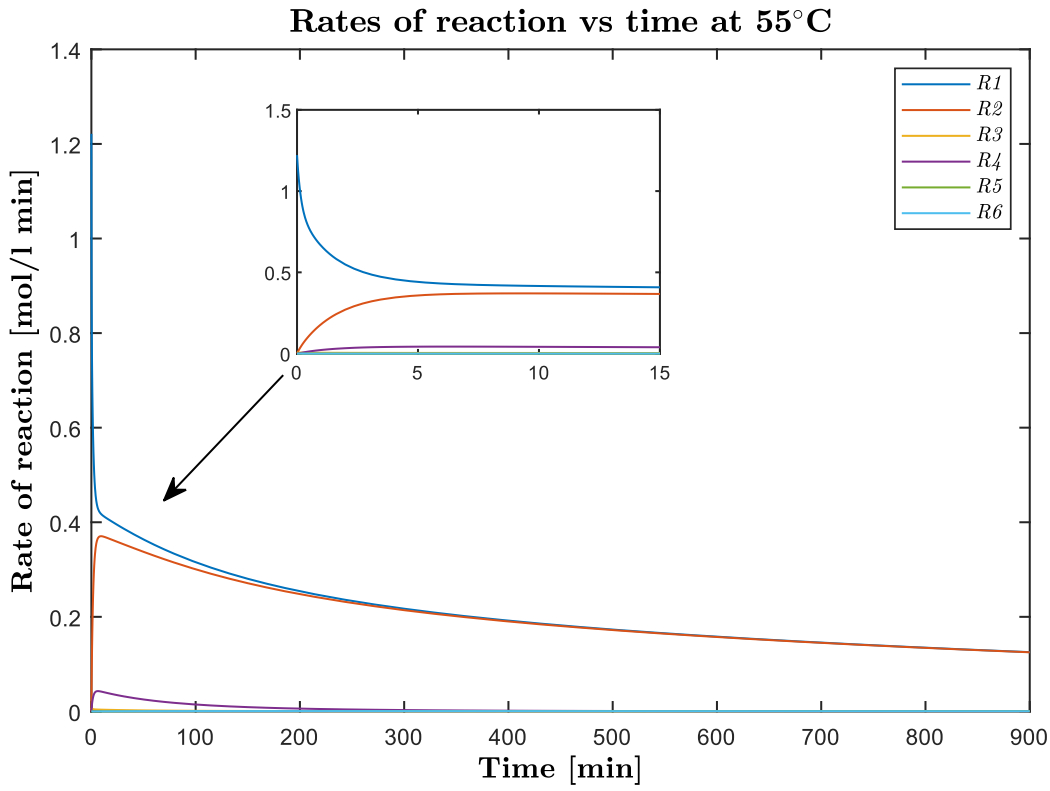

Figure 5.14. *Rate of reactions at 55°C.*

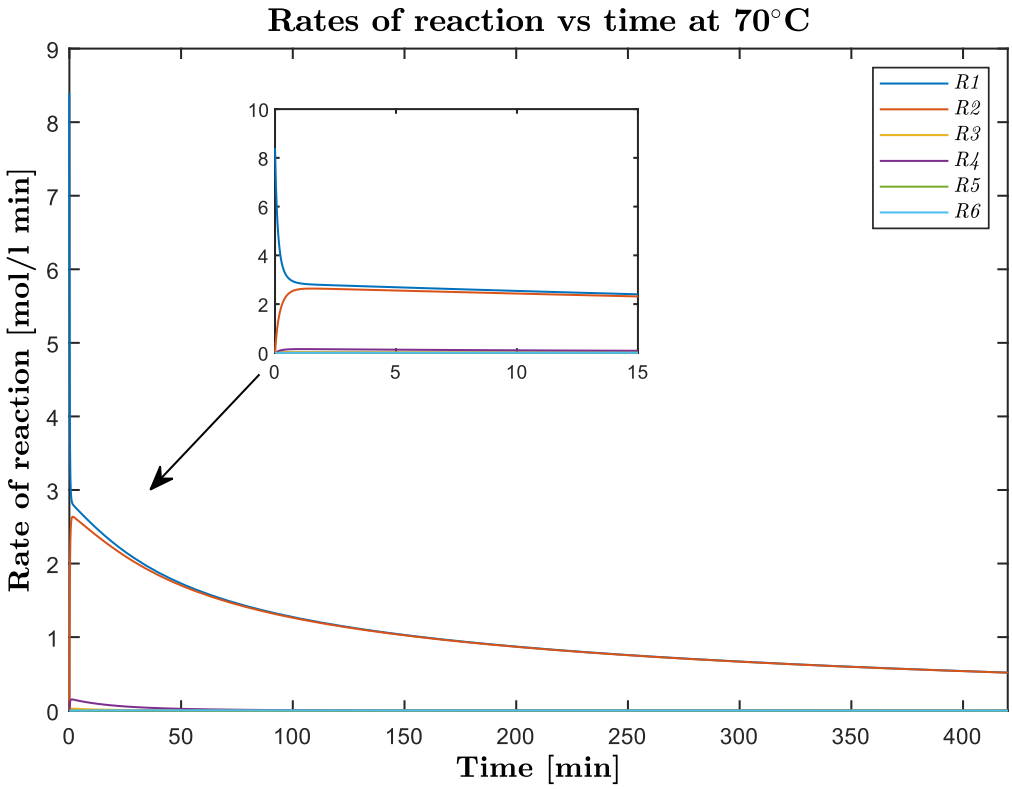

Figure 5.15. *Rate of reactions at 70°C.*

The estimated parameters are reported in Table 5.4.

Table 5.4. *Parameters estimated performing the modelling.*

Parameter	T=40°C	T=55°C	T=70°C	Unit
k_1	$6.49 \cdot 10^{-3}$	$4.94 \cdot 10^{-2}$	0.286	$l/(mol \cdot min)$
k_3	$5.25 \cdot 10^{-17}$	$4.57 \cdot 10^{-6}$	$1.71 \cdot 10^{-4}$	$l^{1.5}/(mol^{1.5} \cdot min)$
k_4	$8.38 \cdot 10^{-2}$	0.212	0.765	$l/(mol \cdot min)$
k_5	$2.99 \cdot 10^{-22}$	$3.49 \cdot 10^{-4}$	$5.51 \cdot 10^{-6}$	$l/(mol \cdot min)$
k_6	$5.83 \cdot 10^{-3}$	$9.69 \cdot 10^{-3}$	$4.91 \cdot 10^{-2}$	$l/(mol \cdot min)$
β^w	$8.82 \cdot 10^{-2}$	1.99	2.35	$1/min$
β^o	3.33	19.28	59.60	$1/min$

As a matter of fact, from table 5.5 it can be seen that all kinetics increase with temperature, as expected. Also mass transfer improves increasing the temperature. This can be due to a faster mass transfer resulting from a higher coefficient of diffusivity, or an increase of the interfacial area, since at high temperature the coalescence between droplets is reduced, according to Souza *et al*. [10].

About the epoxidation reaction, on the base of the kinetic constant estimated performing the modelling, the determination of the pre-exponential factor and of the activation energy was performed, considering the Arrhenius' equation:

$$k = A \cdot e^{-\frac{E_a}{R \cdot T}} \qquad 5.2$$

that can be expressed in the logarithmic form:

$$ln(k) = -\frac{E_a}{R} \cdot \frac{1}{T} + ln(A). \qquad 5.3$$

In this way the equation is a straight line and, performing a linear fitting on the calculated kinetic constants, the result is shown in Figure 5.16.
The estimated parameters are indicated in table 5.5.

Table 5.5. Parameters of the *Arrhenius' equation determined for this system for* k_4.

$A\ [l/mol \cdot min]$	$E_a[kJ/mol]$
$7.16\ 10^6$	65.79

The obtained results are similar to what found by Leveneur *et al.* [9], who found a value of 72.7 kJ/mol.

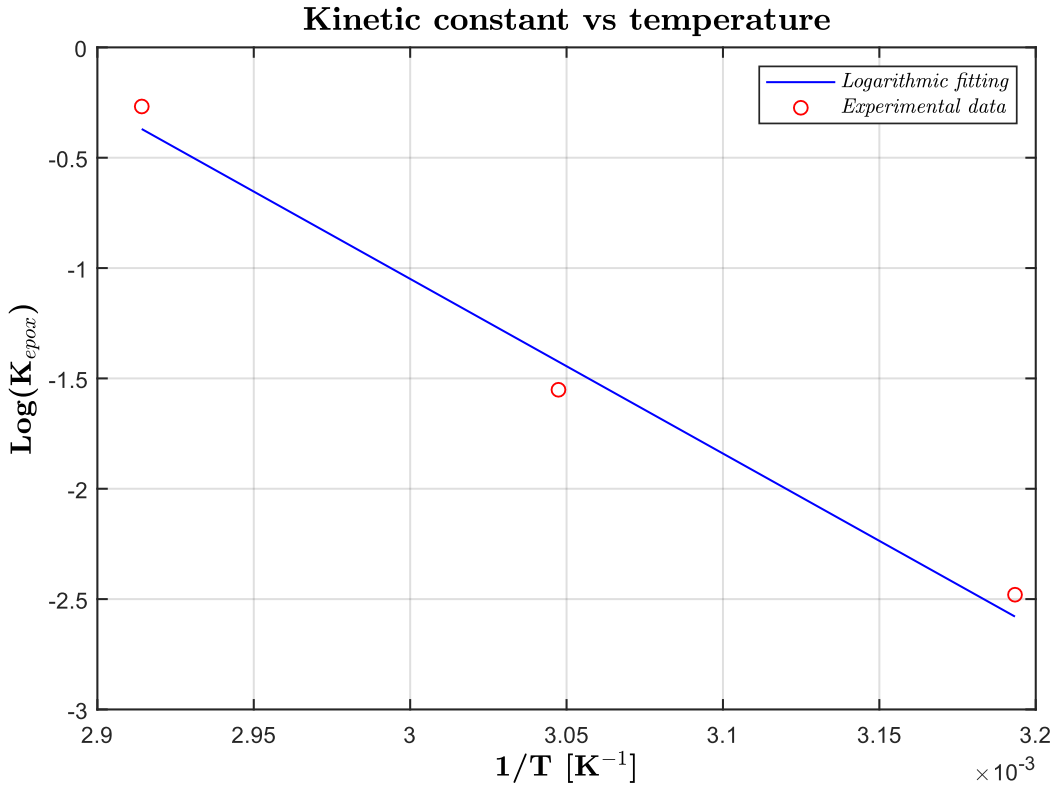

Figure 5.16. *Logarithmic fitting according Arrhenius' law of the experimental data of the kinetic constants of the reaction of the epoxidation reaction at different temperatures.*

5.4 Determination of the heat of reaction

In Chapter 3, an accurate method for the determination of the heat exchange coefficient, including thermal losses and effective heat capacity, was determined. On the base of the that study, it was possible to calculate the heat exchanged during the process. Since it is not possible to calculate the heat of reaction generated by each reaction, the total heat generated by the process is determined. This is comparable to the heat of reaction of the reaction of epoxidation, since other reactions give a negligible enthalpic contribution. Clearly, this is not the most accurate approach, but it is useful to have an estimation of the heat generated by the process, as implemented also by many authors, as De Quadros *et al.* [5] even though the determination of the heat exchange coefficient was sensibly less accurate. This data is useful for future works on scale up design to manage the thermal power produced by the process. The enthalpy is calculated by integration of the thermal profile on the time. The integration is carried out up to 7, 15 and 25 hours for the tests at 40, 55 and 70°C, as shown by Figures 5.3-5.5. It is assumed

that at this time duration the conversion of the double bonds is complete (100%). The results are reported in Table 5.6.

Table 5.6. Experimental determination of the enthalpy of reaction at different temperatures.

Temperature [°C]	Enthalpy [kJ/mol]
40	-292
55	-266
70	-270
Mean	**-276**

The mean value of the enthalpy is -276kJ/mol a value similar to data obtained by Santacesaria *et al.*[8] (-230 kJ/mol), but quite different from De Quadros *et al.* [5] (-196 kJ/mol) and Leveneur *et al.* (-116 kJ/mol).

5.5 Conclusions

Epoxidation in the calorimetric reactor was successfully implemented. The calorimetric reactor is a batch, jacketed, stirred reactor, equipped with a stack of thermocouples for accurate measurement of the temperatures. A preliminary homogeneity test was carried out to verify that no segregation phenomena take place, using a glass beaker with the same diameter of the reactor. The reaction mixture appears homogeneous, without segregation.

Experimental data were collected at different times and different temperature to obtain the yield vs time curves, parametric to the temperature. The maximum yield was always higher than 90%, and the time required to achieve this maximum reduces from 25 to 7 and 3 hours increasing the temperature from 40°C to 55°C and 70°C. At 70°C the degradation is quite fast, hence particular attention should be paid for this aspect at the industrial scale.

A detailed biphasic mathematical model was implemented in Matlab®, performing a fitting on the experimental data with good accuracy. By means of the modelling, several results were obtained. The system did not have mass transfer limitation for all three temperatures. The concentration profiles of the peracetic acid along time of the bulk and the interface are comparable, hence spatial concentration gradient are low. This is valid for both phases.

Moreover, the rate determining step was the perhydrolysis reaction, i.e. the formation of the peracetic acid. This step is about 50 times faster than the epoxidation, and this result is an important novelty. Consequently, the process is controlled only by the epoxidation.
Also a thermal study was carried out, and the thermal profiles were collected and integrated along time. Once the heat exchange coefficient was preliminary evaluated, the heat of reaction was determined, giving a value of -276 kJ/kg and it is in the order of magnitude of the value that can be found in the literature.

Bibliographic references

[1] Piccolo D., "Epoxidation of soybean oil by conventional and non-conventional methods", *Master Degree Thesis in Chemical and Process Engineering*, University of Padova, 2016.

[2] C. Vianello, D. Piccolo, E. Salzano, and G. Maschio, "Preliminary study of epoxidation of soybean oil in stirred tank reactor: The effect of the mixing program," *Chem. Eng. Trans.*, vol. 57, no. 2015, pp. 1051–1056, 2017.

[3] C. Vianello, D. Piccolo, A. Lorenzetti, E. Salzano, and G. Maschio, "Study of soybean oil epoxidation: effects of sulfuric acid and the mixing program," *Ind. Eng. Chem. Res.*, vol. In press, 2018.

[4] E. Santacesaria, R. Tesser, M. Di Serio, R. Turco, V. Russo, and D. Verde, "A biphasic model describing soybean oil epoxidation with H2O2 in a fed-batch reactor," *Chem. Eng. J.*, vol. 173, no. 1, pp. 198–209, 2011.

[5] J. V. de Quadros and R. Giudici, "Epoxidation of soybean oil at maximum heat removal and single addition of all reactants," *Chem. Eng. Process. Process Intensif.*, vol. 100, pp. 87–93, 2016.

[6] E. L. P. V. A. A. S. M. Kresta, *Handbook of Industrial Mixing: Science and Practice*. John Wiley & Sons, 2003.

[7] Z. Wu *et al.*, "Mass transfer and reaction kinetics of soybean oil epoxidation in a formic acid-autocatalyzed reaction system," *Can. J. Chem. Eng.*, vol. 94, no. 8, pp.

1576–1582, 2016.

[8] E. Santacesaria, R. Tesser, M. Di Serio, R. Turco, V. Russo, and D. Verde, “A biphasic model describing soybean oil epoxidation with H 2O 2 in a fed-batch reactor,” *Chem. Eng. J.*, vol. 173, no. 1, pp. 198–209, 2011.

[9] S. Leveneur, J. Zheng, B. Taouk, F. Burel, J. Wärnå, and T. Salmi, “Interaction of thermal and kinetic parameters for a liquid-liquid reaction system: Application to vegetable oils epoxidation by peroxycarboxylic acid,” *J. Taiwan Inst. Chem. Eng.*, vol. 45, no. 4, pp. 1449–1458, 2014.

[10] W. J. Souza *et al.*, “Effect of water content, temperature and average droplet size on the settling velocity of water-in-oil emulsions,” *Brazilian J. Chem. Eng.*, vol. 32, no. 2, pp. 455–464, 2015.

Chapter 6

Epoxidation under microwave heating

In this chapter, the effect of microwave (MW) heating in the process is studied. For this purpose, two reactors were set up, both with the same geometry in order to make the comparison of the tests as rigorous as possible (§2.1.2 - §2.1.3). Experiments were carried out on the two batch reactors using different heating sources: a MW multimodal reactor and a conventional heating reactor heated by a thermostatic bath. The time of reaction starts from the end of the heating transient (10 minutes).

6.1 Experimental results

The quantities of the reactants used for the tests are indicated in Table 6.1.

Table 6.1. *Table of the quantities of all the reactants.*

Reactant	Mass [g]
Soybean	10
Acetic acid	1.659
Hydrogen peroxide	8.041
Sulfuric acid	0.3

The total mass was equal to 20 g for each test. The concentration of the reactants is the same for both the MW and conventional reactors, and is based on the optimization determined in Chapter 4 for the calorimetric reactor.

In the case of MW heating, Leveneur *et al* [1] demonstrated that changing the amount of the reactants and increasing the percentage of aqueous phase is particularly effective. In fact, MW field mainly targets the aqueous phase, hence the system is particularly sensible to the aqueous phase amount. The percentage of aqueous phase is a variable that must be taken into

consideration in process optimization. In this case, this variable was fixed to have the same concentrations of the conventional heating reactor and of the calorimetric reactor.

6.1.2 Effect of stirring velocity

The effect of stirring velocity was studied in both cases of MW and conventional heating. Tests were performed for 3 hours at 60 °C. The results are shown in Figure 6.1. In the case of conventional heating (Figure 6.1), the velocity was varied from 100 to 650 rpm. At low stirring velocity (100 rpm), the yield of epoxides is very low (about 10%). The threshold stirring velocity is in the range of 250-300 rpm, as in the case of Leveneur *et al* [1] and similar to [2]. At a lower stirring velocity, the two phases are completely segregated and a good mixing cannot be achieved. Above this threshold, the yield noticeably increases, and remains approximately constant. This means that the stirring velocity does not significantly influence the process, that a good mass transfer is reached, and that the process is kinetically controlled. Values of stirring velocity higher than 300 rpm permits to properly perform the process. A value next to 450rpm could be considered a value sufficiently higher than the threshold. Moreover, it is recalled that high stirring velocities promote the formation of by-products since the epoxidized oil is more exposed to acid and water, which are responsible of the epoxy ring opening [3].

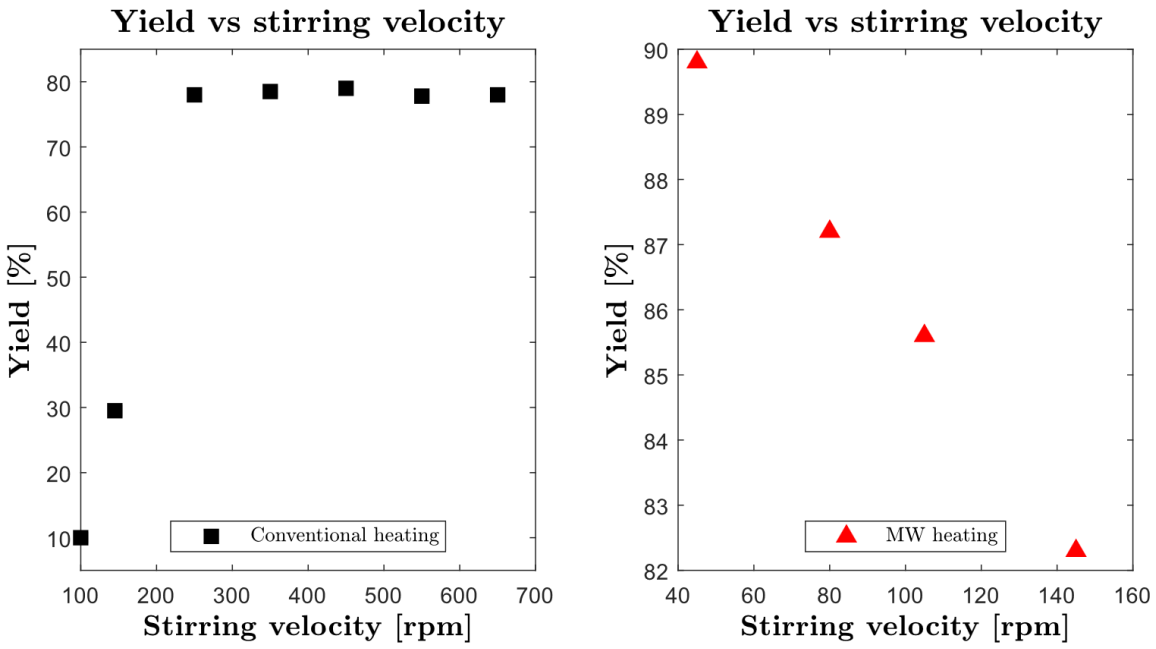

Figure 6.1. *Yield vs stirring velocity, conventional and MW heating tests. Time: 3 hours. Temperature: 60 °C.*

In the case of MW heating (Figure 6.1), the stirring velocity was varied between 45 and 150 rpm. The yield of the epoxides is always higher than 80% (explaining the different ranges for the y-axes). The results show that the maximum yield can be obtained at very low stirring velocity (45 rpm) and that the yield decreases with increasing stirring velocity.

a)  b) 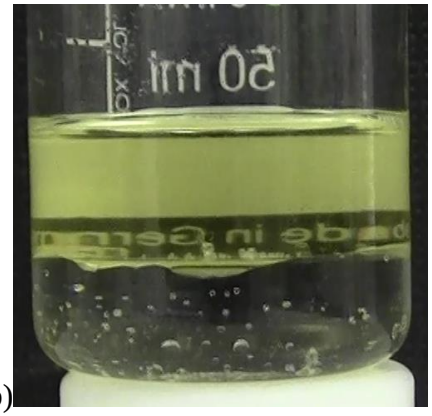

Figure 6.2. *Images of the reaction mixture taken as soon as the process was shut down, at 70°C and 45 rpm: a) MW process, b) conventional process.*

At a visual observation, it is evident that the MW field can create a uniform fine suspension even with such a weak agitation. In Figure 6.2 a comparison between the suspension of the MW and conventional tests is shown. Pictures were taken at the end of the process (90 minutes, 70°C, 45 rpm). This suspension cannot be achieved by the only simple action of the stirrer in the conventional heating at this very low stirring velocity. In fact, at 45 rpm the two phases remain segregated because the stirring velocity is so low and dispersion is not possible. In this case, only above-threshold velocities generate good suspensions. This could be due to the selective MW heating that mainly targets the aqueous phase, thus reducing the surface tension and easing the creation of the suspension. This is an important novelty because a uniform suspension between oil and aqueous phase can be created using MW heating whereas the impeller seems to affect its stability. To further investigate this aspect, the yield vs time curves were obtained at 60°C at different stirring velocities (45 and 145 rpm) to understand the effect of the impeller velocity (Figure 6.3).

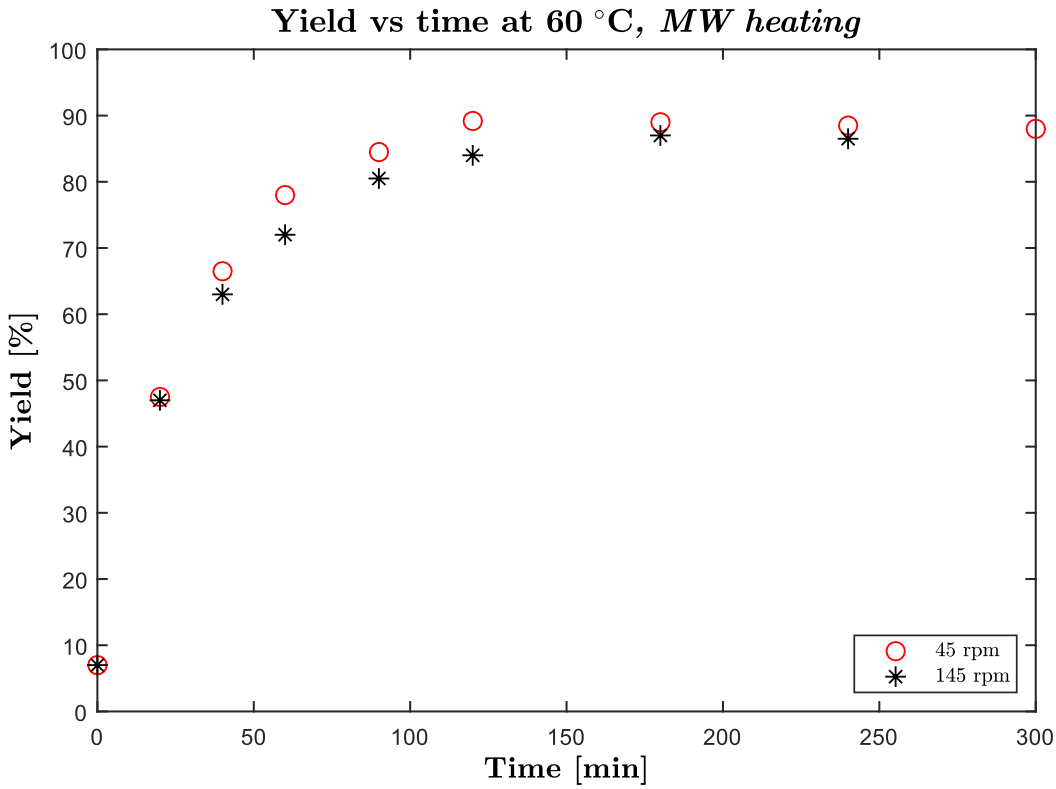

Figure 6.3. *Yield vs time curves obtained by MW heating at two different stirring velocities: 45 rpm (stars), 145 rpm (circles).*

The yield vs time curves in Figure 6.3 demonstrate that an increase in stirring velocity is not beneficial for the process, both in terms of rate of reaction and selectivity from the beginning to the end. In this range of stirring velocity, the impeller does not contribute to the creation of the suspension (as this would require at least 300 rpm), but could promote the coalescence between droplets (as it happens in a clarifier/fluocculator) in the suspension created by the MW field. Given the below-threshold stirring velocity, and the observations from Figure 6.2, the conclusion is that the contribution of the impeller in the formation of the suspension is negligible. To summarize, in the conventional process the optimal stirring velocity is at about 450 rpm, whereas in the case of MW process is at 45 rpm. The MW process needs a much weaker stirring (one order of magnitude less) with good opportunities for energy savings. In fact, a lot of energy for vigorously mixing the reactor is saved, since the stirring velocity is noticeably lower. Moreover, MW heating always permits to save energy compared to conventional heating, because it targets only the aqueous phase, without heating walls, instrumentations etc.

The Reynolds number at 45 rpm a 450 rpm is in the order of 150 and 1500 respectively. This means that at 45 rpm the system is perfectly laminar whereas at 450 rpm the fluid dynamics is in a case between the transition and the turbulent regime.

6.1.3 Effect of the temperature

Different temperatures were tested, 50, 60 and 70°C. The stirring velocity was chosen at the optimum that was determined in the previous tests, so 45 and 450 rpm for MW and conventional heating, respectively. All the tests were repeated in the case of MW and conventional heating (Figure 6.4-6.6).

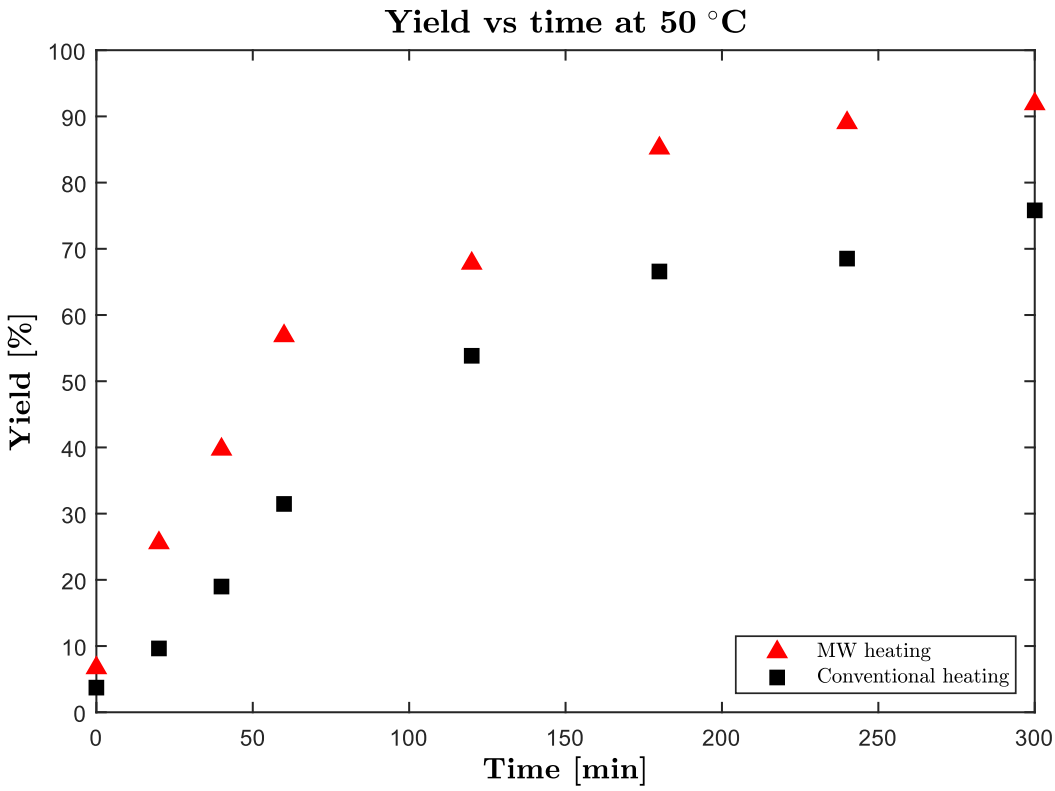

Figure 5.4. Yield vs time curves at 50°C in conventional and MW heating systems.

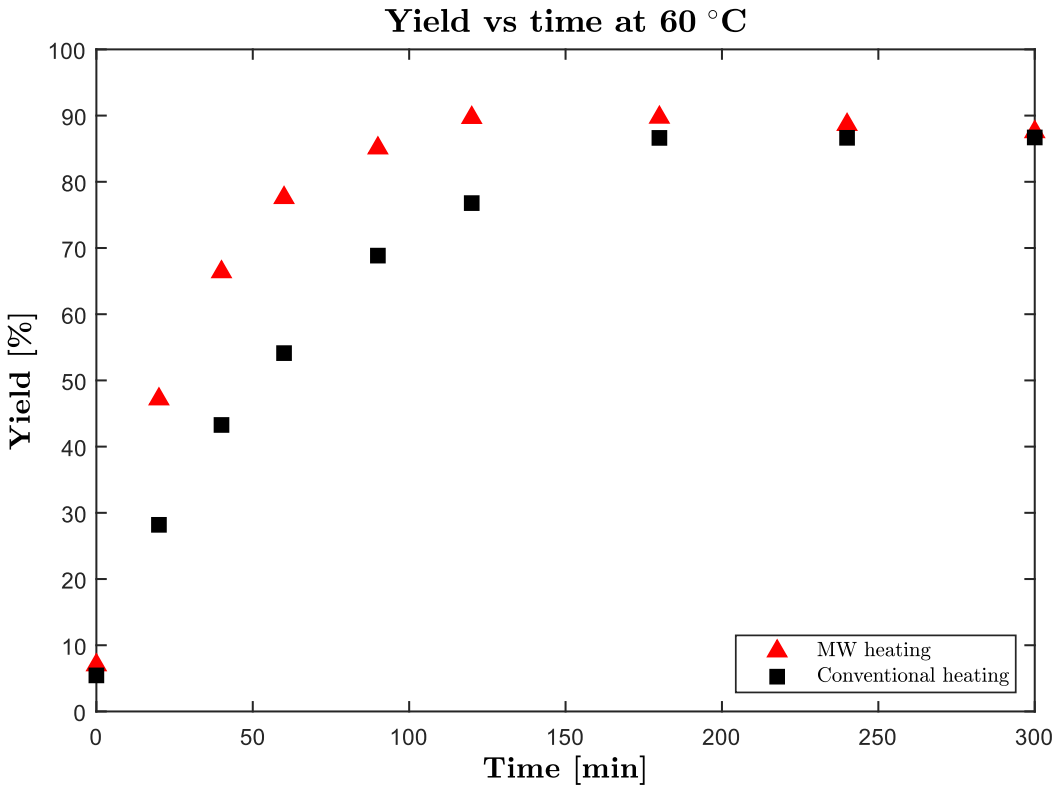

Figure 6.5. Yield vs time curves at 60°C in conventional and MW heating systems.

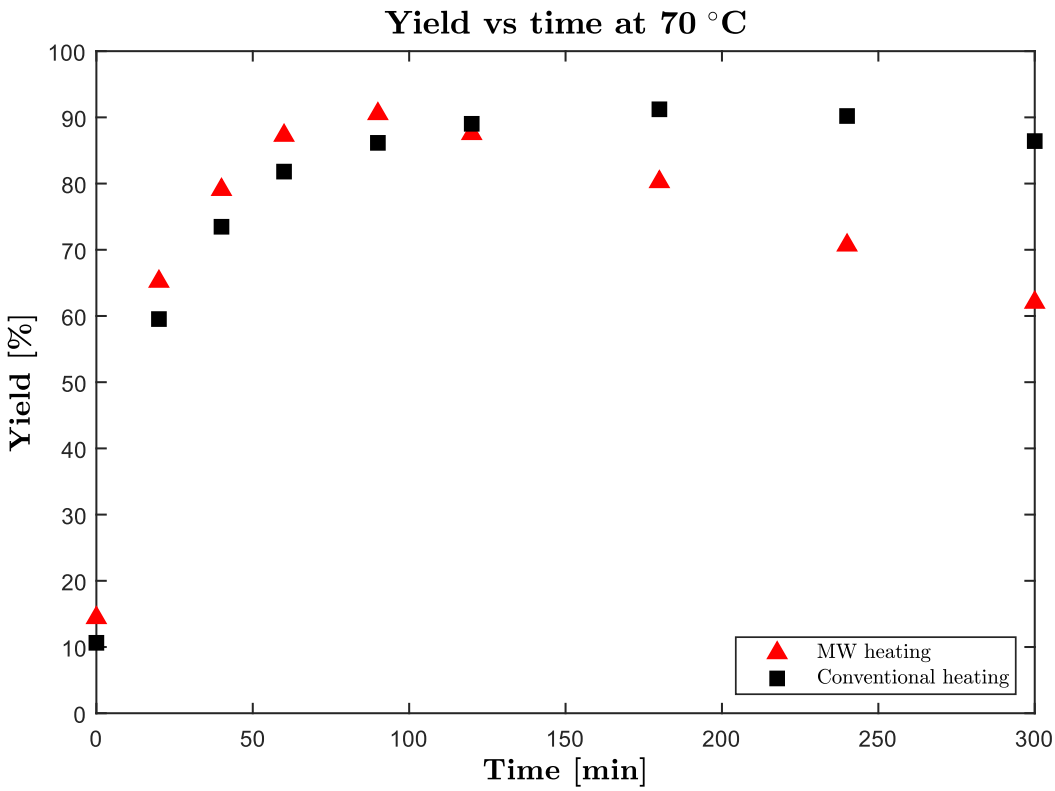

Figure 6.6. Yield vs time curves at 70°C in conventional and MW heating systems.

At 70°C, in the case of conventional heating, the time to maximum yield is slightly more than 3 hours whereas the MW heating reduces it to 1 hour and 30 minutes. In this case, about 50% of time could be saved maintaining the same quality of the product (comparable yield). However, the process must be shut down exactly at the maximum because the epoxy opening is very fast. Therefore, MW heating permits to boost the entire process, including the undesired reaction, as highlighted also by Aguilera *et al.* [4], [5] and by Leveneur *et al.* [1]. MW in fact could strongly act on the reaction between hydrogen peroxide (unstable and strongly polar) and the acetic acid (polar), increasing the rate of reaction of the perhydrolysis step. The degradation of the epoxides is very fast, probably due to the fact that MW field particularly acts on water and acids, which are also responsible of the opening of the epoxy-groups. At 60°C the result is similar, and the maximum yield using conventional heating was at about 4 hours, whereas MW heating shortened the time to 2 hours, saving 50% of time. In this case the yield obtained by MW heating is even slightly higher. At these conditions, the epoxy ring opening is noticeably slower than the previous case, and the MW field allows saving time increasing both the selectivity and the yield. Finally, also the tests at 50°C show that higher rate of reaction in the case of MW with respect to the conventional case, even if the kinetics are very slow.

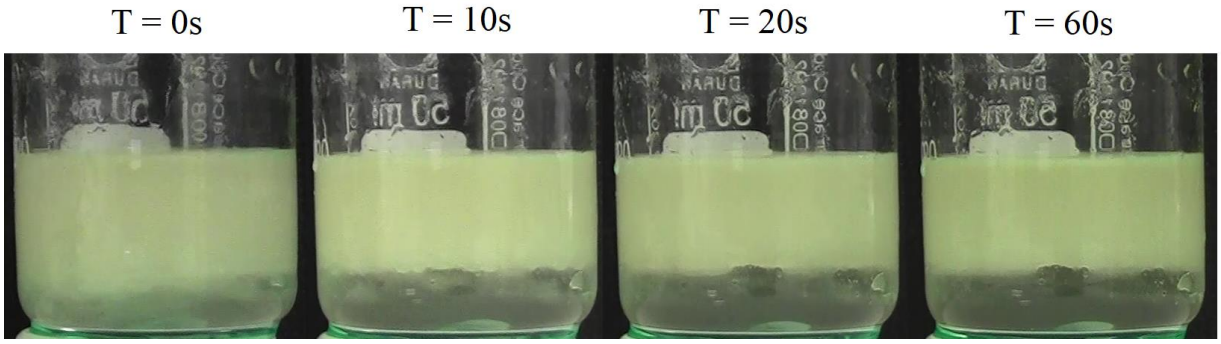

Figure 6.7. *Stability of the suspension after the process was stopped in the case of conventional process.*

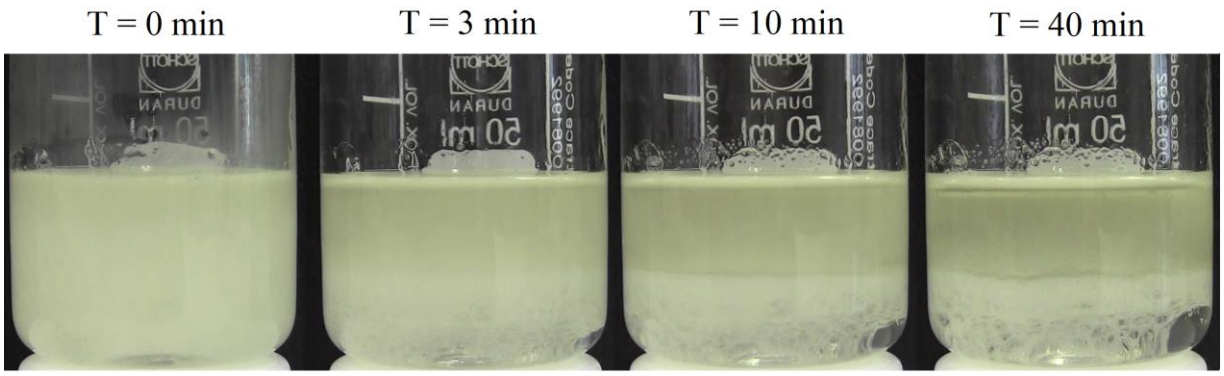

Figure 6.8. *Stability of the suspension after the process was stopped in the case of MWprocess.*

At 70°C, the stability of the suspension of the reaction mixture was assessed both for the conventional and the MW case after the process was stopped. Tests were performed at the stirring velocities and time durations previously identified (450 rpm and 180 minutes and 45 rpm and 90 minutes respectively) to check the system near the point of maximum yield. From Figure 6.8 it can be noticed that in the conventional process at 450 rpm a good dispersion is achieved, because the stirring velocity is one order of magnitude higher than that in Figure 6.2 and higher than the threshold velocity. However, in the conventional case segregation occurs in a few seconds, whereas in the case of the MW the mixture is quite stable for minutes (Figure 6.7-6.8). This can be due to the fact that in the case of the MW process the dimension of the droplets is lower and contributes to increase the stability of the suspension.

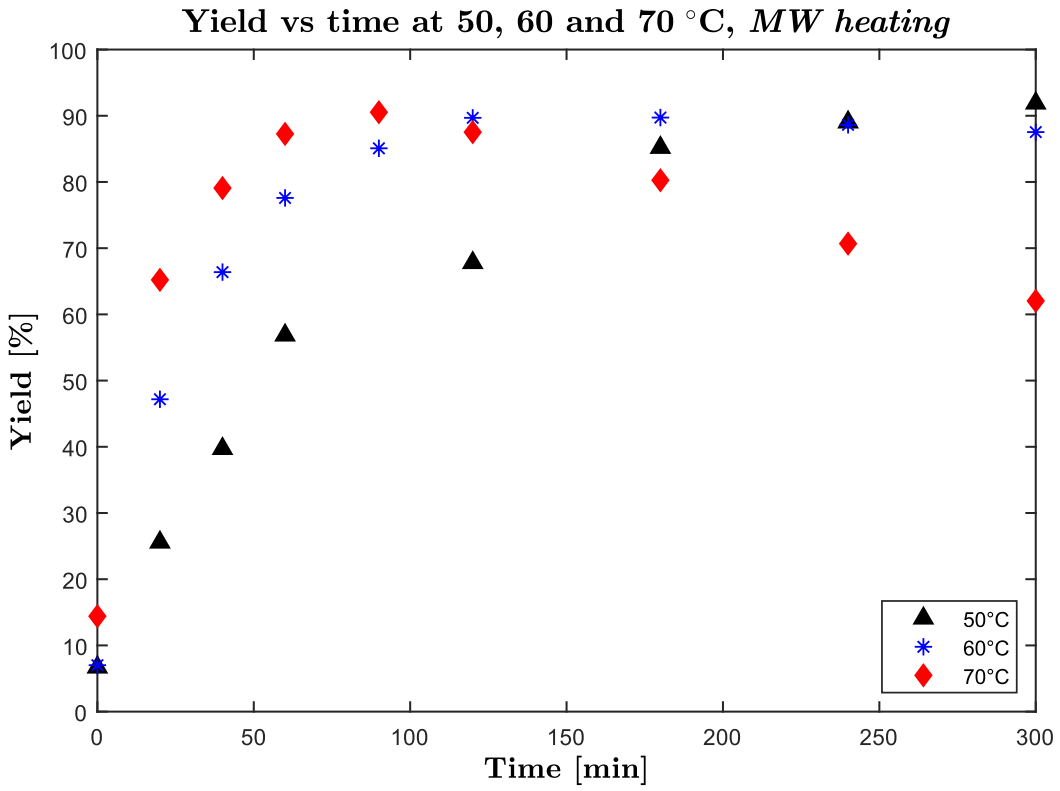

Figure 6.9. *Comparative representation of the yield vs time curves at different temperatures in the case of MW heating.*

In Figure 6.9 the comparison between the curves at 50, 60 and 70°C obtained by MW heating is reported. Increasing the temperature, the peaks of the maximum yield shift towards a lower time of reaction and the maximum value seems to not be affected by temperature. For this reason, the optimal temperature for the process seems to be 70°C even if the process must be shut down exactly at the maximum, otherwise the oxirane ring opening is quite fast. For this

reason, a good compromise between low time of reaction and slow degradation of the epoxides could fall in the range between 60 and 70°C. In this way, the time of reaction is between 90 and 120 minutes that is a great improvement than the conventional process.

6.2 Mathematical modelling

The mathematical approach followed in Chapter 4 was applied for the modelling of the data shown in this chapter. Mathematical modelling was performed for both cases of conventional and MW reactors. The fitting of the experimental data of the conventional reactor is shown in Figures6.10-6.15. Figures 6.10-6.12 report the fitting of the previous yield-vs time data. Figure 6.13-6.15 show the concentration time profiles.

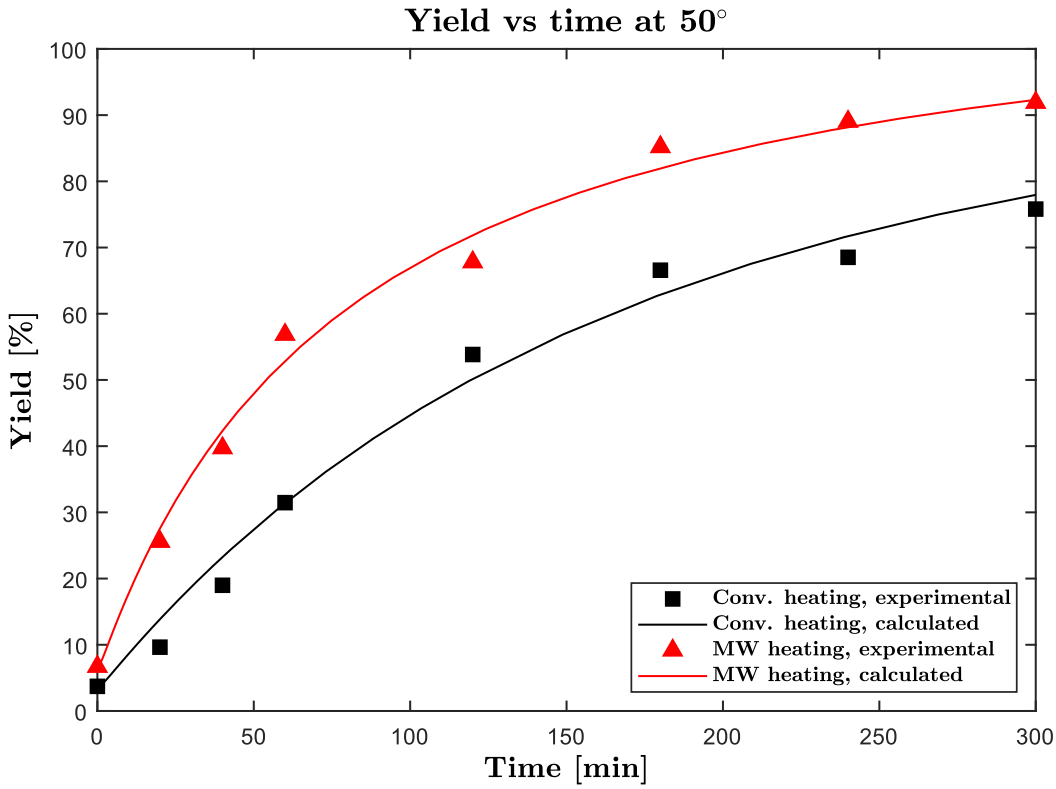

Figure 6.10. *Yield vs time curves at 50°C (experimental and calculated) in the case of conventional and MW heating.*

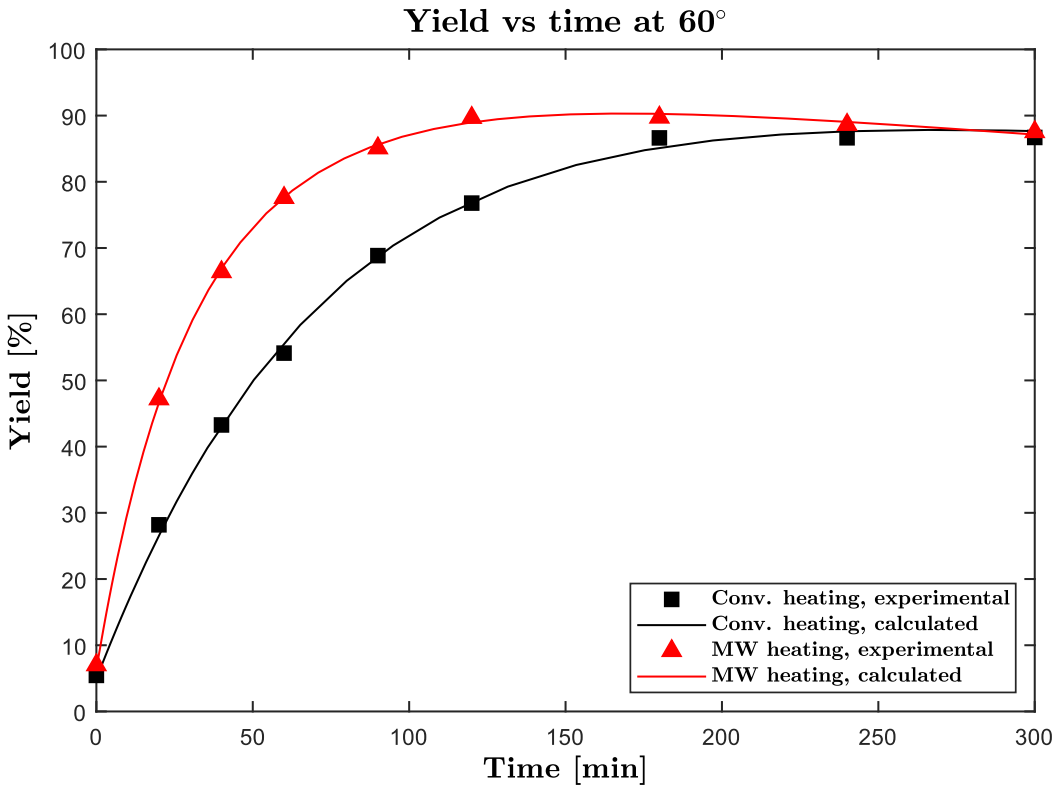

Figure 6.11. *Yield vs time curves at 60°C (experimental and calculated) in the case of conventional and MW heating.*

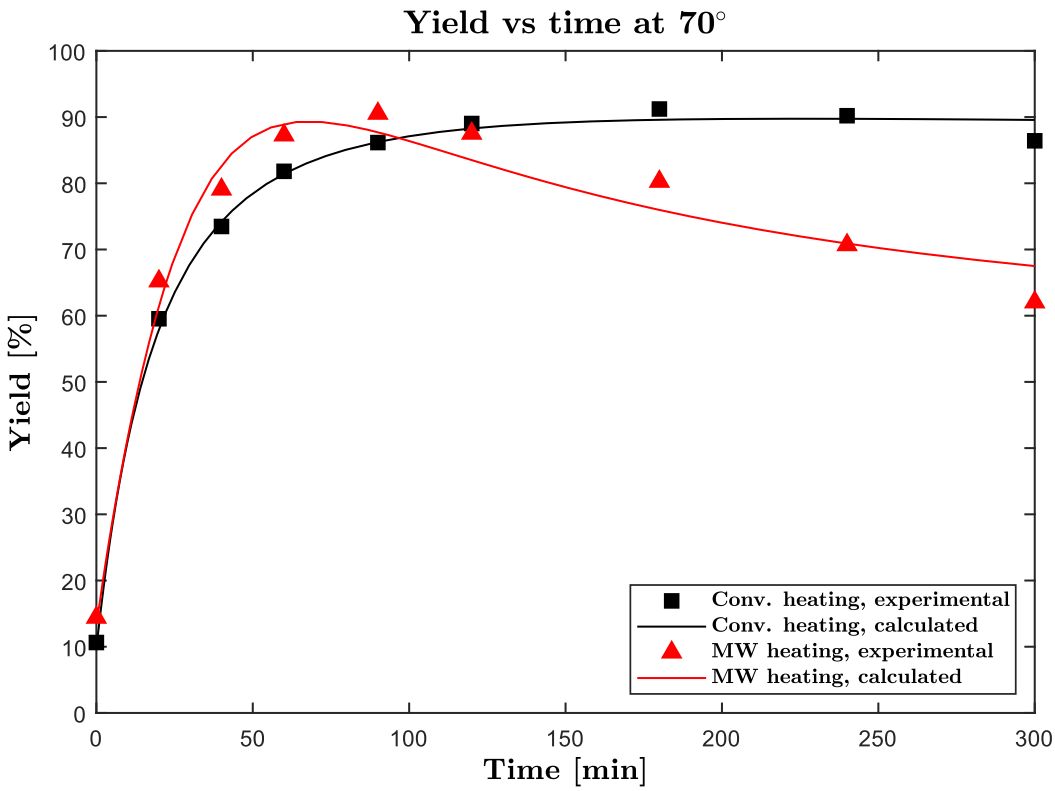

Figure 6.12. *Yield vs time curves at 70°C (experimental and fitted) in the case of conventional and MW heating.*

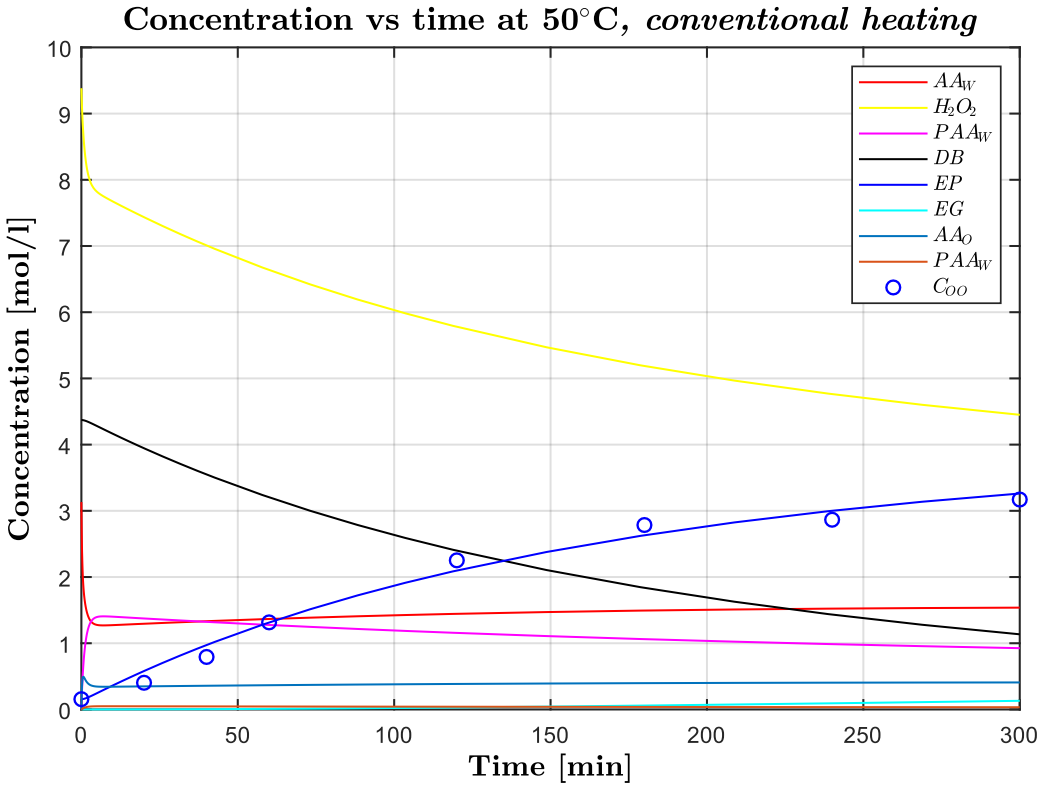

Figure 6.13. *Profile of concentration of the different species involved in the process at 50°C (conventional heating) and experimental point (circles). The concentration of water is neglected*

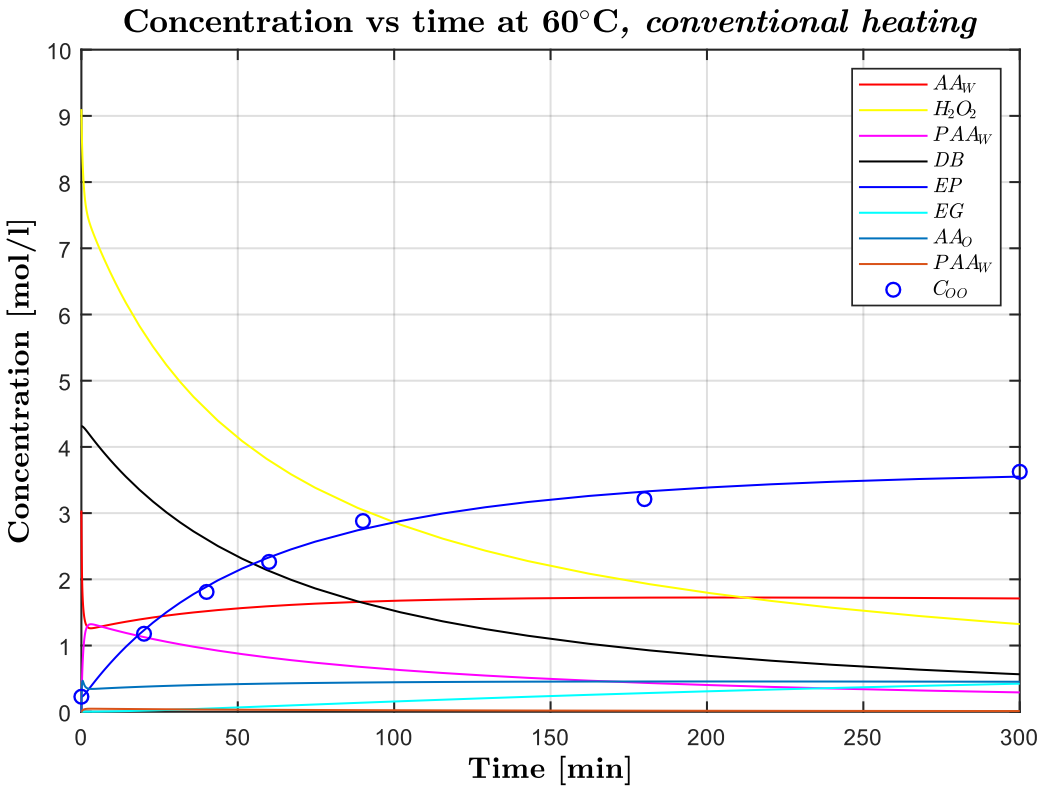

Figure 6.14. *Profile of concentration of the different species involved in the process at 60°C (conventional heating) and experimental point (circles). The concentration of water is neglected*

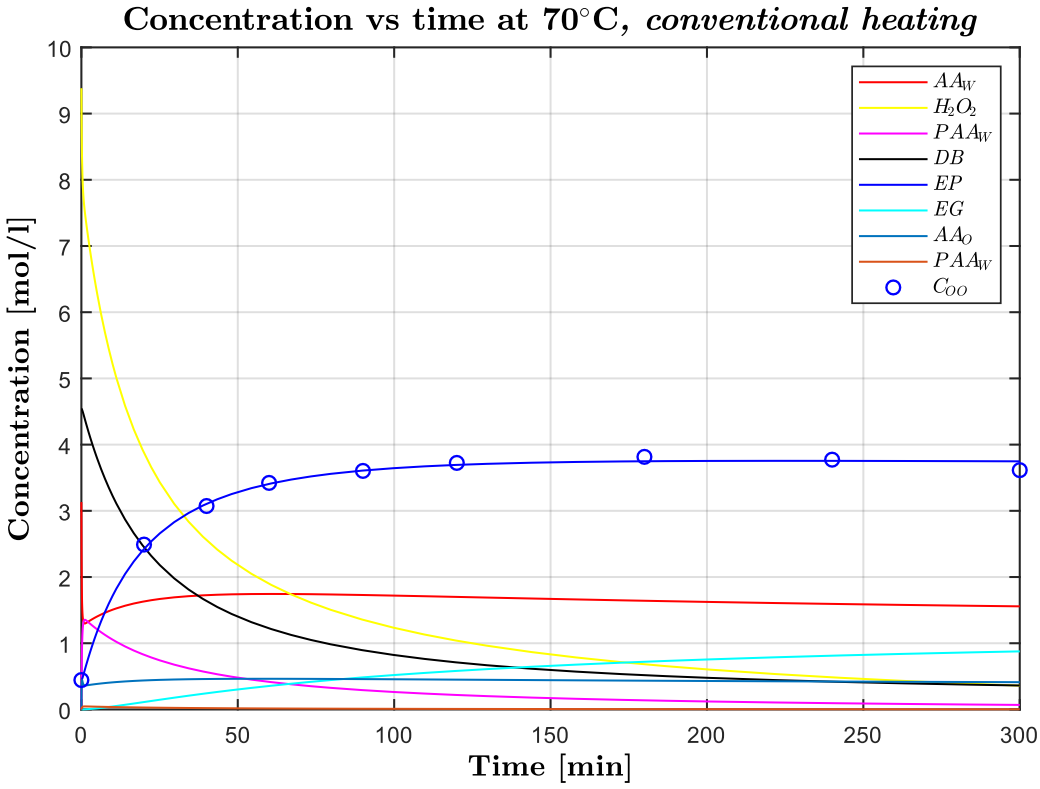

Figure 6.15. *Profile of concentration of the different species involved in the process at 70°C (conventional heating) and experimental point (circles). The concentration of water is neglected*

In every case the fitting is acceptable because the coefficient of determination is always larger than 0.99. In the case of the conventional heating method, the results and the kinetic constants are very close to the one obtained for the calorimetric reactor (Table 6.1). As anticipated in §6.1, with stirring velocity larger than 300 rpm, mass transfer is not limiting, hence also changing the reactor scale (one order of magnitude), the geometry does not affect the results. Modelling confirms that the process is not mass transfer limited, as indicated by Figures 6.16-6.18 that show the time profile of the concentration of the PAA in the bulk and interface for both phases. In this case the difference of concentration between bulk and interface of the concentration of peracetic acid is negligible in both phases. This indicates low space gradient of concentration, i.e. flat concentration profiles, hence the process is kinetically controlled. The gradient is a little higher at 50°C, because of increased viscosity and lower diffusivity of the PAA.

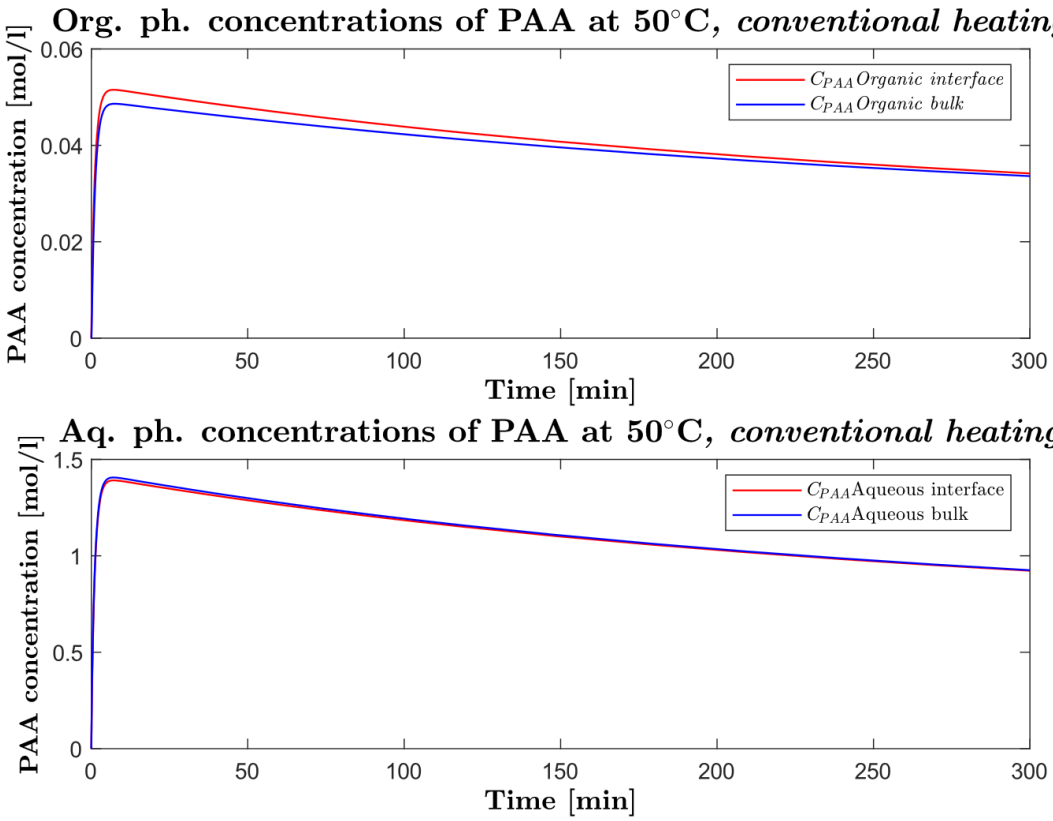

Figure 6.16. *Concentrations of PAA in the organic and aqueous phase (bulk and interface) at 50°C, conventional heating*

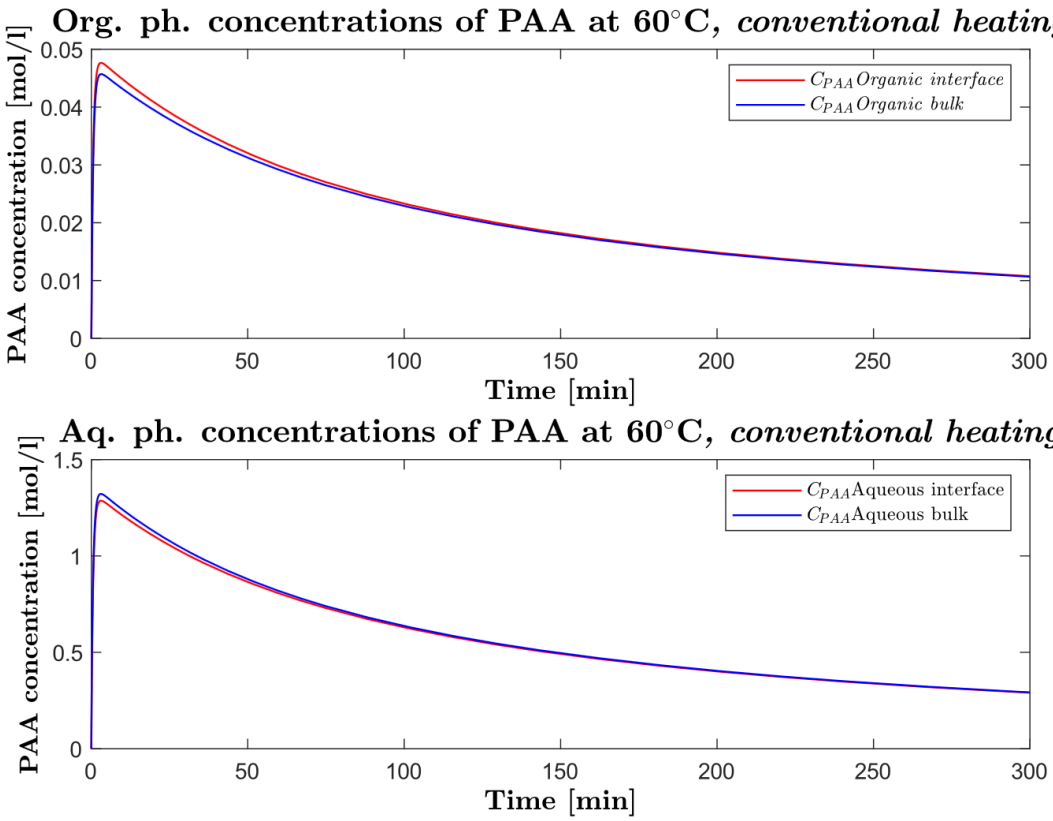

Figure 6.17. *Concentrations of PAA in the organic and aqueous phase (bulk and interface) at 60°C, conventional heating.*

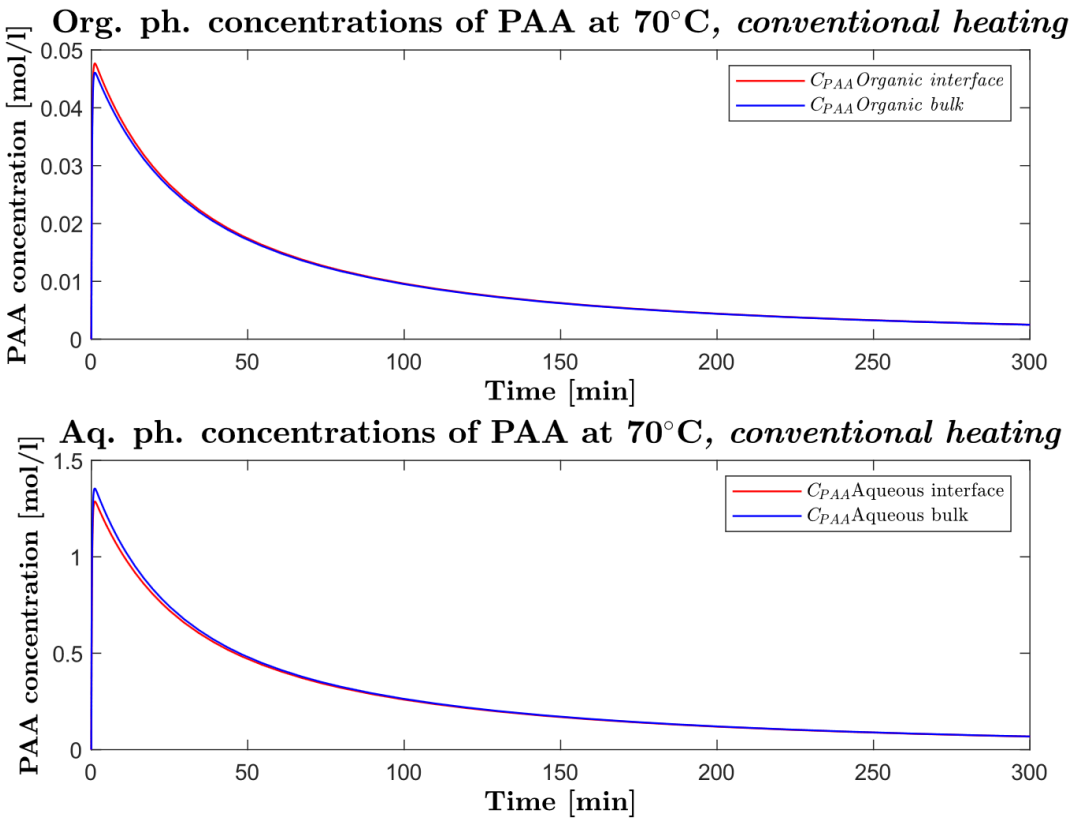

Figure 6.18. *Concentrations of PAA in the organic and aqueous phase (bulk and interface) at 70°C, conventional heating*

Mathematical modelling was performed also for the experimental data obtained by the MW process. The approach is the same used for the previous modelling, and it was intended to understand how much the MW field impacts on the kinetics of formation of PAA and epoxidation. The fitting carried out for the three temperatures is shown in Figures 6.19-6.21. The quality of the fitting is good and the coefficient of determination is always higher than 0.99.

As in the case of the conventional process, also for MW process mass transfer is not the rate determining step even though the impeller velocity is noticeably lower (45 vs 450 rpm). The plots of concentration of the peracetic acid are shown in Figure 6.22-6.24 indicate that the difference of concentration between bulk and interface in both phases are very low (less than 5%) in every case, so spatial concentration gradients are low. This confirms what observed from the experimental evidences exposed at §6.2, according to which the MW field is able to produce a stable suspension even if the stirring velocity is noticeably low.

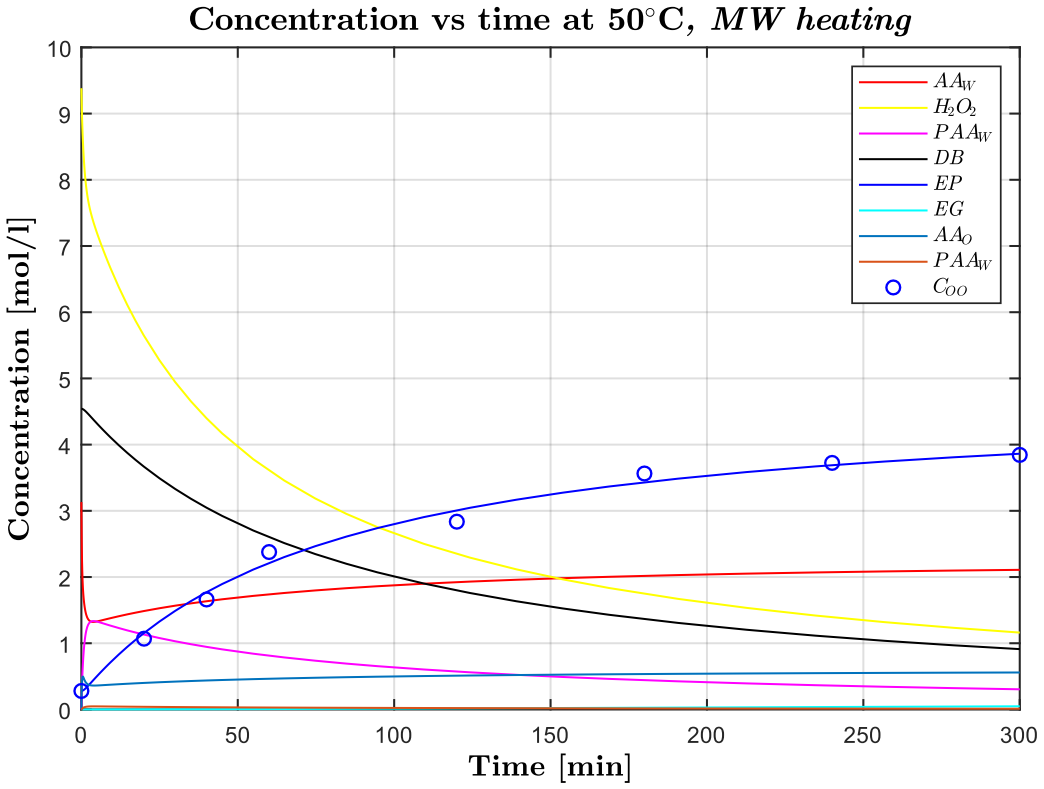

Figure 6.19. *Profile of concentration of the different species involved in the process at 50°C (MW heating) and experimental point (circles). The concentration of water is neglected*

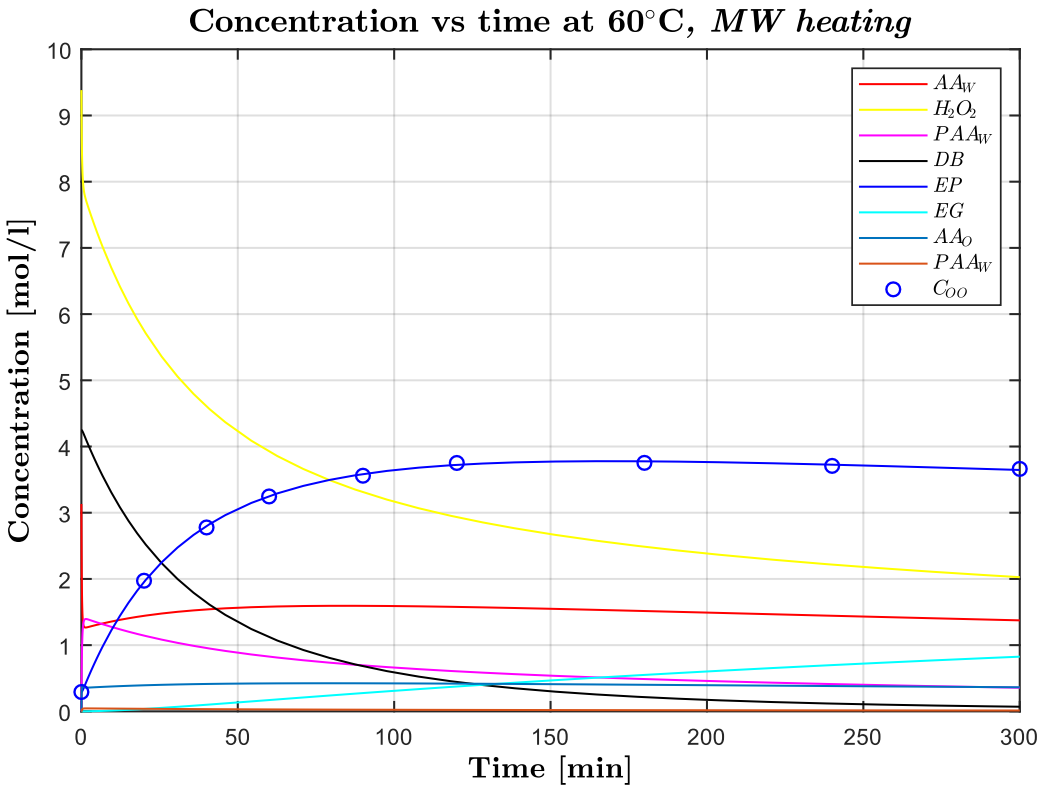

Figure 6.20. *Profile of concentration of the different species involved in the process at 60°C (MW heating) and experimental point (circles). The concentration of water is neglected*

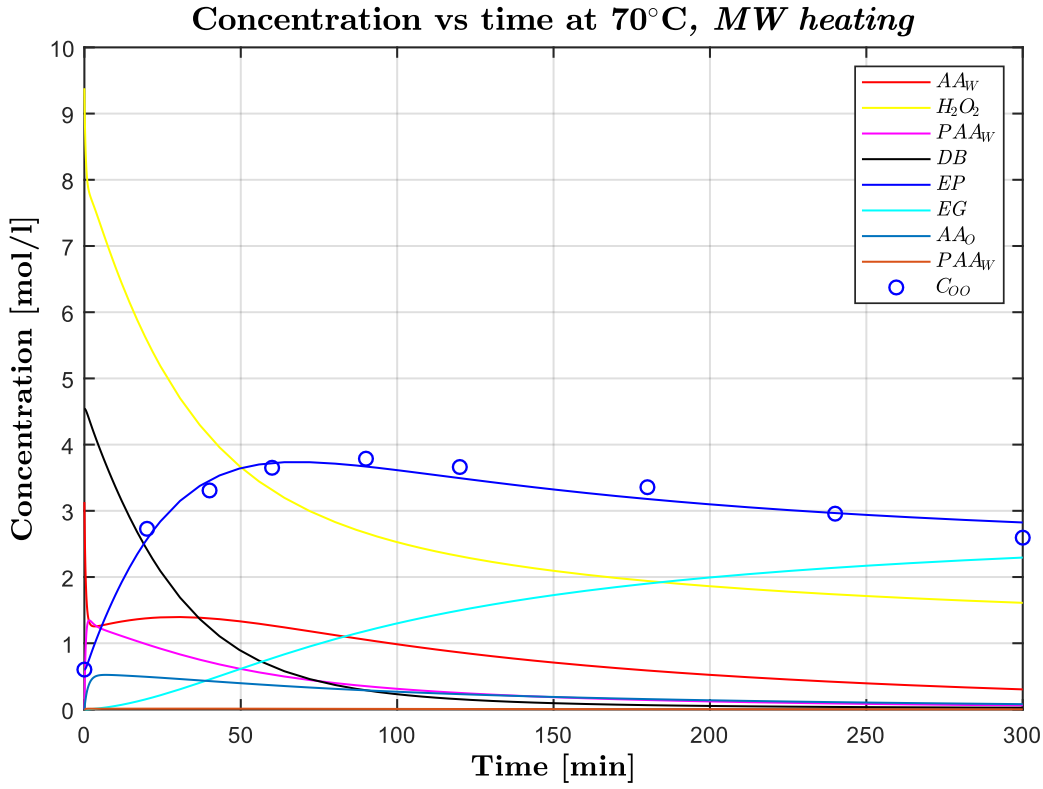

Figure 6.21. *Profile of concentration of the different species involved in the process at 70°C (MW heating) and experimental point (circles). The concentration of water is neglected.*

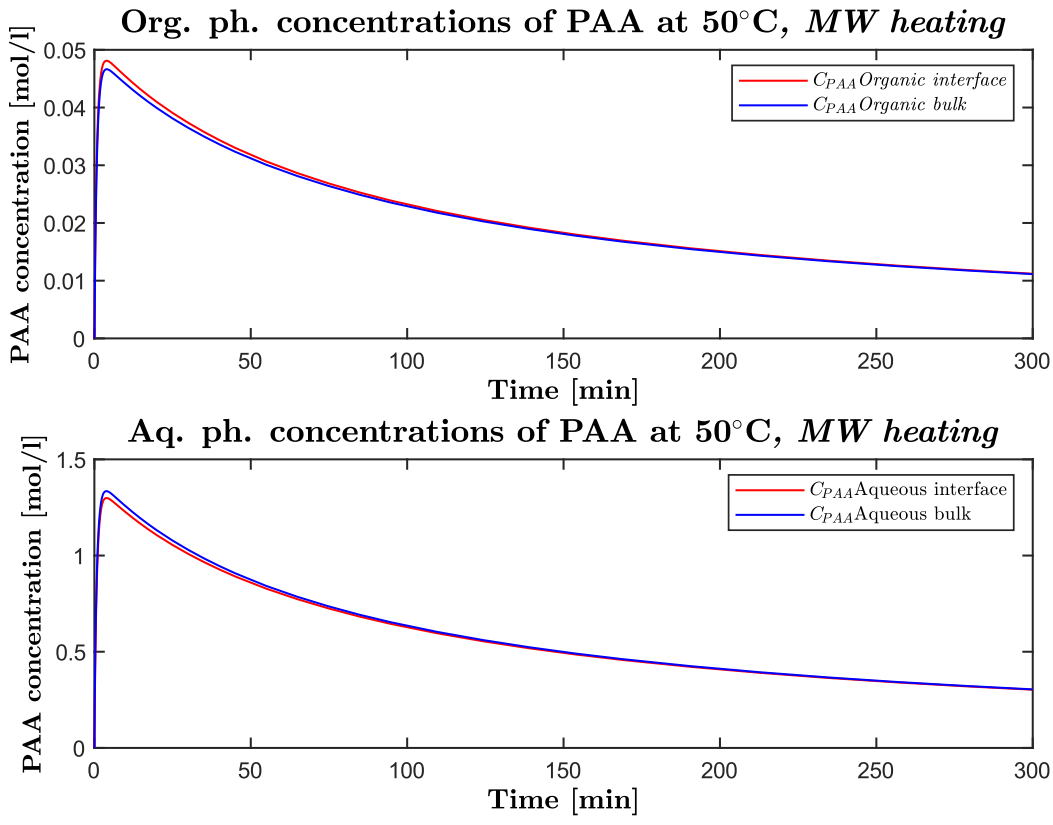

Figure 6.22. *Concentrations of PAA in the organic and aqueous phase (bulk and interface) at 50°C, MW heating*

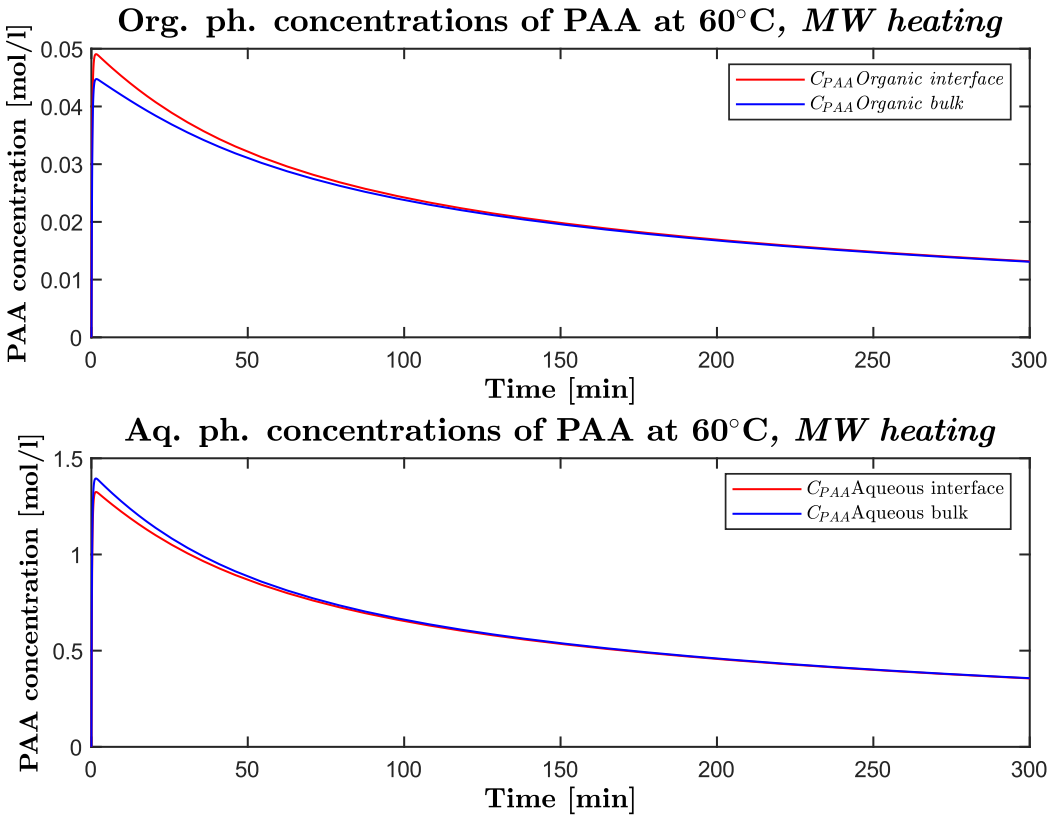

Figure 6.23. *Concentrations of PAA in the organic and aqueous phase (bulk and interface) at 60°C, MW heating*

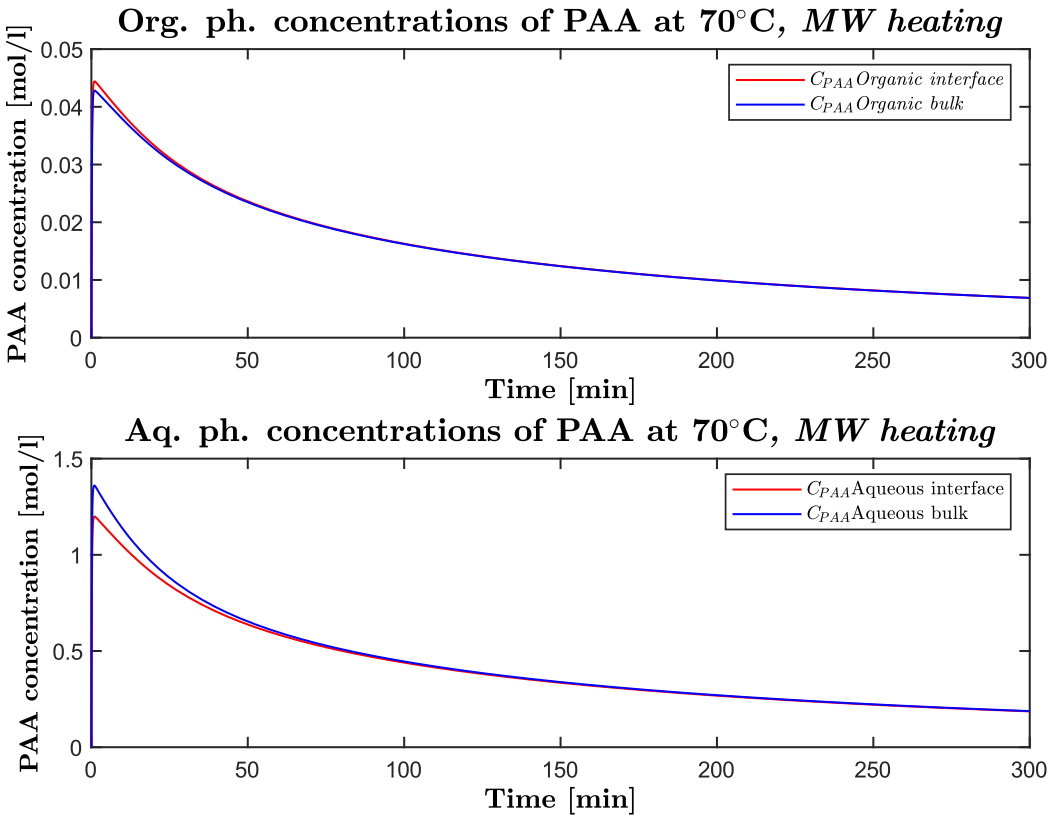

Figure 6.24. *Concentrations of PAA in the organic and aqueous phase (bulk and interface) at 70°C, MW heating*

With regards to the rate of reactions, in the case of MW process both the kinetics of formation of peracetic acid and the epoxidation increase, as can be seen from Table 6.2. This is due to the strong effect of the microwave field on polar groups as hydrogen peroxide, acetic acid and peracetic acid.

Table 6.2. *Kinetic constants of the epoxidation and perhydrolysis reactions obtained by modelling of the experimental data in the cases of conventional and MW heating.*

Temperature	Reaction constant [l/mol·min]	Conventional heating	MW heating	Relative difference
50 °C	k_1	0.0313	0.0940	**+200%**
	k_4	0.1658	0.3804	**+130%**
60°C	k_1	0.1191	0.3401	**+190%**
	k_4	0.3230	0.6734	**+110%**
70°C	k_1	0.3107	0.6942	**+120%**
	k_4	0.8409	1.9053	**+130%**

The effect on the kinetics is an increase of reaction constant of the formation of the peracetic acid of about 200% and 100% of the reaction of epoxidation. The effect is stronger on the step of formation of peracetic acid because it involves two strongly polar species, that are very sensible to the field. However, since among the two reactions the rate determining step is the epoxidation, the net effect on the process is due to the increase of the kinetic constant of this step. In fact, the experimental data shows that the time required to reach the maximum in the case of the MW process is about 50% lower than the case of conventional heating. This is confirmed from the results of the modelling since the kinetic constant of the epoxidation reaction in MW process is doubled when compared to the conventional one (+100%). This is an important novelty because in the literature there is no evidence of the effect of the MW field on the reacting system. From Figures 6.25-6.27 it appears evident that also in MW process the rate of formation of PAA is noticeably faster than the rate of epoxidation (about 50 times) hence the formation of the oxirane ring is for sure the rate determining step of the entire process.

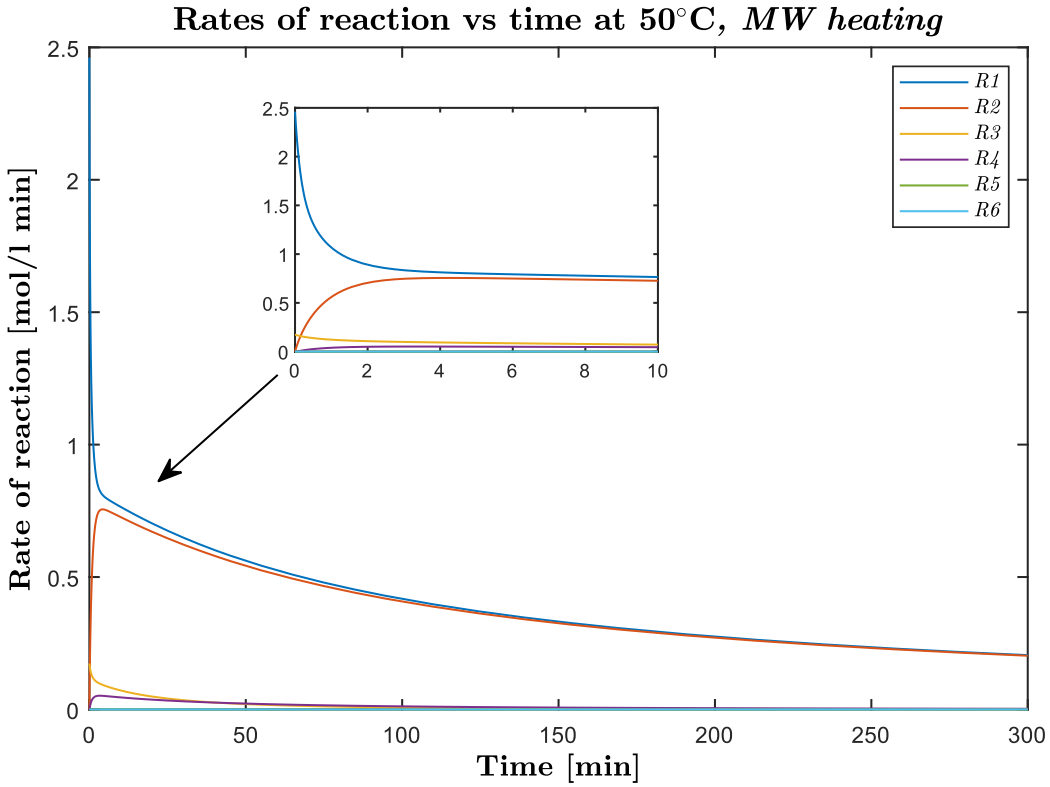

Figure 6.25. *Rates of reaction vs time at 50°C, MW heating process; r_1 is the rate of formation of PAA, r_1 is the rate of epoxidation of double bonds.*

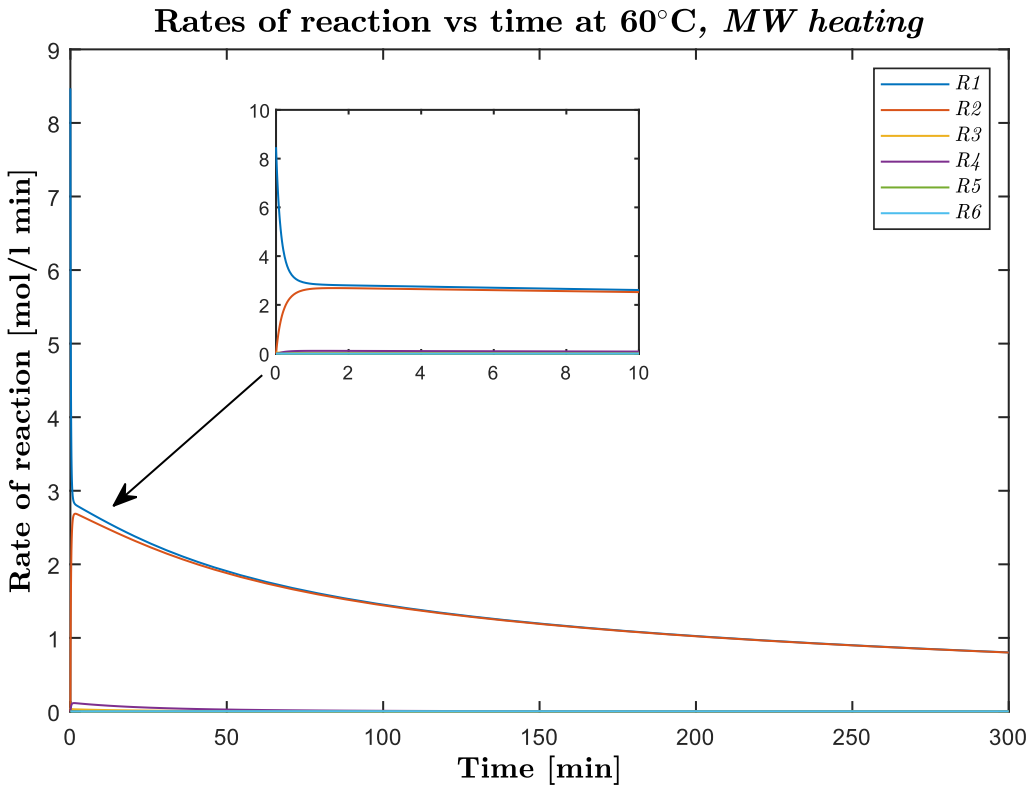

Figure 6.26. *Rates of reaction vs time at 60°C, MW heating process; r_1 is the rate of formation of PAA, r_1 is the rate of epoxidation of double bonds.*

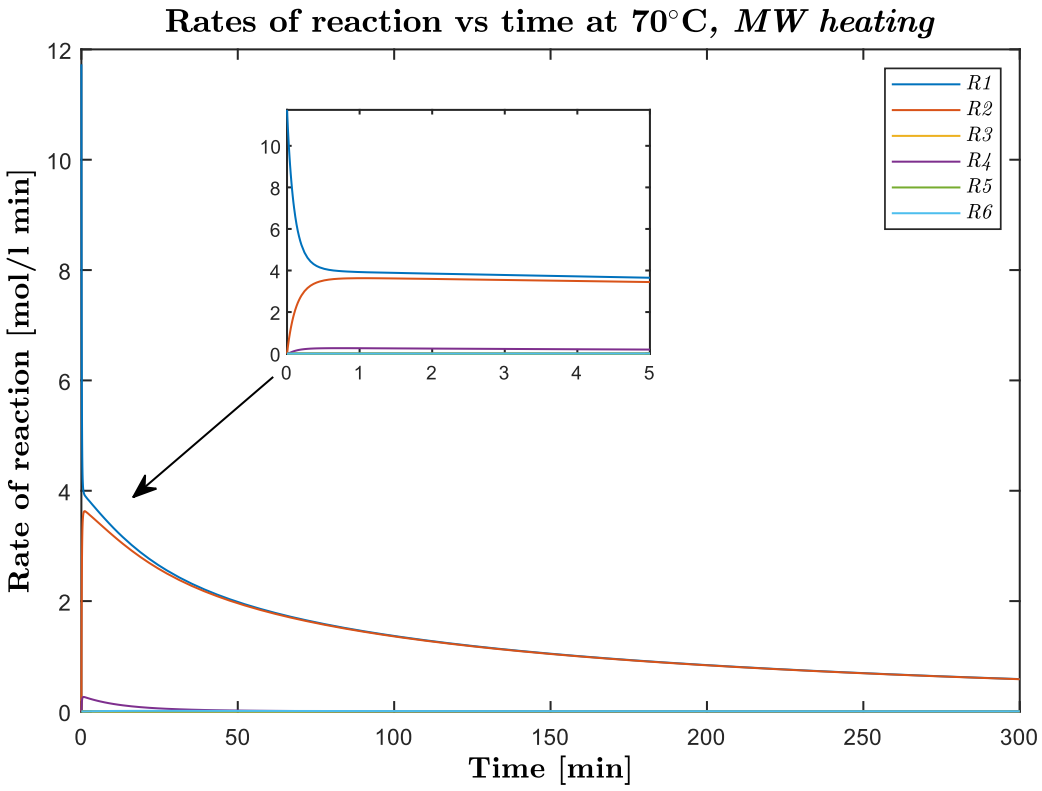

Figure 6.27. *Rates of reaction vs time at 70°C, MW heating process; r_1 is the rate of formation of PAA, r_1 is the rate of epoxidation of double bonds.*

6.3 Conclusions

In this chapter it was demonstrated that MW heating has several beneficial effects on the process of epoxidation of soybean oil. It was discovered that the MW field could create a uniform suspension thanks to the selective heat generation inside the mixture. In fact, since MW heating is much more intense in the aqueous than the oil phase, the elevated temperature decreases the superficial tension of the aqueous phase, promoting the creation of a uniform suspension. The action of the impeller seems to affect the stability of this suspension by promoting the coalescence between droplets. Instead, in the case of the conventional heating the optimal stirring velocity was found to be 450 rpm (turbulent flow), in the case of the MW heating the stirring velocity is one order of magnitude lower, 45 rpm (laminar flow). The MW process, even if it is costlier in terms of equipment, allows saving significant energy that would be used for mixing. Moreover, the MW process permits to save 50% of time in comparison to the conventional one. In fact, the maximum yield (higher than 90%) can be reached in one hour and a half at 70 °C, with the same quality of product than the conventional case. However, once the maximum yield is reached, the epoxy ring opening is quite fast, so the process should be

shut down exactly at the maximum. At 60 °C, the maximum yield was reached in two hours (50% time saved) with a higher yield than in the conventional case and with the additional advantage of a much slower oxirane degradation. The optimal temperature is chosen in a range between 60 and 70 °C, a good compromise between low reaction time and slow degradation of the product.

Thanks to the mathematical modelling, it was demonstrated that the process is kinetically controlled and that mass transfer is sufficiently fast. Moreover, the formation of peracid is about 50 times faster than the epoxidation of double bonds, that is the rate determining step. An important novel result is that the MW field has a strong effect on the rate of formation of PAA (+200%) and on epoxidation (+100%). However, since the process is controlled by the epoxidation, the net effect on the process is due to the increase of the kinetic constant of the epoxidation step.

In conclusion, the MW process allows to halve the time of the process and to operate with a much lower stirring velocity.

Bibliographic references

[1] S. Leveneur, A. Ledoux, L. Estel, B. Taouk, and T. Salmi, “Epoxidation of vegetable oils under microwave irradiation,” *Chem. Eng. Res. Des.*, vol. 92, no. 8, pp. 1495–1502, 2014.

[2] M. Musik and E. Milchert, “Selective epoxidation of sesame oil with peracetic acid,” *Mol. Catal.*, vol. 433, pp. 170–174, 2017.

[3] C. Vianello, D. Piccolo, A. Lorenzetti, E. Salzano, and G. Maschio, “Study of soybean oil epoxidation: effects of sulfuric acid and the mixing program,” *Ind. Eng. Chem. Res.*, vol. In press, 2018.

[4] A. F. Aguilera, P. Tolvanen, K. Eränen, S. Leveneur, and T. Salmi, “Epoxidation of oleic acid under conventional heating and microwave radiation,” *Chem. Eng. Process. Process Intensif.*, vol. 102, pp. 70–87, 2016.

[5] A. F. Aguilera *et al.*, “Kinetic modelling of Prileschajew epoxidation of oleic acid under conventional heating and microwave irradiation,” *Chem. Eng. Sci.*, vol. 199, pp. 426–438, 2019.

Chapter 7

Epoxidation in a continuous reactor under conventional and RF heating

This chapter shows the work carried out to perform the epoxidation in a continuous reactor. The change from batch to continuous processes allows approaching innovative applications at industrial scale, although the shift is not trivial. In fact, passing from batch to continuous involves additional issues, such as the production of a stable suspension/emulsion and the post-process treatments that had to be modified compared with the previous cases. A mixer and a reactor were developed *ad-hoc* exploiting the techniques traditionally used for microfluidics reactors for biological applications. The system was based on a modular design, so that several identical reactors could be connected in series (for different residence times) or in parallel (for larger flowrates).

The study involved the creation of the biphasic mixture, that should be maintained stable in the reactor. For this purpose, a proper surfactant was chosen among different possibilities. The post process treatment was optimized to achieve complete breakage of the emulsion and complete extraction of the oil. The procedure led to the obtainment of pure anhydrous oil. The reactor was also adapted for RF heating and preliminary results were achieved, suggesting that a new more effective geometry should be designed.

The following chapter deals with the study of the complete set-up of the continuous system, from the design and building of the reactor to the procedure for carrying out the process and the post treatment section. The system was tested and experimental runs of epoxidation were carried out.

7.1 Experimental results

7.1.1 Production of the reactor

The protocol for the production of the mixer and the reactor was optimized starting from existing techniques. The methodology is similar to one usually exploited in the microfluidic technology for biologic applications [1]–[5]. Microfluidic reactors are typically produced by PDMS casting on silicon molds. These molds are produced by soft-litography on silicon wafers. The dimension of the channels is in the order of magnitude micrometers, hence these reactors work on the microscale. Once the mold is finished, multiple replicas of the devices are produced by PDMS casting and reticulation. The resulting piece is a flat PDMS chip with channels carved on a face. This face is sealed to a thin glass sheet after R.F: plasma treatment.
The production of the continuous reactor was based on these procedures, and considering that the dimensions of the channels are 1-2 millimetres, it works on the mesoscale.

The molds were produced by CNC milling of aluminium blocks. The pieces were polished to achieve low rugosity for maximum accuracy of the molds. PDMS was casted in the molds and due to the height of the channels, particular attention had to be devoted to the removal of the chips, in order to avoid the formation of cracks that could lead to subsequent fluid leaks.

Plasma treatment was performed on both PDMS chips and glass slides, according to standard protocols for microfluidics, but because of the excessive dimensions of the pieces, the functionalisation of the surfaces was only partial. In fact, PDMS bonded to the glass with poor repeatability and only partial sealing. The solution was found changing the polymer used for the replica molding process and using Crystal 15 resin, that is an economical silicon resin used for artistic models. Crystal 15 has different characteristics from PDMS [6], [7], such as higher elongation to rupture, relevant anti-adherent property, but lower transparency. For this reason, chips removal was much easier and without cracks. Moreover, the unreacted resin can easily stick to cross-linked resin, so it can be used as glue to bind pieces creating a seamless connection between layers. This property is quite uncommon among silicone resins since unreacted resin usually cannot stick to completely cross-linked silicone. Since plasma treatment was not effective, a different protocol was set up. In fact, glass slides were substituted with Crystal 15 sheets (1 mm thickness) and replica-molded chips were glued to the sheets by means of the same unreacted resin. Complete cross-linking could be achieved at room temperature after 18-24 hours.

7.1.2 Creation of a biphasic mixture

Since the reactants are distributed in two phases, the production of a biphasic mixture can be achieved producing a suspension or an emulsion. In the previous cases (batch reactors), the suspension was achieved by the action of the impeller or thanks to the MW field. In this case, the formation of a stable suspension is fundamental to perform the process continuously, avoiding the segregation of the reactants inside the tubular reactor.

The suspension was produced by using the V-mixer (§2.1.4). The fluid dynamics of the system was tested using oil and water, coloured by a little amount of crystal violet to better distinguish the two phases in the suspension. The mixer was able to produce a train of aqueous droplets in oil phase (Figure 7.1) and the dimension of the droplets was fairly uniform, with an approximate diameter of 2 millimetres. Despite this good result, the repeatability of the process was low. In fact, coalescence was responsible of the formation of macro-droplets inside the reactor, thus limiting stability and repeatability. The system was tested in different conditions of mass ratio oil/water and flow rates and in all the cases the system was unable to reach a stable steady state, with large coalesced and segregated zones. The fluid dynamic regime is strongly laminar, since the Reynolds number are in the range 0.5-5. The velocity is in the range of 0.3-2 mm/s, higher than the microfluidics standards [5]. Higher velocities could lead to the internal breakage of the reactor and would have a great impact on the reduction of the residence time which would be in the order of seconds, too low for the process, which requires several minutes or hours. Moreover, the average dimension of the droplets is in the order of magnitude of millimeters, noticeably higher than the cases (micrometers) of tests in the calorimetric or MW reactor. Consequently, the process was not carried out in these conditions otherwise mass transfer would be strongly limiting.

Figure 7.1. *Biphasic stream of water droplets in oil.*

Since the process is not feasible by means of a suspension, it was modified stabilising the two phases in an emulsion. The V-mixer was used to mix two streams, one made of an emulsion, and the other of the catalytic mixture. The principle was based on producing a bi-phasic emulsion made of hydrogen peroxide, acetic acid, oil and a proper surfactant, without catalyst. The reactive system was activated at the V-mixer with the injection of the catalyst and sent to the tubular reactor, as indicated in Chapter 2 (§2.1.4). The surfactant stabilizes the mixture both in the syringe and inside the reactor.

It is recalled that a generic surfactant when dispersed in aqueous phase, creates micelles with a hydrophilic shell and a hydrophobic core [8]. When oil is added, it moves inside the micelles and the coalescence between particles is prevented by the repulsion between surfactant shells, thus stabilizing the system. An important parameter in the case of ionic surfactant is the Z parameter. High value of the Z potential promotes the formation of electrostatic forces that strongly prevent coalescence phenomena. Z potential strongly decreases in presence of ions or variation of pH. For this reason, ionic surfactants were avoided because of their instability in strongly acid and ionised solutions. In fact, the reactive system is made of acetic acid, hydrogen peroxide and sulfuric acid, and the ionic strength of the solution can strongly affect the stability of the emulsion. For this reason, non-ionic surfactants were chosen: in fact, even though less effective, they are noticeably less sensitive to pH.

For the choice of a proper surfactant, HLB number must be considered. It is defined as [9]:

$$HLB = 20 \cdot \frac{M_h}{M} \qquad 7.1$$

where M_h is the mass of the hydrophilic section of the surfactant and M is the mass of the whole molecule. Each oil has $HLBr$, i.e. the HLB required by the oil for an optimally stable emulsion, is equal to 7, so the HLB of the chosen surfactant should be around this value. The two most important families of surfactant available in the market are the Tweens (polyoxyethylene esters) and the Spans (sorbitan esters) [10].

Span 40 could be used since its HLB is similar to the one of the soybean oil, but it was not commercially available. Different surfactants can be mixed together to obtain a mixture with the desired HLB. In particular, the HLB of the mixture can be roughly assumed equal to the weight linear combination of the HLB values of the components [9]. Span 80 and Tween 80 are easily available in the market, and they were chosen to produce a surfactant mixture with HLB equal to 7. For this purpose, a mixture made of 25% Tween80 and 75% Span 80 was produced.

Table 7.1. *HLB values of different surfactant of the Tweens and Spans family* [11].

Surfactant	HLB
Tween 20	16.7
Tween 40	15.6
Tween 60	14.9
Tween 65	10.5
Tween 80	15.0
Tween 85	11.0
Span 20	8.6
Span 40	6.7
Span 60	4.7
Span 65	2.1
Span 80	4.3
Span 85	1.8

Several combinations were tested, using pure Span 80, pure Tween 80, Span80 / Tween80 mixture, and an ionic surfactant as ammonium lauryl suphate (ALS). The mixture was made by

acetic acid and hydrogen peroxide (17.1wt.% and 82.9wt.% respectively, as the previous tests), adding the surfactant dropwise in the proportion of 5wt.%. Oil was added dropwise at 10wt.% concentration. The results are reported in Table 7.2.

Table 7.2. *Comparison between different surfactants.*

Surfactant	Ionic / non ionic	HLB	Performance
ALS	Ionic	40	very poor
Triton X100	Non ionic	13.4	poor
Tween 80	Non ionic	15	poor
Span 80	Non ionic	4.3	medium
Mix Span80 / Tween 80	Non ionic	7	good

The evaluation of the performance of the surfactants was carried out by a simple visual analysis after 10 minutes, evaluating the segregation of the emulsion. Figure 7.2 shows the difference between an emulsion with ammonium lauryl sulfate and Span 80 / Tween 80 mixture after 10 minutes. In the case of the ammonium lauryl sulfate, segregation takes place in a few minutes. In the case of Span 80 / Tween 80 the emulsion is homogeneous and without segregation.

Figure 7.2. *Emulsions with ammonium lauryl sulfate (left) and Span 80 / Tween 80 (right)*

These tests confirmed that most effective solution is the mixture of non-ionic surfactants with *HLB* equal to 7. The system was optimised to maximise the amount of solubilised oil in the emulsion. The concentration of the surfactant is 5wt% compared to oil. Several tests were carried out to understand the maximum concentration of oil without segregation of the emulsion. It was discovered that high concentration of oil (7-8wt.%) can be quite stable. However, the concentration of oil was fixed to 5wt.% to achieve a fully stable emulsion.

7.1.3 Breakage of the emulsion

Since a surfactant was used, the post-process treatment implemented for the other methods (§2.3.6) had to be adapted. Typically, salts or acids are added to change the ionic strength of the mixture and break an emulsion. However, since in this case the surfactant is non-ionic, this is not effective. To overcome this issue, simple diethyl ether was used to solubilise the oil and break the micelles. Nevertheless, the separation was very slow and the obtained product was particularly turbid, indicating presence of residual water in the oil, which resulted not anhydrous, as confirmed by the FTIR analysis (Figure 7.3).

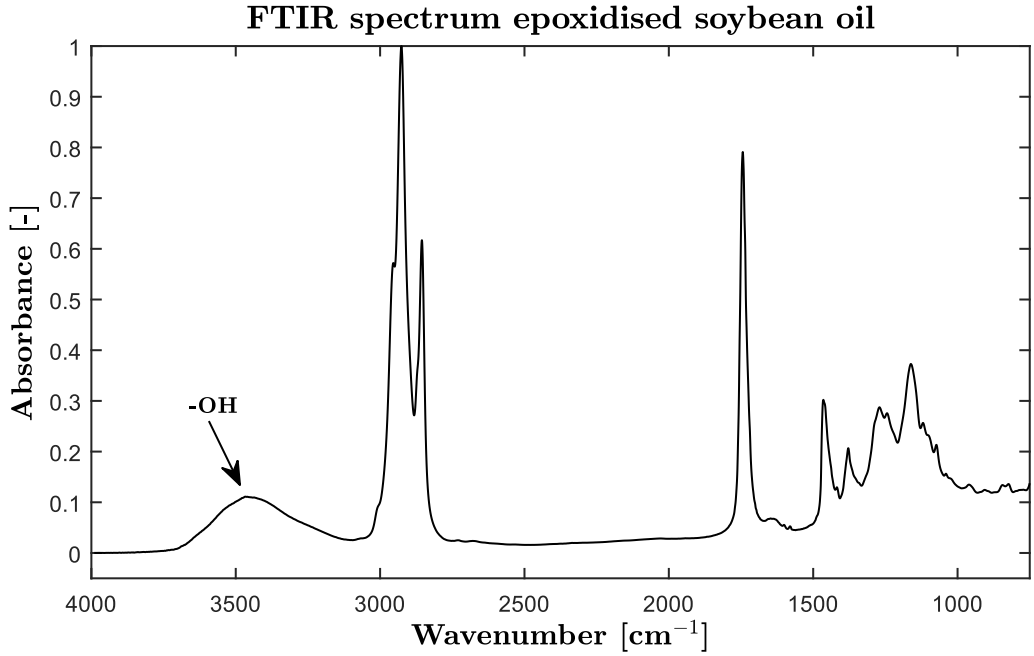

Figure 7.3. *FTIR spectrum of sample of oil treated with diethyl ether.*

Figure 7.3 shows a relevant band corresponding to the hydroxy group. This proves that the amount of water entrained in the oil phase is not negligible. The reason of this problem is that diethyl ether is not completely non-polar, thus reducing its effect in the presence of a surfactant. For this reason, n-hexane was used because it is completely non-polar, has a density comparable to that of diethyl ether, even though the boiling temperature is higher (Table 7.3).

Table 7.3. *Properties of diethyl ether and hexane* [10].

Property	Diethyl ether	Hexane
Polar / Non polar	Weakly polar	Non polar
Density	713 kg/m^3	660 kg/m^3

Boiling point	34.6 °C	68 °C
Solubility in water	69 g/l	0.0095 g/l

Table 7.3 shows that the solubility of hexane in water is 3-4 orders of magnitude lower than that of diethyl ether, thanks to the difference in the polarity of the molecule. Nevertheless, the boiling point of hexane is sensibly higher (68°C vs 34.6°C), so the removal of the solvent is slightly more difficult and the temperature of the thermostatic bath is increased from 55°C to 65°-70°C.

The FTIR spectrum of a sample treated with hexane is shown in Figure 7.4.

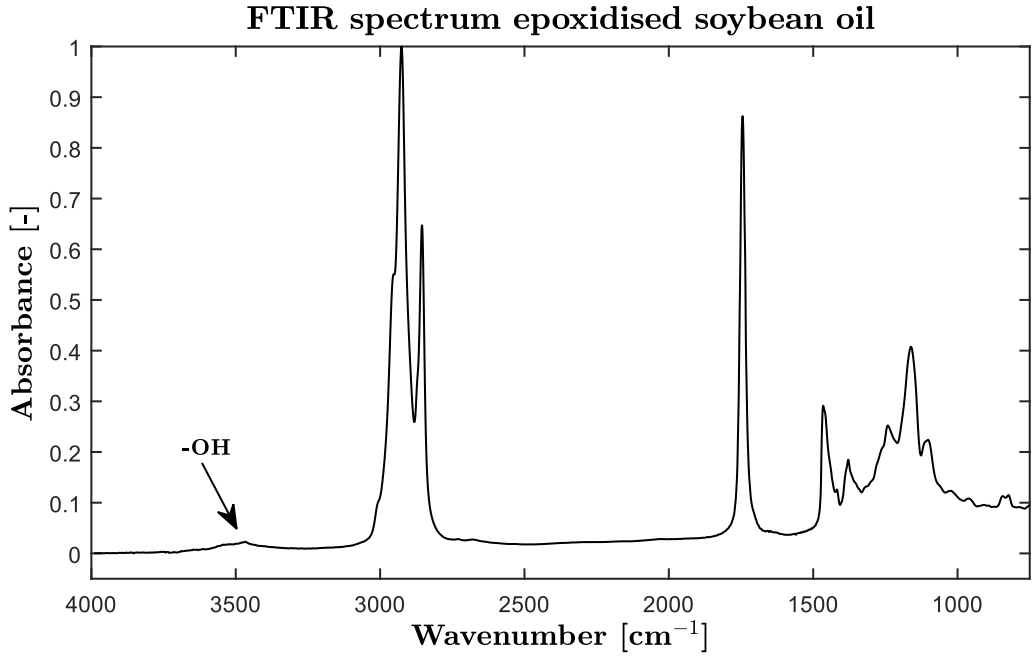

Figure 7.4. *FTIR spectrum of sample of oil treated with hexane.*

Figure 7.4 shows that the hydroxy band is noticeably lower than in the previous case, demonstrating that the treatment is effective. In this way, anhydrous oil can be obtained.

7.1.4 Yield vs time curve – conventional heating

The yield vs time curve was obtained collecting different points at different residence times. Since the volume of the reactor is constant, the residence time was varied acting on the flowrate.

Table 7.4. *Composition of the system*

Chemicals (Emulsion)	Mass [g]	Chemicals (Catalyst solution)	Mass [g]
Soybean oil	3	Sulfuric acid	3.33
Acetic acid	9.747	Hydrogen peroxide	16.67
Hydrogen peroxide	47.253		
Surfactant	0.15		

Changes in the flowrate did not modify the dimension of the oil droplets since the emulsion was preliminary produced using a standard procedure by means of a high shear mixer and stocked in the syringe, mounted on the pump. Moreover, as stated before, in all the cases the fluid regime is fully laminar, since the Reynolds number is in the range 0.5-5.
The composition of the system is reported in Table 7.4.

The points were collected from 5 to 30 minutes at 70°C and Figure 7.5 shows the yield vs time curve. Each point of this curve was obtained maintaining fixed the volume of the reactor and varying the total inlet flowrate. Table 7.5 shows different values of inlet flowrate for different residence times.

Table 7.5. *Correlation between flowrates and residence time.*

Time [min]	Emulsion[ml/h]	Catalyst[ml/h]
5	53.52	9.08
10	26.76	4.54
15	17.84	3.03
20	13.38	2.27
30	8.92	1.52

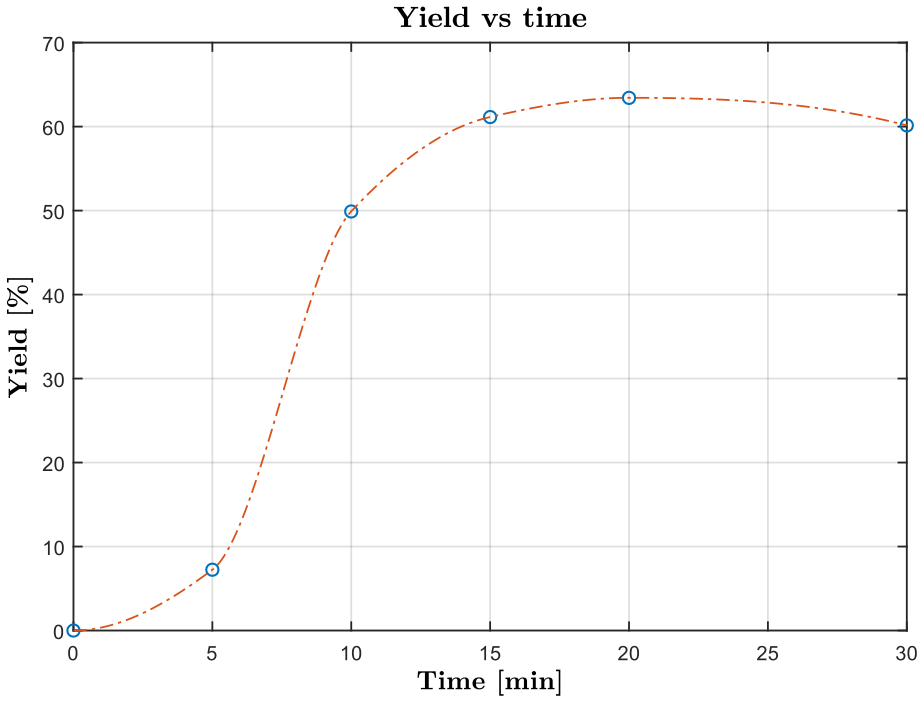

Figure 7.5. *Yield vs time curve at 70°C. Points are joined only for clarity purposes.*

The yield vs time curve highlights that the maximum is achieved at 20 minutes and it is equal to about 63%. Compared to the previous cases (Chapter 5 and 6), the maximum is achieved faster when compared to the 3 hours needed with the calorimetric reactor. However, the maximum yield is sensibly lower than in the tests carried out using the calorimetric reactor (higher than 90%). This is due to the different water phase / oil ratio, that in these tests is 10 times lower. In fact, water phase / oil ratio is constrained by the surfactant, that is not able to guarantee the stability of the emulsion with a large oil loiding. For this reason the oil loading was 5%, one order of magnitude lower than previous cases (about 50%). Consequently, the amount of available peracetic acid is higher, promoting faster formation of epoxides but also faster degradation of epoxides at the same time.

The process has an initial lead time of 5 minutes due to the preliminary formation of the peracid and mostly to the time of mixing between the catalyst solution and the emulsion. In fact, in these conditions mixing is governed by diffusion mechanisms, since the fluid dynamic regime is strictly laminar.

7.2 Mathematical modelling results

The system was modelled according the model exposed in Chapter 4. The fitting of the experimental data was not possible because of the initial lead time due to the mixing issues described above. For this reason, the system was modelled according to the kinetic parameters found for the calorimetric reactor. Figure 7.6 shows that the model follows quite accurately the experimental data, even though it fails to describe the initial lead time due to the mixing. This issue could be overcome by an accurate redesigning of the mixer to achieve better micromixing. In fact, the mixing between phases is diffusion controlled, due to the strongly laminar regime. Moreover, these limitations could be due to the assumption of the model that considers the reactor as a PFR. This assumption is partially verified, but due to the low Reynolds number, concentration profiles are not flat, and axial diffusion could be not negligible. However, given the fact that the implementation of such a model is considerably more complex, the accuracy achieved by this model is considered good for the purpose of the present studies.

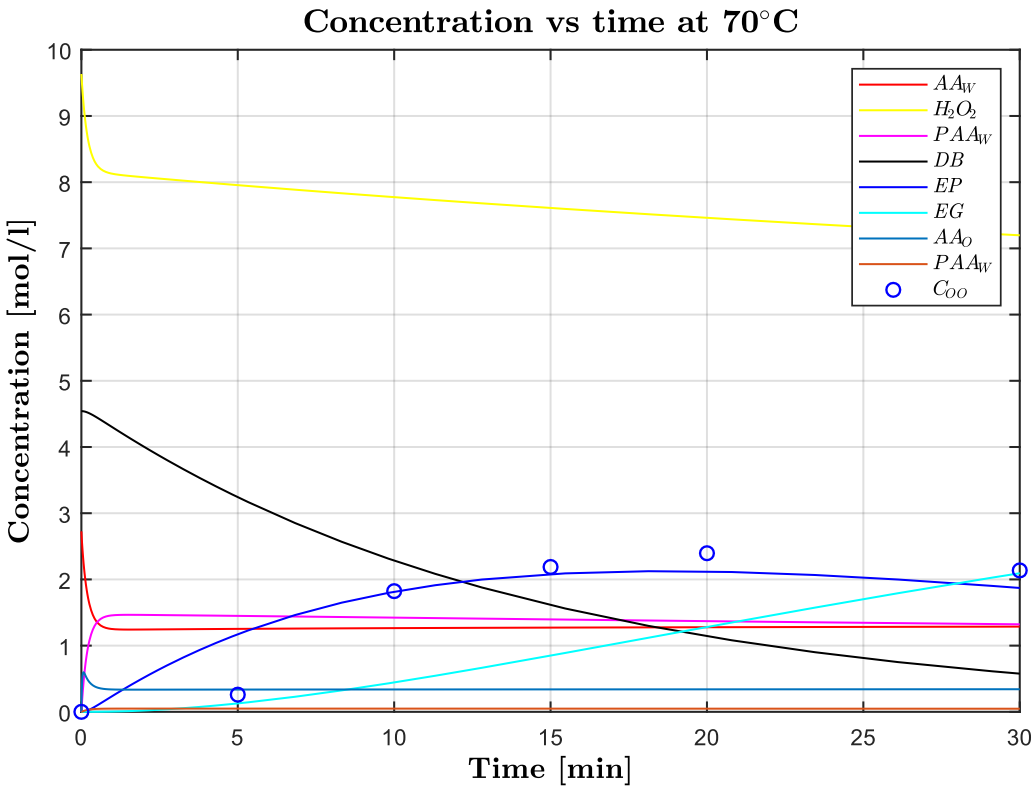

Figure 7.6. *Mathematical modelling of the experimental data.*

7.3 RF heating system: set up and analysis

RF network is reported in Chapter 2 (§2.1.4). A shielded planar condenser applicator was designed and built to heat the tubular section of the reactor. RF application requires a preliminary electromagnetic characterisation of the load. This analysis is useful to correctly operate the RF generator, since it must work at 50 ohms impedance loads with negligible imaginary part. In this way, the RF generator can operate with minimum reflected power. To match the load to the RF generator, a PI-network impedance adapter is used. The impedance matcher cannot operate with loads with a real component of the impedance lower than 2 ohms. From a VNA (Vector Network Analyser) analysis, the impedance of the load line resulted equal to 3-4 ohms (real part) and -250 ohms (imaginary part). The load is strongly capacitive and must be tuned by means of the impedance matcher, to reduce as much as possible the module of the reactance and to increase the real part to 50 ohms. In this way, the impedance of the load can be matched. Because of the strongly capacitive component of the load, the impedance adapter was modified substituting the coil of the PI-network with a larger inductance coil, wound ad-hoc using a 5mm copper rod. A shunt was used to correctly adjust the inductance of the coil and proper impedance match was achieved.

The RF field was applied with 130W and negligible reflected power obtaining the heating of the reaction mixture. Despite this result, the system must be shut down because the excessive heating of the cable between the RF applicator and the impedance adapter due to standing waves. For this reasons, the amount of chemicals to be heated should be larger to increase the real part of the load, in such a way that RF power is totally absorbed by the load and not by the cable. Moreover, planar condenser geometry does not have uniform distribution of field, so the reactor should be redesigned possibly with a coaxial geometry.

7.5 Conclusions

A method to make continuous the epoxidation process of soybean oil was set up. A robust method was found for producing the mesoscale modular reactor, made of a mixer and a tubular section. This method was based on microfluidic techniques, with adjustments on the fabrication of the platforms. An accurate study on the production of stable emulsions under very strong conditions was performed, as well as the post-process treatment. Different surfactants were tested and a mixture of Tween 80 and Span 80 was demonstrated the most effective. For the breakage of the emulsion in the post-process section, n-hexane was the best solution.

Yield vs time curve was obtained up to 30 minutes, collecting experimental data at intermediate times. Tests at different times were obtained varying the volume flowrate, and the resulting curve has a maximum near to 60% at only 20 minutes. Compared to the other processes, the time to reach the maximum is shorter (20 mins vs 3 hours) with lower yield (60% vs 90%), hence in these conditions both epoxidation and degradation is faster. This is due to the lower amount of oil (ten times lower) that is not a process variable as in the other reactors, but it is constrained by stability of the surfactant. The system was modelled using the parameters obtained by the calorimetric reactor, and experimental results were well represented. The accuracy of the model is good despite the PFR assumption (quite restrictive) and the initial lead time due to the mixing of the catalyst.

The system was also adapted for R.F. heating. An applicator was made according a planar geometry, and the load was characterised by means of Vector Network Analyser. According to real and complex components of the impedance, the impedance matcher was designed. R.F. field was applied to the reactor and heating was successfully obtained. Despite this result, excessive heating in the line was observed due to standing waves. The reactor should be redesigned with a different scale and geometry to solve this issue.

Bibliographic references

[1] M. Srisa-Art, S. D. Noblitt, A. T. Krummel, and C. S. Henry, "IR-Compatible PDMS microfluidic devices for monitoring of enzyme kinetics," *Anal. Chim. Acta*, vol. 1021, pp. 95–102, 2018.

[2] C. M. Olmos *et al.*, "Epoxy resin mold and PDMS microfluidic devices through photopolymer flexographic printing plate," *Sensors Actuators, B Chem.*, vol. 288, no. October 2018, pp. 742–748, 2019.

[3] A. A. Aziz *et al.*, "Rapid fabrication and characterization of PDMS microfluidics device using printed conductive silver ink," *Mater. Today Proc.*, vol. 16, pp. 1661–1667, 2019.

[4] A. Plecis and Y. Chen, "Fabrication of microfluidic devices based on glass-PDMS-glass technology," *Microelectron. Eng.*, vol. 84, no. 5–8, pp. 1265–1269, 2007.

[5] T. M. Squires and S. R, "Quake: Micro uidics: Fluid physics at the nanoliter scale," *Electrophoresis*, vol. 22, no. July, p. 3902, 2005.

[6] A. C. M. Kuo, "Polymer Data Handbook, 2nd ed. Polymer Data Handbook, 2nd ed . Edited by James E. Mark (University of Cincinnati, OH). Oxford University Press: New York. 2009 . xii + 1250 pp. $195.00. ISBN 978-0-19-518101-2 .," *J. Am. Chem. Soc.*, vol. 131, no. 44, pp. 16330–16330, 2009.

[7] Gomma siliconica trasparente crystal 15, pp. 1–3, http://www.antichitabelsito.it/gomma_siliconica_trasparente.html, accessed 10/6/2019

[8] C. Read, "The Theory," *Corp. Financ.*, vol. 883, 2014.

[9] F. Acids and Y. Zheng, "Hydrophilic-Lipophilic Balance Learn more about Hydrophilic-Lipophilic Balance Sugar Fatty Acid Esters Stabilization of omega-3 oils and en- riched foods using emulsifiers," 2015.

[10] Pubchem, "U.S. National Library of Medicine." [Online]. Available: https://pubchem.ncbi.nlm.nih.gov/. [Accessed: 29-Aug-2019].

[11] Croda Europe Ltd, "Span and Tween HLBs," *Www.Croda.Com/Europe*, vol. 44, no. 0, pp. 6–11, 2009.

Chapter 8
Final considerations and future perspectives

The epoxidation process was studied following different experimental approaches, whereas a mathematical model enabled a complete understanding of kinetic and mass transfer phenomena. Epoxidation in the calorimetric reactor allowed simulating large batch processes in lab scale, with accurate calorimetric measurements. Based on the thermal profiles, the process is quite exothermic (-276 kJ/mol) and has a strong initial overshoot, highlighting how thermal control of this system is an issue, especially for safety reasons. In addition, the system operates with hydrogen peroxide that has a strong tendency to decompose. The biphasic mixture was intensely agitated at 500 rpm by means of a Rushton turbine, obtaining a uniform biphasic suspension. In these conditions, the flow regime is completely turbulent. The time to reach maximum yield decreases from 25 hours to 3 hours increasing the temperature from 40 to 70°C. Degradation is much faster at higher temperatures, whereas the maximum yield is constant and over 90%. The model assessed that the process is kinetically controlled and that peracid formation is two orders of magnitude higher than epoxidation, which is the rate-determining step.

The study on the effect of MW heating was carried out in two reactors, with similar geometry but different heating sources: MW in a case, conventional heating in the other. Experimental data showed that the conventional heating process achieved very low yield with stirring velocity below a threshold velocity of 300 rpm. In fact, the reactor must be operated in fully turbulent regime to avoid segregation between phases. On the contrary, the MW process is able to produce a remarkable uniform and stable suspension in fully laminar conditions (45 rpm), whereas stirring seems to affect its stability promoting coalescence. The study highlighted that MW heating boosts both peracid formation and epoxidation, with an overall enhancement of 100%. Therefore, MW process can guarantee high yields over 90%, and a 50% saving in time.

The study on the continuous system highlighted the need for a stable emulsion to avoid segregation in the reactor. The reactor was operated in strongly laminar regime, with very low velocity to achieve reasonably a high residence time for sufficient conversion. The maximum

yield was good (60%), but fast degradation took places because of the relevant amount of aqueous phase.

Since this work was intended to be useful for industrial applications, some considerations at the industrial scale could be drawn. The simplest solution at the industrial scale is a batch reactor, which is nowadays commonly employed for this process. However, its scale-up is not trivial, because thermal control can be highly problematic in very large reactors. In fact, especially at the early stages when strong thermal overshoots occur, local hot spots can degrade epoxides, decreasing the final yield and the value of the product. Moreover, this biphasic system needs turbulent conditions with strong stirring. In these conditions, scale up could be not totally effective because local segregation as well as dead zones can be a serious issue. It is clear that mixing plays a key role in the process, and thus achieving proper dispersion could be remarkably energy-consuming, especially if scale up is operated at constant power density. For these reasons, a proper CFD biphasic simulation could be useful to properly scale up the reactor, minimizing these problems with acceptable energy consumption.

However, the MW heating process permitted to obtain a very stable and uniform suspension, even when operating in strongly laminar regime. In these conditions, impeller consumption would be strongly reduced. Furthermore, the time required for maximum yield with this kind of heating source would be reduced by 50%, a remarkable improvement on process time. On the other hand, the plant investment should be considerably higher than a standard batch reactor, considering that the reactor should be made by low loss material (inert plastics as polypropylene, PVDF or PTFE). Moreover, for these reasons, the mixing system should be complex and metal parts should be avoided. Nevertheless, the process was more effective in fully laminar regime and very low stirring velocity, hence an industrial reactor could be designed without any moving part, and the mixing could be carried out by the sole MW field. Thermal control should be properly studied, even though it could be less problematic since magnetrons can be immediately shut down. It is evident that MW heating process offers several relevant advantages and its feasibility could be studied further, evaluating whether or not the higher investment plant could be paid by the 50% time saving. Moreover, from the energetic point of view, it should be considered that MW heating is an efficient way to deliver energy to materials, more than conventional heating methods.

Furthermore, continuous processes are particularly interesting for industrial application when large flowrates are required. In this case, the biphasic mixture had to be stabilised to avoid segregation. For this problem, two solutions can be proposed: the creation of an emulsion by

means of a surfactant or that of a suspension by means of a static mixer. Static mixers have a minimum fluid velocity in the order of meters per seconds; hence the reactor should be remarkably long (in the order of 10^2 meters). A solution for reducing the length of the reactor could be tubular reactor with feedback recirculation to achieve sufficient residence time. About the other solution, the creation of an emulsion permits to obtain a stable mixture independently from the velocity. Nevertheless, the use of a surfactant seriously constraints the amount of oil that can be loaded to about 5%, hence a low percentage of oil can be obtained from this process. Another possible way to stabilise the biphasic mixture could be to carry out the continuous process under MW heating, in order to take advantage of the MW-mediated stabilization effect. However, since a tubular reactor can be seriously difficult to be adapted for MW application, R.F. heating is more suitable for this application. For this reason, the R.F. continuous reactor could be a good solution to achieve both stabilisation of the mixture and enhancement of the rate of the process. In this work, some technical difficulties were encountered when testing the R.F. process for excessive standing waves due to the fact that load was poorly reactive, i.e. the amount of reactants was too low. Moreover, planar geometry could not be the most appropriate. In fact, a suitable solution is that of a coaxial geometry in which a screwed tubular reactor is placed as dielectric between the two cylindrical coaxial plates of a capacitor, that can act as R.F. applicator. In this way, good shielding is achieved as well as a uniform distribution of the field in the dielectric.

In addition, some considerations can be drawn on the separation process, a relevant step both for its impact on economical and environmental sustainability. In fact, a large amount of reactants, washing water and solvents are used for separation and purification. For this reason, a closed loop purification stage should be designed for a more environmental friendly process. Centrifugation can be used to reduce the amount of light solvent that is used to enhance separation.

Furthermore, in this work only sulphuric acid was employed as acid catalyst. However, other catalysts as alumina can be used for simpler separation, even though they are less efficient. On the other hand, solid catalyst can be particularly active under MW / RF heating and they could be used as dispersing agent in a tubular reactor for better mixing.

In conclusion, this work showed many novelties in epoxidation of soybean oil, with several ideas for future improvements, always focusing on self-sustainable processes at the industrial scale.

Conclusions

The aim of this work is producing epoxidized soybean oil in newer, safer and more efficient ways. The study was organised according different experimental approaches. Furthermore, diluted hydrogen peroxide and acetic acid were chosen instead of commonly used concentrated hydrogen peroxide and formic acid for safer conditions. Soybean oil was preferred among different vegetable oils thanks to its large production. The process is carried out in a biphasic system in which hydrogen peroxide and acetic acid react producing peroxyacetic acid, that is soluble in the organic phase and acts as oxygen carrier. Peroxyacetic acid reacts with double bonds of the oil producing epoxidised soybean oil. For this reasons, the process is made of two steps of reaction and two steps of mass transfer. This study involves the epoxidation in a batch calorimetric reactor, that is a batch, well-stirred, jacketed reactor. Temperature control was accurately achieved by means of a thermal control system by *Huber*. This system permitted to study the process in batch conditions, with high quality mixing and accurate data acquisition. This part of the study is a base case, thanks to which it is possible to obtain information useful for future scale-up and calorimetric data, by means. The epoxidation process was carried out in order to obtain yield vs time curves, at different intermediate times and parametric to different temperatures. The set-up of this experimental apparatus required the implementation of a software for the acquisition of data of temperature and pressure of the reactor and the control of the impeller motor. Furthermore, the calibration of the stirrer required the set up of an infrared velocity measurement system. A deep study on the determination of the heat exchange coefficient was carried out, based on both thermal transients and steady states.

Moreover, the effect of MW heating in the reacting system was assessed, for a more effective energy delivery to the system In fact, MW field has both thermal and kinetic effects in reacting system made of polar species. Two systems were implemented, with same geometry but different heating source, MW heating and conventional heating. In this way, an accurate comparison was performed, evaluating the net effect of the MW field on the reactive system. The effect of the stirring velocity was assessed in both cases. Yield vs time curves were obtained for both processes, at different temperatures.

Furthermore, the feasibility of a continuous process was verified, and it was fully implemented and operated, obtaining the yield vs time curves. The system was designed and built according

a modular approach usually followed for microfluidic chips for biological applications. The biphasic reaction mixture was stabilised by means of a surfactant, obtaining a stable emulsion. A study on the stability of the mixture was carried out, using different ionic and non-ionic surfactants.

In addition, R.F. heating was applied and tested on the continuous process, with several advantages in terms of electric control of the system compared to MW.

For all the cases, a kinetic and mass transfer model was implemented for a complete study of the overall system. The biphasic mixture was studied according the approach based on Whitman's two films theory, and it described all the reactions that take place in each phase and mass transfer between phases. The model permitted to determine mass transfer and kinetic parameters by means of a fitting.

Analytical methods were based on FTIR analysis for preliminary semi-quantitative analysis. Moreover, hydrobromic acid titrations were carried out for accurate analysis.

Epoxidation in the calorimetric reactor demonstrated that the process is very sensible to the temperature and time to reach the maximum shits from 25 hours to 3 hours passing from 40 to 70°C whereas maximum yield seems to be nearly constant and remarkably above 90%. Mathematical modelling highlighted that the overall process is not mass transfer controlled whereas the rate determining step is the epoxidation reaction. The reactor was operated in fully turbulent conditions, permitting a uniform mixing of the biphasic system. Furthermore, a calorimetric study was performed and the heat generated by the process was accurately determined. Enthalpy generated by the process was equal to -276 kJ/mol, that is in good agreement with the literature. This result was obtained by time integration of thermal profiles collected by the system. The heat exchange coefficient was experimentally determined according a procedure ad hoc, equal to 2.62 kJ/K. The method was able to evaluate both thermal losses and the heat exchange coefficient with good accuracy.

Furthermore, MW heating effect was studied in two geometrically identical reactors, with different heating sources, in a case MW heating, in the other one conventional heating. MW heating demonstrated a remarkable ability to produce a uniform and stable suspension. In fact, MW heating especially targets aqueous phase, thus creating temperature gradients lowering the surface tension of the aqueous phase. A sensitivity analysis demonstrated a threshold value of stirring velocity (300 rpm) below which yield is noticeably low, because of segregation takes place. Above the threshold value, mixing do not affect the process, since good mixing is achieved and the process is not mass transfer controlled. For this reason, the conventional

heating process was operated in fully turbulent regime (450rpm). Instead, MW process was able to produce a uniform suspension that is stable for several minutes, even with strongly laminar regime (45 rpm). Nevertheless, the impeller action seems to slightly affect the stability of the suspension, since it promotes the coalescence between droplets created by the MW field.
Moreover, yield vs time curves were determined at 50, 60 and 70°C in both cases. MW process halves the time to reach maximum yield, with the same quality of the product (yield higher than 90%). Modelling assessed for both cases that mass transfer was not limiting, and the epoxidation reaction was the time determining step. Moreover, compared to the conventional heating process, MW field boosts both peracid formation (+200%) and epoxidation (+100%). However, since the kinetic rate controlling step is the epoxidation reaction, the overall enhancement is about 100%, hence the rate of the process is doubled. This is in line with the experimental results that showed that the time to maximum yield is halved. Hence, MW process can achieve very high quality product reducing the time by 50%, forming a uniform suspension even with very low stirring velocity.
Furthermore, a continuous reactor was designed, built and set up. The biphasic mixture was stabilised by means of a surfactant. In this way, the mixture was emulsified avoiding segregation in the reactor. The surfactant was properly chosen, and a mixture of non-ionic Span 80 and Tween 80 was sufficiently effective, instead of pH-sensitive ionic surfactants. The process was carried out at 70°C, and maximum yield was obtained in only 20 minutes, even though its only 60%, so lower than previous cases. Modelling was performed with good results, despite the PFR assumption was quite limiting, since the flow regime was strongly laminar.
R.F. heating apparatus was set up to heat the tubular section of the continuous reactor. The system was made of a R.F. generator, an impedance adapter and a R.F. applicator. The system made of the reactor and the applicator was preliminary analysed by means of Vector Network Analyser, and the load was assessed poorly resistive and highly capacitive. On the base of this study, the coil of the impedance adapter was redesigned and wound for correct operation. R.F. heating was achieved even though standing waves problems caused the excessive heating of the line between the applicator and the impedance adapter.

Future works can be carried out on the scale up of reactors, making them interesting for an industrial application. Moreover R.F. apparatus should be redesigned with a different geometry to reduce standing waves problems and to achieve uniform field distribution. Finally, different catalysts could be used, as solid ones since they can be particularly effective in case of MW and RF heating.

Aknowledgments

Ringraziamenti

A conclusione di questo impegnativo lavoro di tre anni, vorrei ringraziare alcune persone che hanno avuto per me un ruolo fondamentale in questa esperienza.
Innanzitutto, desidero ringraziare Prof.re Giuseppe Maschio, il mio supervisore di dottorato, che mi ha seguito costantemente nell'attività di ricerca durante questi tre anni. La sua decennale esperienza ha rappresentato per me un notevole e rilevante supporto per il prosieguo del mio lavoro. Voglio inoltre ringraziare Prof.sa Elisa Cimetta, che mi ha aiutato in questi anni di lavoro in laboratorio e con la quale ho collaborato nel corso di Termodinamica. I suoi consigli professionali e personali, sempre oculati e attenti, sono stati efficaci e utili per la mia crescita personale e professionale.
Vorrei inoltre ringraziare Prof.re Paolo Sgarbossa e Prof.sa Alessandra Lorenzetti, per i consigli dispensati durante questi anni, aiutandomi o consigliandomi con professionalità e gentilezza.
Un sincero grazie ai miei preziosi colleghi di ufficio nonché sinceri amici Alberto, Paolo, Sara e Lorenzo con i quali ho condiviso sia esperienze professionali sia momenti di vera felicità e allegria.
Voglio ringraziare i miei amici del collegio Don Nicola Mazza di Padova, Jacopo, Nicola e Lorenzo con i quali ho vissuto felicemente fianco a fianco questi anni di dottorato.
Ringrazio i miei genitori che hanno creduto in me e mi hanno supportato in questi anni universitari, sia come studente sia come dottorando.
Infine voglio ringraziare di cuore Elisa, persona speciale con la quale condivido una sincera, profonda e gioiosa felicità.

Annex

Determination of the heat exchange coefficient: thermal transient

Thermal transient was studied according the approach in §3.2.1. This procedure permitted the evaluation of the characteristic time and the effective heat capacity. Tests were carried out at 40, 55 and 70°C. For each temeprature, different values of generated power were set, 5, 10, 15, 20, 25 W (15 tests). For the sake of brevity, it is reported the script for 70°C, 10 watts. For the other tests, the approach was similar. The programming software is *Matlab*®.

```
clc, clear all, close all
A=xlsread('calibrazione 70_2.xlsx');
time=A(:,1);
Tr=A(:,2);
plot(Tr)
Tr=Tr(8138:8422);
time=time(8138:8422);
plot(time,Tr);
Tb=69.63; % Jacket temperature
logT=log10(Tr-Tb);
plot(time,logT)
m0_q0= [180 40];
options=optimset('Display','iter','TolFun',1e-8,'TolX',1e-
8,'MaxIter',5000,'MaxFunEvals',15000);
[m_q,fval]=fminsearch(@err,m0_q0,options,Tb,time,logT)
m0_q0=m_q;
function fob=err(m_q,Tb,time,logT)
logTcalc=-1/m_q(1)*time+m_q(2);
fob=norm((logTcalc-logT).^2);
figure (1)
plot (logTcalc,'-. b','LineWidth',0.8), hold on
plot (logT, 'r','LineWidth',0.8), hold on
xlabel('\textbf{Time [s]}', 'FontName', 'Times New Roman', ...
       'FontSize',13,'Color','k', 'Interpreter', 'LaTeX')
ylabel('\textbf{log (${\Delta}$T)}', 'FontName', 'Times New Roman',
...
       'FontSize',13,'Color','k', 'Interpreter', 'LaTeX')
```

```
title(join(['\textbf{Thermal transient at
70}','$^{\circ}$','\textbf{C}']), 'FontName', 'Times New Roman', ...
       'FontSize',14,'Interpreter','Latex')
legend ('Fitting line','Experimental data','Interpreter',
'LaTeX','Location','northeast'), hold on
box on
x_0=50;
y_0=200;
width=700;
height=470;
set(gcf,'position',[x_0,y_0,width,height])
grid on
hold off
drawnow
end
```

Determination of the heat exchange coefficient: thermal steady state

According the procedure previously explained (§3.2.2) the thermal steady states were analysed to determine the heat exchange coefficient. This method was repeated at different temperatures 40, 55 and 70°C. Each experimental run consider the thermal steady states generated by different values of power, 5, 10, 15, 20 and 25W. The following script concerns the determination of the heat exchange coefficient at 70°C. For the other temperatures, the script was similar. The programming language is *Matlab*®.

```
clc, clear all, close all
%%
% ******STEADY STATE ANALYSIS AT 70°c******

%%caricamento dati
A=xlsread('calibrazione 70_2.xlsx');
time=A(:,1);
Tr=A(:,2);
Tin=A(:,3);
Tout=A(:,4);
% figure (1);
% plot(Tr), hold on
% plot(Tin), hold on
% plot(Tout), hold on
Tr_5=Tr(4072:4517);
% Tin_5=Tin(4072:4517);
Tout_5=Tout(4072:4517);
Tr_5=mean(Tr_5)+273.15;
Tb_5=(mean(Tin_5)+mean(Tout_5))/2;
Tr_10=Tr(6049:6319);
Tin_10=Tin(6049:6319);
Tout_10=Tout(6049:6319);
Tr_10=mean(Tr_10)+273.15;
Tb_10=(mean(Tin_10)+mean(Tout_10))/2;
Tr_15=Tr(7759:8122);
Tin_15=Tin(7759:8122)+273.15;
```

```
Tout_15=Tout(7759:8122);
Tr_15=mean(Tr_15)+273.15;
Tb_15=(mean(Tin_15)+mean(Tout_15))/2;
Tr_20=Tr(9603:9918);
Tin_20=Tin(9603:9918);
Tout_20=Tout(9603:9918);
Tr_20=mean(Tr_20)+273.15;
Tb_20=(mean(Tin_20)+mean(Tout_20))/2;
Tr_25=Tr(1.136e4:1.172e4);
Tin_25=Tin(1.136e4:1.172e4);
Tout_25=Tout(1.136e4:1.172e4);
Tr_25=mean(Tr_25)+273.15;
Tb_25=(mean(Tin_25)+mean(Tout_25))/2;

%% temperature reattore e camicia
Tr=[Tr_5 Tr_10 Tr_15 Tr_20 Tr_25];
Tb=[Tb_5 Tb_10 Tb_15 Tb_20 Tb_25];
Tb=mean(Tb)+273.15;
P=[5 10 15 20 25]; %% power [W]
UA0_Qd0=[5 1.16]; %% inital parameters
options=optimset('Display','iter','TolFun',1e-8,'TolX',1e-
8,'MaxIter',5000,'MaxFunEvals',15000);
[UA_Qd,fval]=fminsearch(@err,UA0_Qd0,options,Tb,Tr,P)
UA0_Qd0=UA_Qd;
function fob=err(UA_Qd,Tb,Tr,P)
Tcalc=1/UA_Qd(1)*(P-UA_Qd(2))+Tb; %%temperature calculation
fob=norm((Tcalc-Tr).^2); %% error (squared)
figure (1)
plot (P,Tcalc,'b'), hold on
plot (P,Tr,'d'), hold on
xlabel('\textbf{Power [W]}', 'FontName', 'Times New Roman', ...
       'FontSize',13,'Color','k', 'Interpreter', 'LaTeX')
ylabel('\textbf{Temperature [${\circ}$T]}', 'FontName', 'Times New
Roman', ...
       'FontSize',13,'Color','k', 'Interpreter', 'LaTeX')
title(join(['\textbf{Steady state analysis at
70}','$^{\circ}$','\textbf{C}']), 'FontName', 'Times New Roman', ...
       'FontSize',14,'Interpreter','Latex')
```

```
legend ('Fitting line','Experimental data','Interpreter',
'LaTeX','Location','southeast'), hold on


grid on
hold off
drawnow
end
```

Kinetic and mass transfer modelling

The kinetic and mass transfer model valid for tests in the calorimetric reactor is here reported. For the sake of brevity, only the script valid for tests at 70°C is reported. For the other temperatures, the scripts were similar, except for the experimental data arrays.

Modelling of the MW heating and conventional heating systems followed the same script, except for the experimental arrays and the initial amount of reactants. The programming language is *Matlab*®.

```
clear all,  clc, format long

%% Fitting *****For 70°C*****
% calculation of the initial concentrations
temp = '\textbf{70}';
temp2 = '70';
nom = 'calorimetrico';
m_olio= 45; %g
m_AA= 0.171*m_olio; %g
m_H2O2_H2O= 0.829*m_olio; %g
m_H2O= m_H2O2_H2O*(1-0.35); %g
m_H2O2= m_H2O2_H2O*0.35; %g
m_H2SO4= m_olio*0.03; %g
MW_AA = 60.05; % g/mol
MW_H2O2 = 34.0147; % g/mol
MW_H2O = 18.0158; % g/mol
n_AA = m_AA / MW_AA;
n_H2O2 = m_H2O2 / MW_H2O2;
n_H2O = m_H2O / MW_H2O;
n_in = [n_AA n_H2O2 n_H2O];
naq_in = sum(n_in);
xi_in = n_in/naq_in;
MW_aq= 60.05*xi_in(1)+34.0147*xi_in(2)+18.015828*xi_in(3);
rho_oil= 0.917*10^3; %g/l
rho_mean= 1.1*10^3; %g/l
I2number=mean([122.7 128.7]); %grams of I2 required to titolate C=C
of 100g of oil
n_I2=I2number*45/253.8089/100; % [mol I2/g oil] MW_I2= 253.8089
g/mol
Cin_DB= n_I2/(45/rho_oil); %[mol/l]
Cin_aq = rho_mean.*xi_in; %[mol/l]
%% initial concentration
y0 = [Cin_aq(1) Cin_aq(2)    0      Cin_aq(3) Cin_DB  0    0   0       0
];
%         AA_w     H2O2       PAA_w     H2O        DB     EP   EG AA_o
PAA_o
```

```
C0= y0(4); % concentration adimensionalization parameter
t0=420;
y0=y0/C0;
%% kinetic constant and mass transfer coefficient guesses
%    k1  k2    k3    k4    k5  Aw_AA   Aw_PAA   Ao_AA   Ao_PAA
k0= [0.09 0.0001 0.15 0.00027 0.0085 1.8 19];
Aj_i = product between mass transfer coeff of
%
species "i" in the phase "j" and the
%
interfacial area between the two phases.
logk0= log10(k0);

%% experimental epoxide concentration values and fitting
%       0  20m    1h

%       0  20m        40m         1h          1.5h       3h
5h
%
7h          15h
OO_70= [0 3.587 5.230 6.038 6.319822458 6.45081622 6.146410278
5.565248977]*(45/(16*100))/0.04907/C0;
texp= [0, 20, 40, 60, 90, 180, 300, 420]/t0; %vettore dei tempi fino
a 7 ore
options=optimset('Display','iter','TolFun',1e-3,'TolX',1e-
7,'MaxIter',1000,'MaxFunEvals',15000);
[logk,fval]=fminsearch(@Calcolo_errore,logk0,options,texp,OO_70,y0,C
0,t0); %fitting prove a 55°C
OO=OO_70;
k=10.^(logk);
k0=k;

 %% Calcolo errore
function S=Calcolo_errore(logk, texp, OO_70, y0, C0,t0) %come
concentrazioni uso quelle a 70°C
k=10.^(logk);
[t,y]=ode15s(@MassBalances,texp,y0,[],k,C0,t0); %risoluzione del
sistema di equazioni
S=norm((y(:,6)-OO_70').^2); % calcolo scarto quadratico
TSS=sum((OO_70'-mean(OO_70)).^2);
RSS=sum((OO_70'-y(:,6)).^2);
R_2=1-RSS/TSS
% figure(1)
% % Grafici delle concentrazioni in funzione del tempo
% plot(t,y(:,1),'-r',t,y(:,2),'-y',t,y(:,3),'-
m',t,y(:,4),'g',t,y(:,5),'b',t,y(:,6),'c',t,y(:,7),'k',t,y(:,8),t,y(
:,9))
```

```
% hold on, grid on
% plot(texp,OO_70,'o')
% legend ('AA_w','H2O2','PAA_w','H2O','DB','EP',
'EG','AA_o','PAA_o','C_O_O_7_0'), hold on
% hold off
% drawnow
end
%% Mass balances
function dydt=MassBalances(t,y,k,C0,t0)
% MASS TRANSFER RATES PER UNIT VOLUME
PC=[3.78 27];     %partition coefficient  Ci_w/Ci_o for AA and PAA,
respectively.
Vw=0.042136; %l        volume aqueous
Vo=0.0491; %l         volume organic
% Concentrations at the organic phase interphase
ci_AA=(Vw*k(6)*y(1)+Vo*k(7)*y(8))/(Vo*k(7)+Vw*k(6)*PC(1));
ci_PAA=(Vw*k(6)*y(3)+Vo*k(7)*y(9))/(Vo*k(7)+Vw*k(6)*PC(2));
%
Jw_AA =  k(6)*t0*(y(1)-PC(1)*ci_AA);
Jo_AA =  k(7)*t0*(ci_AA-y(8));
Jw_PAA = k(6)*t0*(y(3)-PC(2)*ci_PAA);
Jo_PAA = k(7)*t0*(ci_PAA-y(9));
Keq= 5.17; % equilibrium constnt of the peracetic acid formation
% reaction system
% AA_w H2O2 PAA_w H2O  DB  EP  EG    AA_o  PAA_o
% 1     2    3     4   5   6   7      8      9
%
% considered equations:
%                                        k1
% Aqueous phase:          1) AA_w+H2O2 <--> PAA_w + H2O ==> r1) 1 + 2
--> 3 + 4
%                                  k1/Keq                   r2) 3 + 4
--> 1 + 2
%
%                                   k2
%                          2) H2O2 --> H2O +0.5O2        ==> r3) 2 -->
4
%
%
%                                      k3
% Organic phase:          3) PAA_o + DB --> EP + AA_o   ==> r4) 9 + 5
--> 6 + 8
%
%                                     k4
%                          4) EP + AA_o --> EG           ==> r5) 6 + 8
--> 7
%
```

```
%                                        k5
%                          5) EP + PAA_o --> EG          ==> r6) 6 + 9
--> 7
%
%% RATES OF REACTION
r(1)= k(1)*C0*t0*y(1)*y(2);
r(2)= k(1)/Keq*C0*t0*y(3)*y(4);
r(3)= k(2)*C0^1.5*t0*y(2)^2.5;
r(4)= k(3)*C0*t0*y(9)*y(5); % con y(9)^2 k0= [24.8 50.14 0.86
1.650973800355333e+14 6.235504083343732e-29 1.700230006477752e+05
9.58 8.24 0.35 7.647630604095155e+04];
r(6)= k(4)*C0*t0*y(6)*y(8);
r(5)= k(5)*C0*t0*y(6)*y(9);
%% MASS BALANCES (constant volume of both phases)
% aqueous phase
dc1dt= -r(1) +r(2) -Jw_AA;
dc2dt= -r(1) +r(2) -r(3);
dc3dt=  r(1) -r(2) -Jw_PAA;
dc4dt=  r(1) -r(2) +r(3);
% orgnic phase
dc5dt= -r(4);
dc6dt=  r(4) -r(5) -r(6);
dc7dt=  r(5) +r(6);
dc8dt=  r(4) -r(5) +Jo_AA;
dc9dt= -r(4) -r(6) +Jo_PAA;
dydt = [dc1dt dc2dt dc3dt dc4dt dc5dt dc6dt dc7dt dc8dt dc9dt];
dydt=dydt';
end
```

Plots generation

The drawing of the plots was performed by means of the following script. This script is executed after the modelling is completely processed. Plots were generated with fixed dimensions and format and automatically saved in the selected folder. The programming language is *Matlab*®.

```
clc
[t,y]=ode15s(@MassBalances,[0 t0],y0*C0,[],k,C0,t0); %risoluzione
del sistema di equazioni
figure(1), hold on
xlabel('\textbf{Time [min]}', 'FontName', 'Times New Roman', ...
       'FontSize',13,'Color','k', 'Interpreter', 'LaTeX')
ylabel('\textbf{Concentration [mol/l]}', 'FontName', 'Times New
Roman', ...
       'FontSize',13,'Color','k', 'Interpreter', 'LaTeX')
title(join(['\textbf{Concentration vs time at
}',temp,'$^{\circ}$','\textbf{C}']), 'FontName', 'Times New Roman',
...
       'FontSize',14,'Interpreter','Latex')

%% Grafici delle concentrazioni in funzione del tempo
plot(t,y(:,1),'-r',t,y(:,2),'-y',t,y(:,3),'-
m',t,y(:,5),'k',t,y(:,6),'b',t,y(:,7),'c',t,y(:,8),t,y(:,9),
'LineWidth',0.8)
hold on, grid on
plot(texp*t0,OO*C0,'b o','LineWidth',1), xlim([0 t0]), hold on
legend
('$AA_{\!W}$','$H_{\!2}O_{\!2}$','$PAA_{\!W}$','\it{DB}','\it{EP}',
'\it{EG}','$AA_{\!O}$','$PAA_{\!W}$','$C_{\!OO}$','Interpreter',
'LaTeX'), hold on
box on
x_0=50;
y_0=200;
width=700;
height=470;
set(gcf,'position',[x_0,y_0,width,height])
fname =
'C:\Users\Damiano\Dropbox\Tesi\Modello\Modello\calorimetrico\im';
saveas(gca,fullfile(fname,join(['conc_',temp2,'_',nom,'.svg'])))

hold off
drawnow
Keq= 5.17;
PC=[3.78 27];     %partition coefficient  Ci_w/Ci_o for AA and PAA,
respectively.
Vw=0.042136; %l        volume aqueous
Vo=0.0491; %l         volume organic
R=zeros(length(t),6);
R(:,1)= k(1)*y(:,1).*y(:,2);
R(:,2)= k(1)/Keq*y(:,3).*y(:,4);
R(:,3)= k(2)*y(:,2).^2.5;
R(:,4)= k(3)*y(:,9).*y(:,5);
```

```
R(:,5)= k(4)*y(:,6).*y(:,8);
R(:,6)= k(5)*y(:,6).*y(:,9);
%% Grafici velocità di reazione
figure (2), xlabel ('time [min]'), ylabel('reaction rates
[mol/(l*min)]'), hold on
plot(t,R(:,1),t,R(:,2),t,R(:,3),t,R(:,4),t,R(:,5),t,R(:,6),
'LineWidth',0.8), hold  on
xlabel('\textbf{Time [min]}', 'FontName', 'Times New Roman', ...
       'FontSize',13,'Color','k', 'Interpreter', 'LaTeX')
ylabel('\textbf{Rate of reaction [mol/l min]}', 'FontName', 'Times
New Roman', ...
       'FontSize',13,'Color','k', 'Interpreter', 'LaTeX')
title(join(['\textbf{Rates of reaction vs time at
}',temp,'$^{\circ}$','\textbf{C}']), 'FontName', 'Times New Roman',
...
       'FontSize',14,'Interpreter','Latex')
legend
('\textit{R1}','\textit{R2}','\textit{R3}','\textit{R4}','\textit{R5
}','\textit{R6}', 'Interpreter', 'LaTeX')
xlim([0 t0])
box on
x_0=150;
y_0=200;
width=700;
height=470;
set(gcf,'position',[x_0,y_0,width,height])
fname =
'C:\Users\Damiano\Dropbox\Tesi\Modello\Modello\calorimetrico\im';
saveas(gca,fullfile(fname,join(['rate_',temp2,'_',nom,'.svg'])))
%% rate determining step
% PAA concentrations in organic phase
ci_PAAo=(Vw*k(6).*y(:,3)+Vo*k(7).*y(:,9))/(Vo*k(7)+Vw*k(6)*PC(2));
figure (3)
cb_PAAo=y(:,9);

subplot (211)
plot(t,ci_PAAo,'-r',t,cb_PAAo,'-b', 'LineWidth',0.8), xlim([0 t0]),
hold on
xlabel('\textbf{Time [min]}', 'FontName', 'Times New Roman', ...
       'FontSize',12,'Color','k', 'Interpreter', 'LaTeX')
ylabel('\textbf{PAA concentration [mol/l]}', 'FontName', 'Times New
Roman', ...
       'FontSize',11,'Color','k', 'Interpreter', 'LaTeX')
title(join(['\textbf{Organic phase concentrations of PAA at
}',temp,'$^{\circ}$','\textbf{C}']), 'FontName', 'Times New Roman',
...
       'FontSize',14,'Interpreter','Latex')
legend (join(['$C_{\!PAA}$', '\textit{Organic
interface}']),join(['$C_{\!PAA}$', '\textit{Organic
bulk}']),'Interpreter', 'LaTeX'), hold on
x_0=150;
y_0=50;
width=700;
height=500;
set(gcf,'position',[x_0,y_0,width,height])
```

```
xlim([0 t0])



% PAA concentrations in water phase
subplot (212)
ci_PAAw=PC(2).*ci_PAAo;
cb_PAAw=y(:,3);
plot(t,ci_PAAw,'-r',t,cb_PAAw,'-b', 'LineWidth',0.8), xlim([0 t0]),
hold on
xlabel('\textbf{Time [min]}', 'FontName', 'Times New Roman', ...
       'FontSize',12,'Color','k', 'Interpreter', 'LaTeX')
ylabel('\textbf{PAA concentration [mol/l]}', 'FontName', 'Times New
Roman', ...
       'FontSize',11,'Color','k', 'Interpreter', 'LaTeX')
title(join(['\textbf{Aqueous phase concentrations of PAA at
}',temp,'$^{\circ}$','\textbf{C}']), 'FontName', 'Times New Roman',
...
       'FontSize',14,'Interpreter','Latex')
legend (join(['$C_{\!PAA}$', '\textit{Aqueous
interface}']),join(['$C_{\!PAA}$', '\textit{Aqueous
bulk}']),'Interpreter', 'LaTeX'), hold on

fname =
'C:\Users\Damiano\Dropbox\Tesi\Modello\Modello\calorimetrico\im';
xlim([0 t0])
saveas(gca,fullfile(fname,join(['MT_',temp2,'_',nom,'.svg'])))

%% Mass balances
function dydt=MassBalances(t,y,k,C0,t0)
% MASS TRANSFER RATES PER UNIT VOLUME
PC=[3.78 27];     %partition coefficient  Ci_w/Ci_o for AA and PAA,
respectively.
Vw=0.042136; %l        volume aqueous
Vo=0.0491; %l         volume organic
% Concentrations at the organic phase interphase
ci_AA=(Vw*k(6)*y(1)+Vo*k(7)*y(8))/(Vo*k(7)+Vw*k(6)*PC(1));
ci_PAA=(Vw*k(6)*y(3)+Vo*k(7)*y(9))/(Vo*k(7)+Vw*k(6)*PC(2));
%
Jw_AA =  k(6)*(y(1)-PC(1)*ci_AA);
Jo_AA =  k(7)*(ci_AA-y(8));
Jw_PAA = k(6)*(y(3)-PC(2)*ci_PAA);
Jo_PAA = k(7)*(ci_PAA-y(9));
Keq= 5.17; % equilibrium constnt of the peracetic acid formation
% reaction system
% AA_w H2O2 PAA_w H2O  DB  EP  EG    AA_o  PAA_o
% 1     2    3     4   5   6   7      8      9
%
% considered equations:
%                                        k1
% Aqueous phase:          1) AA_w+H2O2 <--> PAA_w + H2O ==> r1) 1 + 2
--> 3 + 4
%                                    k1/Keq                    r2) 3 + 4
--> 1 + 2
%
```

```
%                                  k2
%                          2) H2O2 --> H2O +0.5O2          ==> r3) 2 -->
4
%
%
%                                    k3
% Organic phase:           3) PAA_o + DB --> EP + AA_o     ==> r4) 9 + 5
--> 6 + 8
%
%                                   k4
%                          4) EP + AA_o --> EG             ==> r5) 6 + 8
--> 7
%
%                                    k5
%                          5) EP + PAA_o --> EG            ==> r6) 6 + 9
--> 7
%
%% RATES OF REACTION
r(1)= k(1)*y(1)*y(2);
r(2)= k(1)/Keq*y(3)*y(4);
r(3)= k(2)*y(2)^2.5;
r(4)= k(3)*y(9)*y(5);
r(5)= k(4)*y(6)*y(8);
r(6)= k(5)*y(6)*y(9);
%% MASS BALANCES (constant volume of both phases)
% aqueous phase
dc1dt= -r(1) +r(2) -Jw_AA;
dc2dt= -r(1) +r(2) -r(3);
dc3dt=  r(1) -r(2) -Jw_PAA;
dc4dt=  r(1) -r(2) +r(3);
% orgnic phase
dc5dt= -r(4);
dc6dt=  r(4) -r(5) -r(6);
dc7dt=  r(5) +r(6);
dc8dt=  r(4) -r(5) +Jo_AA;
dc9dt= -r(4) -r(6) +Jo_PAA;
dydt = [dc1dt dc2dt dc3dt dc4dt dc5dt dc6dt dc7dt dc8dt dc9dt];
dydt=dydt';
end
```

Power controlled power generator

The script for the operation of the power controlled power generator is here reported. The programming language is C++.

```
#include <LiquidCrystal.h> //LCD library 16x2
// variables initialization
int val1;
int val2;
double voltD;
double volt;
double curr;
double curD;
float PWR;
int zeroCur=0;
float PWRsetpoint=10;
int voltEXIT=50;
float errore;
int i;
int h;
int t;
int r;
int k=10;
float toll;
LiquidCrystal lcd(12, 11, 10, 9, 8, 7);


void setup() {
  //definition of pins and resolution
  analogReadResolution(12);
  analogWriteResolution(8);
  pinMode(2,INPUT);
  pinMode(4,INPUT);
  pinMode(6,OUTPUT);
```

```
  Serial.begin(9600);
  lcd.begin(16, 2);
  }

void loop() {

 val1 = digitalRead(2);
 val2 = digitalRead(4);
 while (val1==0 or val2==0)
 {
 lcd.clear();
 lcd.setCursor(1,0);
 lcd.print("POWER SETPOINT");

 //user panel reading (setpoint)
  for(t=1; t<=7; t++)
  {
    if(val1==0 && PWRsetpoint<35)
  {
  PWRsetpoint=PWRsetpoint+0.5;
  r=1;
  }
 if(val2==0 && PWRsetpoint>4)
  {
  PWRsetpoint=PWRsetpoint-0.5;
  r=1;
  }
 if(r==1)
 {
 lcd.setCursor(5,1);
 lcd.print(PWRsetpoint);
 lcd.print(" W   ");
 }
```

```
 val1 = digitalRead(2);
 val2 = digitalRead(4);
 r=0;
 delay(500);
  }
  }

// acquisition of current and voltage (average on 50000 values)
  curD = 0;
 voltD = 0;
for(i=1; i<=50000; i++)
 {
  curD = analogRead(4)+curD;
  voltD = analogRead(1)+voltD;
  delayMicroseconds(t);
 }
curD = curD/50000;
voltD = voltD/50000;

//power calculation and error

//volt = 0.021989845493556 + 3.637752055238e-003*voltD +
5.28540116e-007*pow(voltD,2) - 5.35883e-010*pow(voltD,3) + 1.72e-
013*pow(voltD,4);
//volt = 0.009064492085098 + 3.600520429987e-003*voltD +
6.03109228e-007*pow(voltD,2) - 6.23764e-010*pow(voltD,3) + 1.72e-
013*pow(voltD,4);
//volt = 1.086927240883867 + 1.75258673467e-004*voltD +
4.384387268e-006*pow(voltD,2) - 2.335945e-009*pow(voltD,3) + 4.7e-
013*pow(voltD,4);
volt = 1.086927240883867 + 1.75258673467e-004*voltD + 4.384387268e-
006*pow(voltD,2) - 2.335945e-009*pow(voltD,3) + 4.7e-
013*pow(voltD,4); %% correlazione tensione - valori ADC
volt = volt + 0.0114*volt - 0.0336;
curr = 10.035 + 8.26398920046e-004*curD -
0.000001393870224*pow(curD,2) - 0.05; %% correlazone corrente -
valori ADC
```

```
PWR = volt*curr;
errore = PWRsetpoint - PWR;
toll = 0.005*PWRsetpoint;

Serial.print(PWR);
// write voltage, current, real power and setpoint on LCD
  lcd.clear();
  lcd.setCursor(0,0);
  lcd.print("Ps:");
  lcd.print(PWRsetpoint,1);
  lcd.setCursor(8,0);
  lcd.print("Pr:");
  lcd.print(PWR);
  lcd.setCursor(0,1);
  lcd.print("V:");
  lcd.print(volt,3);
  lcd.setCursor(8,1);
  lcd.print("I:");
  lcd.print(curr);

// control algorithm (fast)
 if (errore > (1) && voltEXIT < 242)
 {
  voltEXIT = voltEXIT + 12;
  analogWrite(6,voltEXIT);
  delay(10);
  t=5;
 }

 if (errore < (-1) && voltEXIT > 13)
 {
  voltEXIT = voltEXIT - 12;
  analogWrite(6,voltEXIT);
```

```
  delay(10);
  t=5;
 }

// control algorithm (slow - fine adjustemnt)
 if (errore > toll && errore < 1 && voltEXIT < 253)
 {
  voltEXIT = voltEXIT + 1;
  analogWrite(6,voltEXIT);
  delay(300);
  t=20;
 }

 if (errore<(-toll) && errore > (-1) && voltEXIT > 2)
 {
  voltEXIT = voltEXIT - 1;
  analogWrite(6,voltEXIT);
  delay(300);
  t=20;
 }



 }
```